U.S. ARMY MEDICAL RESEARCH INSTITUTE OF CHEMICAL DEFENSE

USAMRICD-TR-02-03

Efficacy of Laser Debridement with Autologous Split-Thickness Skin Grafting in Promoting Improved Wound Healing of Deep Cutaneous Sulfur Mustard Burns

John S. Graham
Kevin T. Schomacker
Robert D. Glatter
Crystal M. Briscoe
Ernest H. Braue, Jr.
Katherine S. Squibb

July 2002

U.S. Army Medical Research
Institute of Chemical Defense
Aberdeen Proving Ground, MD 21010-5400

DISPOSITION INSTRUCTIONS:

Destroy this report when no longer needed. Do not return to the originator.

DISCLAIMERS:

The findings in this report are not to be construed as an official Department of the Army position unless so designated by other authorized documents.

In conducting the research described in this report, the investigators complied with the regulations and standards of the Animal Welfare Act and adhered to the principles of the Guide for the Care and Use of Laboratory Animals (NRC 1996).

The use of trade names does not constitute an official endorsement or approval of the use of such commercial hardware or software. This document may not be cited for purposes of advertisement.

REPORT DOCUMENTATION PAGE

Form Approved OMB No. 0704-0188

1. REPORT DATE *(DD-MM-YYYY)*	2. REPORT TYPE	3. DATES COVERED *(From - To)*
July 2002	Technical Report	January 1999-May 2001

4. TITLE AND SUBTITLE

Efficacy of Laser Debridement with Autologous Split-thickness Skin Grafting in Promoting Improved Healing of Deep Cutaneous Sulfur Mustard Burns

5a. CONTRACT NUMBER

5b. GRANT NUMBER

5c. PROGRAM ELEMENT NUMBER
63384

6. AUTHOR(S)

Graham JS, Schomacker, KT,[1] Glatter, RD,[1] Briscoe, CM, Braue, EH, Jr., and Squibb, KS[2]

[1] Wellman Laboratories of Photomedicine, Massachusetts General Hospital, Boston, MA

[2]Department of Epidemiology and Preventative Medicine, Division of Environmental Epidemiology and Toxicology, University of Maryland, Baltimore, MD

5d. PROJECT NUMBER
TC3

5e. TASK NUMBER
V.M

5f. WORK UNIT NUMBER

7. PERFORMING ORGANIZATION NAME(S) AND ADDRESS(ES)

US Army Medical Research Institute of Chemical Defense
ATTN: MCMR-UV-CC
3100 Ricketts Point Road
Aberdeen Proving Ground, MD
21010-5400

8. PERFORMING ORGANIZATION REPORT NUMBER

USAMRICD-TR-02-03

9. SPONSORING / MONITORING AGENCY NAME(S) AND ADDRESS(ES)

US Army Medical Research Institute of Institute of Chemical Defense
ATTN: MCMR-UV-RC
3100 Ricketts Point Road
Aberdeen Proving Ground, MD
21010-5400

10. SPONSOR/MONITOR'S ACRONYM(S)

11. SPONSOR/MONITOR'S REPORT NUMBER(S)

12. DISTRIBUTION / AVAILABILITY STATEMENT

Approved for public release; distribution unlimited

13. SUPPLEMENTARY NOTES

This work was supported in part by the US Army Research Office, contract DAAH04-96-C-0086.

14. ABSTRACT

The consequences of receiving a cutaneous sulfur mustard (SM) burn are a prolonged wound healing phase and secondary infection. This study was undertaken to find a treatment that promotes speedier healing with fewer complications and minimal disfigurement. Deep SM burns were generated on the ventrum of weanling pigs and treated at 48 h. Four treatments were compared including (1) full thickness CO_2 laser debridement followed by skin grafting, (2) full thickness sharp surgical tangential excision followed by skin grafting, the "Gold Standard" used in deep thermal burns management, (3) partial thickness laser ablation with no grafting, and (4) partial thickness sharp excision with no grafting. Ulceration, wound morphometry, wound contraction, skin color, epidermal barrier function, cutaneous blood flow, skin hardness and elasticity, and histopathology were evaluated during a 36-day healing period. Laser debridement followed by skin grafting was as efficacious in improving the wound healing of deep SM burns as the "Gold Standard." Laser debridement offered additional benefits that included hemostatic control during surgery and minimal debridement of normal perilesional skin, resulting in significantly less blood loss and an improved cosmetic result. Mid-dermal debridement by sharp excision or laser ablation without grafting produced less desirable results but was better than no treatment.

15. SUBJECT TERMS

sulfur mustard, laser debridement, skin grafting, transepidermal water loss, wound contraction, wound healing, laser Doppler perfusion imaging, image analysis, reflectance colorimetry, ballistometry, pathology

16. SECURITY CLASSIFICATION OF:			17. LIMITATION OF ABSTRACT	18. NUMBER OF PAGES	19a. NAME OF RESPONSIBLE PERSON
a. REPORT	b. ABSTRACT	c. THIS PAGE			John S. Graham
UNCLASSIFIED	UNCLASSIFIED	UNCLASSIFIED	UNLIMITED	118	19b. TELEPHONE NUMBER *(include area code)* 410-436-1197

Summary

Sulfur mustard [*bis*(2-chloroethyl)sulfide; SM] is a blistering chemical warfare agent that remains a threat to war fighters and civilians worldwide. The consequences of receiving a cutaneous SM burn are a prolonged wound healing phase and secondary infection. Blister aspiration, debridement, irrigation, topical antibiotics and sterile dressings have been the main treatments. The reason for undertaking this study was to find a new treatment that promotes speedier healing with fewer complications and less disfigurement. The principal objective of the study was to compare four treatments and establish which achieved the shortest healing time and least amount of wound contraction. These treatments included (1) full thickness debridement with a computer controlled, raster scanned continuous wave CO_2 laser followed by autologous split thickness skin grafting, (2) full thickness sharp surgical tangential excision followed by skin grafting, the "Gold Standard" used in human deep dermal/full-thickness thermal burns management, (3) partial thickness laser ablation with no grafting, and (4) partial thickness sharp excision with no grafting. Fifteen female Yorkshire Cross weanling pigs were used. Liquid SM was applied to the ventral body surface for 2 h to generate six large 4-cm diameter deep dermal/full-thickness burns. The treatments were conducted 48 h post-exposure. A variety of non-invasive bioengineering methods were used to evaluate ulceration, wound size, shape and contraction, skin color, epidermal barrier function, cutaneous blood flow, and skin hardness and elasticity during a 36-day healing period. Vancouver scar assessments and histopathological evaluations were conducted at the end of the healing period. Laser debridement followed by skin grafting was as efficacious in improving the wound healing of deep dermal/full thickness cutaneous SM burns as the "Gold Standard." Engraftment rates and Vancouver scar assessments were similar between both methods of debridement. Laser debridement offered additional benefits that included hemostatic control during surgery and minimal debridement of normal perilesional skin, resulting in significantly less blood loss and an improved cosmetic result. Mid-dermal debridement by sharp excision or laser ablation without grafting produced less desirable results but was better than no surgical treatment of the wounds at all. Non-invasive bioengineering methods were useful in monitoring the progress of wound healing.

This Page Intentionaly
Left Blank

ACKNOWLEDGMENTS

The authors wish to thank the following people for their professional advice and guidance: Wolfgang J. Mergner, M.D., Ph.D., of the University of Maryland, Baltimore, MD; Renate Reimschuessel, D.V.M., Ph.D., of the Food and Drug Administration, Laurel, MD; William J. Smith, Ph.D., Brennie E. Hackley, Ph.D., Michelle C. Ross, D.V.M., Ph.D., Charles G. Hurst, M.D., Larry W. Mitcheltree, V.M.D., Steven M. Duniho, D.V.M., Howard Gobble, D.V.M., and Thomas P. Logan, Ph.D. of the U.S. Army Medical Research Institute of Chemical Defense (USAMRICD), Aberdeen Proving Ground, MD; Mr. Dominic P. Bua of the Wellman Laboratories of Photomedicine, Massachusetts General Hospital, Boston, MA; Robert L. Sheridan, M.D. and Mary Jo Baryza, M.S., P.T. of the Shriners Burns Hospital, Boston, MA; Gary Grove, Ph.D., cyberDERM, Inc., Media, PA; Frances M. Reid, D.V.M., Battelle, West Jefferson, OH; and Ms. Robyn B. Lee, Robyn B. Lee & Associates, LLC, Fawn Grove, PA. We are also appreciative of Mr. F. Steven Tucker, Ms. Jamie L. Martin, Mr. Bryce F. Doxzon, SGT Robert T. Simons, and the veterinary support staff of the USAMRICD for technical assistance provided during various aspects of the study.

This Page Intentionaly
Left Blank

Table of Contents

Table of Contents (continued)

INTRODUCTION

I. Overview

A review of sulfur mustard toxicity is presented followed by (1) a description of current treatment regimens, (2) discussions on wound healing and measurable parameters of good wound healing, (3) descriptions of the non-invasive bioengineering methods that were used in this study to measure those parameters, (4) the rationale and objectives of the study, and (5) the working hypothesis.

II. Sulfur Mustard Toxicity

History

Sulfur mustard [*bis*(2-chloroethyl)sulfide; SM, Fig. 1] is a potent incapacitating chemical warfare agent which was first used in World War I by Germany against French troops at Ypres, Belgium (1917). Since then, there has been evidence or allegations of SM use in 11 conflicts, including use by Italy against Ethiopia in 1936, by Japan against China in 1937, by Poland against Germany in 1939, by Egypt against Yemen from 1963 to 1967, and by Iraq against Iran in the 1980s.[1] In addition, its use was threatened during the recent Gulf War. Dispersed as a vapor, aerosol or in liquid droplets, sulfur mustard remains a threat to war fighters and civilians worldwide. Extensive production and stockpiling during World War II, along with its known effects on epithelial tissues, has since engendered agreements to ban its production and use. There are programs currently underway to destroy these stockpiles in an environmentally safe manner. Nonetheless, this chemical warfare agent remains a threat due to its popularity in certain third world countries that do not abide by these agreements.

The molecular mechanisms of action, chemistry, toxicodynamics and genotoxicity of SM as well as the pathogenesis and histopathology of SM injuries have been widely described.[1-13] Papirmeister et al.[1] wrote an extensive review of SM research, offered several theories of its cytotoxicity, and summarized what is known of its absorption, distribution, biotransformation and excretion. Current research is not only investigating various aspects of Papirmeister's theories, but is also actively pursuing the use of topical skin protectants, and prophylactic and therapeutic measures to counteract the effects of SM.

Clinical Manifestations

SM is a bifunctional alkylating agent that causes extensive incapacitating injuries to the skin, respiratory tract and eyes. It has been shown to be carcinogenic and mutagenic in animal studies, and epidemiological studies of exposed war fighters and factory workers have implicated it in human cancers.[1] It can cross-link complementary strands of DNA and inhibit cell division. Clinical signs of injury are delayed from one to several hours following exposure. Due to this delay and lack of obvious or easily perceived odor, detection is often difficult and can result in a lack of immediate and

adequate decontamination, resulting in severe damage. Characteristic lesions are a function of dose and time after exposure. At low toxic doses, skin lesions are characterized by an initial asymptomatic period of highly variable duration followed by localized erythema. Higher doses initially produce small vesicles in the periphery of the erythematous areas that may later merge to form large blisters. Very high doses produce coagulation necrosis. Secondary bacterial infections of the wound pose a serious threat. Although the formation of blisters has not been successfully duplicated in laboratory animal species (e.g., hairless guinea pigs, weanling pigs), microvesicles are produced showing separation at the dermal-epidermal region. Basal cell necrosis, breakage of anchoring filaments of hemidesmosomes, and accumulation of edema fluid in the forming blister due to increased osmotic pressure at the dermal-epidermal junction characterize pathological changes (see skin pathology discussion below). Multiple subepidermal microvesicles coalesce to produce the characteristic blister. Inhalation of SM vapor induces changes in laryngeal and tracheobronchial mucosa with mild to severe inflammation. Respiratory infections during World War I were a major cause of death following SM exposure. Persistent problems include chronic bronchitis, asthma, laryngitis and recurrent pneumonia. Ocular reactions include severe conjunctivitis, photophobia and corneal damage. Permanent blindness may occur with very high doses. In addition, very high doses may produce a systemic toxicity that includes destruction of bone marrow, lymphoid organs and intestinal mucosa of the small intestine. SM lesions may require weeks to months to heal, depending upon their severity.

Mechanism of Action

There are several hypotheses of SM cytotoxicity. The hypotheses are (1) the Poly(ADP-Ribose) Polymerase Hypothesis, (2) the Thiol-Ca^{2+} Hypothesis, and (3) the Lipid Peroxidation Hypothesis.[1] None of these hypotheses has been fully accepted, and mechanisms invoked by these theories may be active at the same time. At present, the exact mechanism of action of sulfur mustard is not known.

The first hypothesis, originally proposed by Papirmeister, has been coined the "Poly(ADP-Ribose) Polymerase" hypothesis (PADPRP, Fig. 1). Rapid alkylation of DNA initiates SM injury. Alkylated DNA purines undergo spontaneous/enzymatic depurination, resulting in numerous apurinic sites that are subsequently cleaved via apurinic endonucleases to form DNA breaks. Accumulation of these breaks activates the chromosomal enzyme PADPRP, which utilizes NAD^+ as a substrate to ADP-ribosylate several nuclear proteins, resulting in a depletion of cellular NAD^+. NAD^+ depletion appears to be the result of an accelerated rate of utilization, as opposed to interference with its synthesis. This depletion results in the inhibition of glycolysis and subsequent stimulation of the $NADP^+$-dependent hexose monophosphate shunt (HMS) due to accumulation of glucose-6-phosphate. Activation of the HMS results in induction and secretion of proteases, which in turn lead to the typical pathology changes noted above. Results from *in vivo* studies using a human skin graft model and *in vitro* work utilizing human lymphocytes, human keratinocytes and human skin organ cultures suggest that NAD^+ levels must decrease below a critical value before depression becomes irreversible and injury-producing. Nuclear pathology appears to precede

cytoplasmic damage. This nuclear damage is characterized by loss of euchromatin, and condensation and margination of heterochromatin. Severe damage to the nuclear envelope has been demonstrated by electron microscopy, such as blebbing and breakage of this envelope, along with the formation of perinuclear vacuoles. The extent of nuclear damage has been shown to be dose- and time-related.

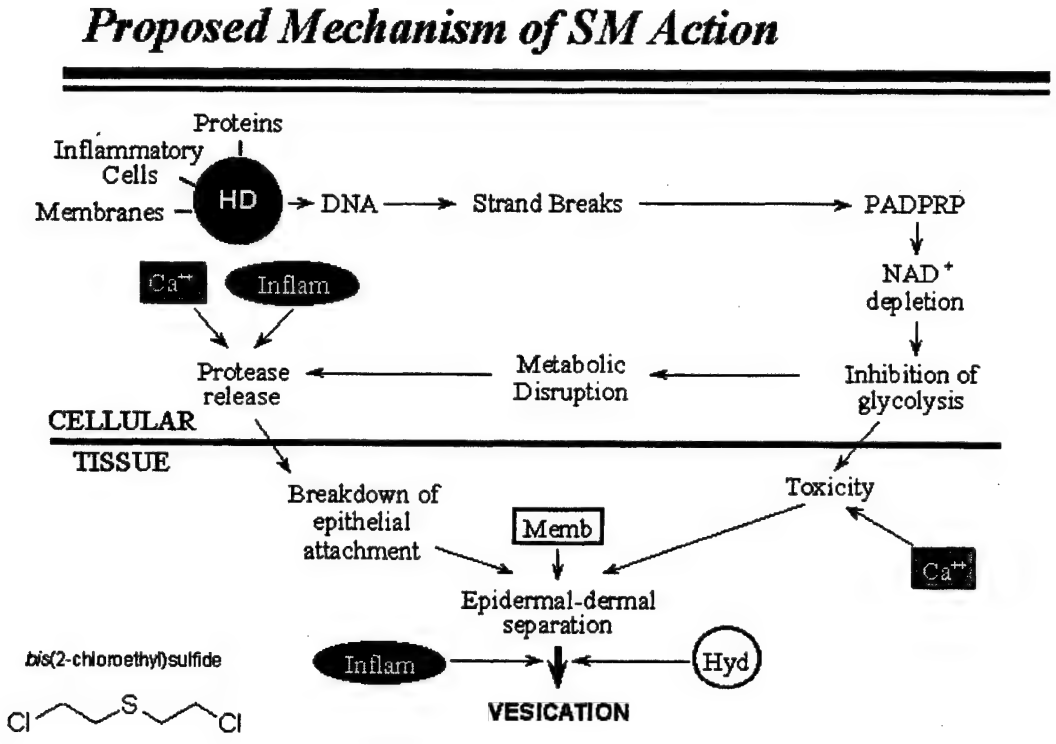

Fig. 1. Proposed mechanism of sulfur mustard (SM) action, the "Poly(ADP-Ribose) Polymerase (PADPRP)" hypothesis. Used by permission, Dr. William J. Smith, U.S. Army Medical Research Institute of Chemical Defense, Aberdeen Proving Ground, MD 21010-5400.

The second hypothesis of SM cytotoxicity, the thiol-Ca^{2+} theory, is based on a mechanism originally proposed by Orrenius and Nicotera in their studies in rat hepatocytes.[14] The initiating event here is a reduction in cellular protein thiol levels leading to toxic increases in free cytosolic Ca^{2+} levels. The thiol levels are depleted as a result of direct reactions of glutathione (GSH) and protein sulfhydryls with oxidants or other electrophilic xenobiotics. GSH is an intracellular scavenger of SM, which may be the cause of GSH depletion. Depletion of GSH occurs following reaction with electrophiles, thus exposing protein sulfhydryls to damage by the xenobiotic or by endogenously produced toxic oxygen species that arise as toxic by-products of oxidative metabolism. Alternatively, SM may also react directly with protein thiols to

cause the inactivation of enzymes. One group of enzymes affected by modification of its sulfhydryl groups is Ca^{2+} translocases, resulting in alteration of intracellular Ca^{2+} homeostasis. This leads to an increase in cytosolic free Ca^{2+}, which in turn leads to activation of Ca^{2+}-dependent catabolic processes including proteases, endonucleases and phospholipases. Protease activity leads to protein degradation and ultimate perturbation of the cytoskeleton. Changes in the cytoskeleton may also arise from direct alkylation by SM on microfilamentous proteins, although this does not appear to play a critical role. Endonuclease activity leads to DNA breaks leading to chromatin condensation and energy loss in the cell. Activation of phospholipases leads to phospholipid hydrolysis with subsequent alterations in membrane fluidity, and loss of membrane protein function and integrity. The cytoskeletal, nuclear and membrane changes all lead to cell death. It is not known whether vesicating doses of SM deplete GSH sufficiently to produce these cytotoxic effects. Slow GSH depletion may be less toxic because it allows time for cell adaption. The lengthy latent period prior to clinical manifestation of SM lesions is inconsistent with the more rapid appearance of injury expected from an alkylation-induced GSH depletion, suggesting that damage to a cellular target other than GSH is responsible for initiating the cytotoxicity and that any involvement of the thiol-Ca^{2+} cytotoxic pathway results from this initial damage.[1]

The third hypothesis involves lipid peroxidation distinct from the thiol-Ca^{2+} hypothesis, where the principal toxic consequence of GSH depletion is the formation of toxic lipid peroxides. Cell death is thus proposed to be due to an accumulation of endogenous oxidants (e.g., H_2O_2 accumulation resulting in hydroxyl and perferryl ion formation) leading to lipid peroxidation and irreversible membrane damage.

Due to the multiple molecular targets of SM, multiple pathways to cell death may be initiated. These multiple pathways may have some common steps; hence, all three of these hypotheses may play a role in the cytotoxicity of sulfur mustard. Papirmeister[15] also explained how SM could induce apoptosis (programmed cell death) and postulated how it might contribute to or modify the pathogenesis of SM injury.

Skin Pathology

Sulfur mustard is known to form a cyclic sulfonium ion, which alkylates nucleophilic cellular sites such as nitrogen bases on DNA strands. The cytotoxic effects of SM on skin have been widely described for a number of species.[1, 3, 5, 9, 16-24] The primary cell population targeted by SM is the basal cell of the epidermis. Blisters/microblisters occur upon separation of the epidermis from the dermis at the dermal-epidermal junction. This separation is dependent upon the loss of integrity of basal cells as well as anchoring filaments. In skin model studies, the development of an apparent initial nuclear pathologic condition of basal cells of the stratum germinativum was followed by progressive cytoplasmic changes leading to the eventual death of affected basal cells. Petrali *et al.*[3] described degenerative subcellular effects of SM on the skin of hairless guinea pigs twenty-four hours after exposure. Degeneration was also observed in human lymphocytes and keratinocytes *in vitro* by Petrali,[3] in a variety of animal models by Papirmeister,[1, 23] and in rabbits and guinea pigs by Vogt.[5] While degenerative changes are noted in the upper layers of the epidermis as well as in epidermal cells of hair follicles, changes are most prevalent among basal cells, with the

earliest and most severe degeneration seen in cells located above the dermal papillae.[1] Microblisters are observed to arise from focal areas of epidermal-dermal separation in areas of widespread basal cell pyknosis, 24-48 hours after SM exposure, as seen by light microscopy. Progressive changes reported in basal epithelial cells include formation of peri- or paranuclear vacuoles, a decrease in nuclear staining intensity, cytoplasmic swelling, loss of chromatin and relocation of chromatin to the periphery of the nucleus, and pyknosis, followed by or accompanied by necrosis, vacuolization, or hydropic degeneration of the cytoplasm.[22] While the extent of nuclear damage is dose- and time-related, it does not take place simultaneously in all basal cells examined, probably reflecting differing repair efficiencies of cells in various phases of the cell cycle. Nuclear pyknosis has also been described following SM exposure in human skin equivalent.[25, 26] It was also described in isolated perfused porcine skin flaps exposed to the SM simulant 2-chloroethyl methyl sulfide, a monofunctional analog of SM.[27] In general, pyknotic nuclei begin to appear in the basal cell layer 3-6 hours after SM exposure. By 12 hours, focal areas of pyknosis are seen and become widespread by 24 hours, with the nuclei of many suprabasal keratinocytes becoming involved.

The pathogenesis of microblisters is not fully understood. Petrali *et al.*[4, 28] found indications that proteins of extracellular matrices of the basement membrane zone are affected during the development of SM-induced skin pathology in hairless guinea pigs, and postulated that they may contribute to the formation of microblisters. Immunohistochemical staining for bullous pemphigoid antigen (BPA), a noncollagenous protein shared between basal cell hemidesmosomes and the lamina lucida, revealed a diminishing of BPA reactivity at early times and subsequent loss of antigenicity at later time periods after an 8-minute SM vapor exposure (tissues were harvested at selected post-exposure time periods up to 24 hours). Laminin, the major glycoprotein of the lamina lucida, showed scanty immunolocalization at the later time periods, conforming to the structurally altered lamina lucida at microblister lesion sites. The reactivity of Type IV collagen, a ubiquitous protein assigned to the lamina densa of basement membranes, was unaltered to specific antisera throughout prevesication and vesication time periods. The influence of these altered macromolecules on repair mechanisms following SM toxicity is not known. Other proteins of the basement membrane zone yet to be discovered likely play a role in the pathogenesis of SM-induced microblisters.

III. Current Treatment Regimens

Severe cutaneous SM lesions can take several months to heal. This lengthy healing process may be due not only to cells at the margin that cannot replicate due to DNA damage, but also to a damaged dermis that may not provide a satisfactory matrix over which the new epidermal cells can spread.[1, 11, 29] In the past, treatment of SM-blistered human patients did not typically involve skin grafting. Blister aspiration and/or deroofing (epidermal removal), debridement, irrigation, topical antibiotics and sterile dressings have been the main courses of action in the medical management of cutaneous SM burns.[11, 13, 30-32] Secondary infection has been noted to be a complication of sulfur mustard burns in both humans and animals.[1] Wound contraction resulting from cutaneous SM exposure has not been well documented. Split-thickness skin grafting was used late in a few cases during the Iran-Iraq conflict where healing

was particularly slow,[11] and for the late treatment of some poorly healing, deep burns sustained in 1992 by a civilian who came across an unexploded artillery shell from World War I.[30]

IV. Wound Healing

Wound healing is a complex process that involves the interplay of a variety of cells, proteins, chemoattractants, growth factors, proteinases, and angiogenic factors.[33] Whether it occurs by primary or secondary intention, wound healing follows a series of cellular and biochemical events. Certain disease processes can cause the progression of healing to falter (e.g., infection, poor nutrition, impaired host defense mechanisms, metabolic imbalances, diabetes, availability of molecular oxygen). Removal of significant amounts of cellular debris by debridement speeds up the healing process by iatrogenically ridding the body of damaged tissue faster than it occurs via the autolytic process.

There are four major overlapping phases of wound healing: coagulation, inflammation, fibroplasia, and remodeling. Different sets of cells, cytokines, and growth factors are involved in each phase, with a high degree of integration, organization and control.[33] Completion of any stage of the healing process can be delayed by a variety of intrinsic (e.g., disease) and extrinsic (e.g., medicinal steroid) factors. The goal of medical intervention in speeding up the healing process is to prevent or minimize the detrimental effects of those factors, and to offer treatments that help to accelerate the process (e.g., wound debridement, growth factors).

During coagulation, platelets aggregate at sites of endothelial damage, activate, and release a number of factors important for hemostasis. The resultant fibrin matrix serves as a scaffold that allows cell migration and helps to deter the movement of bacteria. Important growth factors released by platelets include platelet-derived growth factor (PDGF), transforming growth factor-∀ (TGF-∀), TGF-∃, basic fibroblast growth factor (bFGF), epidermal growth factor (EGF), and insulin-like growth factor-1 (IGF-1).

An acute inflammatory response occurs within hours of injury, typically lasting 5-7 days. The primary active cells in this phase are neutrophils, macrophages, and lymphocytes. Platelets release chemoattractants (platelet factor-IV, TGF-∃), stimulating the influx of neutrophils and macrophages whose function is to kill and digest bacteria as well as remove damaged tissue. Neutrophils release IL-1 and PDGF. They produce elastase and matrix metalloproteinase 8, which can contribute to excessive matrix degradation and destruction of peptide growth factors.[33] Macrophages release collagenase, lactate (which in turn causes the release of angiogenic factors such as tumor necrosis factor-∀ [TNF-∀], interleukin-1 [IL-1], and bFGF), and a number of important growth factors that regulate this and subsequent phases (PDGF, EGF, TGF-∀, TGF-∃, IL-1, and heparin-binding epidermal growth factor [HB-EGF]). Controlling an excessive or chronic inflammatory response is critical in allowing the wound healing process to progress.

Fibroplasia, or the proliferative phase, results in a restored vascular network (neovascularization), replacement of absent or damaged tissue, and re-epithelialization. During angiogenesis, endothelial cells bud off from nearby functioning blood vessels, migrate to the site of injury, and begin to proliferate. The budding off and migration

processes are controlled by proteases and chemotactic factors released from local inflammatory cells. The growth factors involved in neovascularization include basic and acidic fibroblast growth factor, TNF-∃, EGF, and wound angiogenesis factor (WAF). Many of the factors are released from macrophages. Endothelial cells themselves produce bFGF, PDGF, and IGF-1. The migrating and proliferating endothelial cells eventually organize into tubular structures and connect to form a capillary network. PDGF and other chemoattractants recruit fibroblasts, which activate, proliferate, and deposit extracellular matrix components such as collagen, elastic fibers, fibronectin, laminin, and glucosaminoglycans. Fibroblasts also act as precursors to myofibroblasts, which contract and help to bring opposing edges of the wound closer together. Fibroblasts produce TGF-∃, PDGF, and keratinocyte growth factor (KGF, or FGF-7). Large gaps are filled in by large amounts of granulation tissue. The progression of this organization and repair process is a transition from vascular granulation tissue (new capillary network, with recruited macrophages and fibroblasts), to fibrovascular granulation tissue (progressive growth and activity of fibroblasts within the capillary network), to fibrous granulation tissue (active deposition of collagen, along with a regression of many of the newly formed capillaries), to a dense collagenous scar.[34] Collagen deposition generally follows the lines of tissue stress. Growth inhibitory factors such as ∃-fibroblast interferon (IFN-∃) and interferon-((IFN-() help to counterbalance the fibroplasia. After an adequate dermal matrix has been laid down, the reepithelialization process can conclude to reestablish a protective epithelial barrier function. Keratinocytes migrate from the edges of the wound and surviving adnexal structures (e.g., hair follicles, sebaceous glands) to resurface the entire wound. These cells express adhesive surface integrins and secrete matrix metalloproteinases and other collagenases to degrade proteins and allow migration to occur. Movement of the cells is in a "leap-frog" manner (epiboly). The keratinocytes also produce basement membrane components such as fibronectin, collagen, and laminin. The keratinocytes eventually form strong contacts with the underlying basement membrane, and proceed to proliferate and differentiate into a full-thickness, multilayered epidermis. A keratinized horny layer eventually forms the uppermost layer, thereby restoring barrier function. During the process of reepithelialization, the keratinocytes produce IL-1, TGF-∀, TGF-∃, vascular endothelial growth factor (VEGF), and keratinocyte-derived autocrine factor (KAF).

During the remodeling phase of wound healing, (1) excess collagen and matrix are removed by proteolytic enzymes, (2) immature, thin type III collagen is replaced by mature, thick type I collagen, and (3) intra- and inter-molecular crosslinking of collagen strands occurs. The growth factors primarily responsible for the remodeling process include TGF-∃, PDGF, FGF, IL-1, and EGF. TGF-∃ causes an increase in production of tissue inhibitors of metalloproteinases (TIMPs), which help to increase collagen deposition.

The coagulation phase generally lasts for a few hours, the inflammatory and proliferative phases from days to weeks, and the remodeling phase from weeks to months or years.[35] For adult human skin, keratinocytes require 2-4 weeks to migrate from the stratum basale to the stratum granulosum, and an additional 2 weeks to move through the stratum corneum.[36] It can thus take 4-6 weeks following initial wound coverage (thin confluent layer of keratinocytes) for complete stratification to occur and a

disrupted barrier function to return to normal. Wound healing can last as long as two years, and represents a continual process of fibroblast-induced collagen synthesis, breakdown by collagenase, regression of inflammatory cells, and formation of a mature scar.[33] The resultant remodeled tissue, however, never attains its original tensile strength. For a surgical wound that has been sutured, tensile strength is about 10% of normal by 7 days, 50% by 30 days, and a maximal 80% by 3 months.[34]

V. Measurable Parameters of Good Wound Healing

There are a number of characteristics of healed wounds that are important to the patient from both a functional and cosmetic point of view. The wound must be reepithelialized, with no ulcerated areas. Severe wound contraction is detrimental. Surface contour, color/pigmentation and general appearance should be as close to that of surrounding perilesional skin as possible. The epidermal barrier should be functioning to keep bacteria and various chemicals out and water in. There should be adequate blood flow and transcutaneous oxygen tension. The skin should have normal moisture content for the particular area of that patient's body, with normal, slightly acidic pH. The mechanical properties of the skin should be similar to that of surrounding skin (e.g., hardness, elasticity, tensile strength). Neural supply and sensory function should be normal, and hair growth/pelage density should blend in with the surrounding area. The ultimate goal in treating wounds is to return damaged skin to normal appearance and function in the shortest period of time.

Invasive biopsies are useful in characterizing the pathogenesis of wounds and in studying the progression of wound healing. Routine histopathological analyses of formalin-fixed, paraffin-embedded hemotoxylin and eosin-stained tissue offer unique insights into the pathology of the lesion. Supplemented by special histological stains, immunohistochemistry, and electron microscopic examination, light microscopy is a powerful tool for studying the mechanisms of action of various toxic substances. However, widespread use of histopathology in wound healing studies poses several challenges. Using only histopathology requires a large number of animals if the researcher wishes to avoid the deleterious effects on wound healing that multiple sampling from the same site on the same animal will cause. In addition, histopathology does not provide functional measurements. A variety of non-invasive bioengineering methods that are typically used in dermatological research labs and hospitals are available. Several of these have been adapted for use in this study as a way to monitor the progress of wound healing over time. These methods were used, along with histopathology conducted at the end of the study, to characterize the efficacies of the various treatment regimens in improving the healing of liquid SM burns in a weanling pig model.

In the current study, we concentrated on several of the characteristics of healed wounds that were described above: ulceration, wound size and contraction, skin color, epidermal barrier function, cutaneous blood flow, and the mechanical properties of harness and elasticity. To measure areas of ulceration, wound size, and contraction, we performed image analysis on digitized images taken of the lesions throughout the healing period. For skin color, we utilized reflectance colorimetry. To evaluate barrier function, we measured transepidermal water loss (TEWL) using evaporimetry.

Cutaneous blood flow was studied with laser Doppler perfusion imaging. Ballistometry was utilized to measure skin hardness and elasticity. A brief synopsis of these non-invasive bioengineering methods follows.

VI. Non-invasive Bioengineering Methods Employed

In general, multiple measurements were taken from the center of each experimental site during each observation time point, and the results averaged.

Reflectance colorimetry was performed using a chromameter. The chromameter uses reflected light and reads color in a three-dimensional format giving the brightness between black and white, the balance between red and green, and the relative amounts of yellow and blue. The unit includes a small hand-held measuring head connected to a portable data-processing unit by a flexible cord. Three photocells measure the light reflected by the surface of the sample (over an area of an 8-mm diameter circle). The detected signal is converted into three coordinates (L^*, a^*, b^*) of a three-dimensional color system recommended by the CIE (Commission Internationale de l'Eclairage, 1976). This color coordinate system most closely represents human sensitivity to color. The coordinate L^* represents levels of brightness between white (+100) and black (-100); the a^* coordinate represents the relative chromaticity between red (+60) and green (-60); the b^* coordinate represents the relative amounts of yellow (+60) and blue (-60). The a* coordinate is directly related to the degree of color redness and is the most appropriate parameter to use for evaluating erythema. The chromameter is better able to discriminate close shades of redness than the human eye, especially for bright red shades. Braue et. al.[16,17] utilized reflectance colorimetry to assess vesicant skin injury in a hairless guinea pig model, and compared the results with visual scoring based upon a modified Draize scoring scheme. A score of zero (0) was given for no erythema, a score of 1 was given for very slight erythema that was barely perceptible, a score of 2 was given for well-defined erythema, a score of 3 was given for moderate-to-severe erythema, and a score of 4 was given for severe erythema. A plot of visual Draize erythema scores vs a^* values suggested a linear relationship between the two scores.[16]

Stratum corneum barrier function was tested by measuring transepidermal water loss (evaporimetry), based upon the vapor pressure gradient estimation method first described by Nilsson.[37] The stratum corneum forms a barrier against diffusion of water through the epidermis, and thus also the penetration of various chemicals that come in contact with the skin. The efficiency of this layer depends upon the integrity of the stacking of the corneocytes and their intracellular adhesion, as well as upon the water content of the layer. Evaporimetry has been used in the testing of cutaneous irritants, and in the evaluation of clinical skin conditions (irritations or diseases) and occlusive pharmaceutical/cosmetic preparations.[38-41] This methodology holds promise as a non-invasive way of determining how soon after agent exposure barrier function has been compromised, and when normal barrier function has returned. Basically, the human body has a zone of water diffusion around it that is approximately 10 mm thick. A TEWL probe is placed against the skin to make the water loss measurement. Within the probe are two electrodes, one of which sits 3 mm above the skin surface, and the other at 9 mm above the skin surface. Thus, both electrodes sit within the zone of

diffusion. Each electrode measures both temperature and humidity. From these measurements are calculated water vapor pressures, and it is the gradient in water vapor pressure between the two electrodes that yields the TEWL measurement, stated as so many grams of water per square meter per hour. Many variables affect baseline TEWL rates, including species, sweating, skin surface temperature, environmental factors, stress factors, age, sex, race, and anatomical location.[38, 39, 41]

Laser Doppler perfusion imaging (LDPI) was used to study cutaneous blood flow (microcirculation). The complex vascular network of the dermis plays a crucial role in thermoregulation, nutrition and metabolism. Laser Doppler flowmetry and LDPI have been used for prolonged, non-invasive monitoring of tissue viability and wound healing, and for the assessment of peripheral vascular disease, inflammation, ischemia, reperfusion, skin graft acceptance (take) and burn depth.[42-57] LDPI may prove useful in delineating the areas of damage that need to be debrided, avoiding areas with sufficient blood flow. It also has the potential for being a useful tool in evaluating the effects of pharmacologic agents that decrease edema and/or increase blood flow in the microcirculation, therapies we may be exploring in the future. Basically, low power laser light is directed via a moving mirror to execute a raster pattern across the tissue surface. In skin both red and infrared wavelengths penetrate full thickness. The incident light is scattered by static tissue and moving blood. The Doppler shifted light from moving blood and the non-shifted light from tissue are then redirected by the same moving mirror onto detectors in the imaging unit. The signals are translated into "flux" and "conc" levels, which are unitless measurements proportional to tissue blood flow and concentration of moving blood cells, respectively. Brown et al.[58] found that laser Doppler perfusion images of vesicant vapor burns on the backs of swine correlated well with histopathological findings (thrombosis and necrosis of subepidermal capillaries) between 1 h and 7 days post-exposure, and suggested that clinical management decision making on how to treat early vesicant burns could be aided by LDPI. Chilcott et al.[59] concluded that, while reflectance colorimetry and TEWL measurements could provide quantitative, non-invasive methods for determining efficacy of candidate treatment regimens, neither is comparable to the prognostic capabilities of LDPI.

Ballistometry, using impacting masses to measure material properties through their interaction, can be used to measure certain elastic parameters below the surface of the skin.[60] The probe of the torsional ballistometer used in this study contains a rigid aluminum alloy arm which is mounted on a torsion wire. At the correct contact pressure, an internal holding magnet is activated and energy is stored in the torsion spring. Under computer control, the holding magnet is switched off, releasing the arm to vibrate. The vibrating tip of the probe is a spherical ruby ball 2 mm in diameter. The deflection of this ball is monitored. As it bounces on the skin, a bounce profile is generated. From this bounce profile, the indentation (downward deflection) of the ball against the skin is recorded. The harder the skin surface, the smaller the amount of initial indentation. After recoiling, the ball again hits the skin and continues to bounce up and down until it comes to rest. Alpha values, representing elasticity, are determined by fitting an exponential decay function to the peaks on the bounce profile generated by oscillations of the probe. A large alpha value indicates rapid damping (rapid energy loss) thus low elasticity.

VII. Rationale for Conducting the Study

The consequences of receiving a cutaneous SM burn are a prolonged healing phase and secondary infection. The reason for undertaking the current study was to find a treatment regimen that promotes speedier healing with fewer complications and less disfigurement.

VIII. Objectives of the Study

The current study explores the healing of severe, deep dermal/full-thickness SM-induced cutaneous burns in a weanling pig model. It is estimated that it would take between 48 and 96 h to transport an exposed war fighter from the battlefield arena to a properly equipped treatment facility. Waiting 48 h after a burn injury, before wound complications start occurring, is an acceptable elapse for a treatment decision as to whether or not debridement or full-thickness excision is necessary.[61] We thus focused our attention on the treatment of deep cutaneous lesions that were 2 days old.

The principal objective of the study was to compare four treatment regimens and establish which achieved the shortest healing time, lowest rate of infection, and least amount of wound contraction. These treatments included (1) full thickness debridement of the burns with a computer controlled, raster scanned continuous wave CO_2 laser followed by autologous split thickness skin grafting, (2) full thickness sharp surgical tangential excision followed by skin grafting, the "Gold Standard" used in human deep dermal/full-thickness thermal burns management, (3) partial thickness laser ablation with no grafting, and (4) partial thickness sharp surgical excision with no grafting. Based upon observations that viable chondrocytes have been found in thermally altered collagen of lasered meniscus tissue[62] (hence viable fibroblasts may be present in SM-damaged dermis to help in dermal reconstruction), we thought it feasible to examine the efficacy of partial-thickness debridement without autologous split-thickness skin grafting.

Other objectives were to examine differences in engraftment rates (graft acceptance), debridement efficiency and hemostasis between laser debridement and sharp surgical excision.

IX. Rationale for Use of Swine

The pig was chosen as our model of choice due to the similarities between human and porcine skin.[63-69] The histological characteristics of pig and human skin are comparable, with similarities in epidermal thickness and composition, pelage density, dermal structure, lipid content, and general morphology.[66] In addition, pig skin is antigenically closer to human skin than is rodent skin. Recent EPA guidelines for dermal exposure assessment state that the percutaneous absorption of many compounds in the pig is similar to that found in humans.[67] Dick and Scott[66] found that pig skin permeability to selected lipophilic penetrants was closer to that of human skin than was rat skin. Klain *et al.*[68] concluded that pig skin was a good model for human skin metabolic studies. Meyer *et al.*[69] concluded that among the domestic species, the pig provides the most suitable experimental model for dermatological research on humans. These findings suggest that the pig is a very good research animal to use for

predicting cutaneous effects of xenobiotics in humans. While there is no common laboratory animal species including the pig that generates frank blisters as do humans, sulfur mustard has been noted to induce microblisters in this species.[9]

X. Rationale for Using a Laser to Debride Deep SM Burns

Debridement of cutaneous SM lesions has proven efficacious in the past. Approaches have included powered dermabrasion[70, 71] (swine) and sharp surgical excision[72] (guinea pigs). Rice[70] indicated that dermal abrasion of cutaneous SM-vapor lesions on the backs of swine significantly reduced the time to healing. He proposed that the collagen of the papillary dermis in his pigs was altered by sulfur mustard and no longer functioned normally. Physical removal of the alkylated, sublethally injured epidermis and superficial papillary dermis by dermabrasion resulted in enhanced growth of the proliferating epidermis at the edge of the wound. Rice used sandpaper, applied with a drill under anesthesia, to abrade the lesions at 3-4 days following exposure to sulfur mustard. Lesions not subjected to the abrasion took in excess of eight weeks to re-epithelialize, with secondary infection a significant clinical problem. Complete re-epithelialization occurred in 3-4 weeks with the dermabrasion procedure. Both powered dermabrasion and erbium:yttrium-aluminium-garnet (Erb:YAG) laser ablation have been shown to accelerate the rate of healing of cutaneous Lewisite (vesicant) vapor burns (10 cm^2) in swine.[73] Eldad et al.[74] found that Excimer laser ablation and Debridase chemical debridement were efficacious in improving the healing of partial-thickness nitrogen mustard burns. They did not find sharp surgical tangential excisions to be efficacious in their guinea pig model.

Laser debridement was chosen as a potential treatment for deep SM burns because of prior success in the treatment of less severe SM burns.[75] The healing of small, mild to moderately severe cutaneous SM vapor burns following pulsed CO_2 laser debridement was examined at our laboratory in weanling pigs. Viability, thickness, and organization of the epidermis were all significantly improved by laser debridement into the upper papillary dermis. The debridement removed apoptotic/necrotic and cytologically atypical cells from the SM-damaged epidermis, as well as alkylated basement membrane and dermal components. This likely contributed to a faster rate of wound healing by providing a healthy, functional scaffold over which newly formed keratinocytes could migrate and organize.

The use of pulsed CO_2 lasers in dermatology has been widely described.[76-85] They have been shown to offer precise, micron-depth removal of tissue, and to vaporize tissue rapidly and efficiently with coagulation of blood vessels.[79] As an improvement over conventional continuous wave lasers, pulsed CO_2 lasers were designed to promote rapid healing by minimizing laser-induced residual thermal damage.[77, 78, 80-84] Early CO_2 lasers showed promising results in excision of burn eschar.[86-89] Pulsed CO_2 lasers have been shown to be efficacious in preparing adequate graft beds,[78] and have been shown to be potentially valuable in the conservative ablation of skin lesions.[90] An advantage of these lasers is that they emit short pulses, keeping laser-associated thermal damage to a minimum. This effect was first noticed by research at the Wellman Laboratories of Photomedicine, Massachusetts General Hospital, Boston, MA.[77] However, because of the low average power available from a pulsed laser system, this laser may be

inefficient while debriding burns covering large body surface areas. Continuous wave (cw) lasers can be quite efficient in removing tissue but tend to create significant amounts of thermal damage, sometimes creating more damage than the initial burn being treated. Research at the Wellman Laboratories has shown that the residual thermal damage of cw lasers can be minimized if the laser is rapidly scanned over the surface such that the amount of time the laser spends on any one point mimics a short laser pulse.[91, 92] The TX1A Burn Debridement Laser System, developed at the Wellman Laboratories and used in the current study, accomplishes this goal and provides both high power and efficient laser debridement of burn eschar. This laser has previously been shown to be efficacious in a porcine thermal burn model.[93] Sheridan et al.[94] demonstrated the technical feasibility of laser vaporization of burn eschar in humans using a similar rapidly scanned cw CO_2 laser system.

XI. Hypothesis

Laser debridement followed by autologous split-thickness skin grafting is as efficacious in improving the healing of severe (deep) cutaneous SM burns as is sharp surgical debridement followed by autologous split-thickness grafting (the "Gold Standard"). Either method yields better results than partial-thickness debridement with no grafting, or no treatment at all, with improved cutaneous microcirculation, a functioning barrier, minimal scar tissue formation, minimal wound contraction, and near-normal skin color, hardness, elasticity, and histological appearance by 36 days post-surgery.

MATERIALS AND METHODS

I. Animal Model

Fifteen female Yorkshire Cross pigs (weanlings), *Sus scrofa*, 9-11 kg, were used (Archer Farms, Belcamp, MD). They were quarantined upon arrival for seven days and screened for evidence of disease before use. They were maintained under an animal care and use program accredited by the Association for Assessment and Accreditation of Laboratory Animal Care International (AAALAC International). Animals were supplied tap water *ad libitum* and fed approximately 1250 g of Teklad Mini-Swine Breeder Sterilizable Diet (Harlan Teklad 7037, Harlan Teklad, Madison, WI) twice a day. Animals were housed individually in 4 x 6 ft pens with slatted aluminum floors. The animal holding room was maintained at 21° ± 2°C with 50% ± 10% relative humidity using at least 10 complete air changes per h of 100% conditioned fresh air. Animal rooms were maintained on a 12-h light/dark, full spectrum lighting cycle with no twilight.

II. Sulfur Mustard Exposure

Eighteen to 24 h before agent exposure, each animal was sedated by intramuscular injections of xylazine HCl (Rompun®; 1.0 mL @ 20 mg/mL) and a combination of tiletamine HCl and zolazepam HCl (Telazol®; weighed out in equal parts, reconstituted to 100 mg/mL, and 0.5 mL administered), and hair removed from the ventral body surface. The ventral surface was first clipped with an electric clipper, and then depilated using MAGIC (Carson Products Co., Savannah, GA). The MAGIC powder was mixed with an equal weight of water, and the paste mixture applied. After 10 min the paste was removed with wetted gauze applied with gentle pressure. The treated areas were then gently washed with a soap solution (1:20 ivory liquid) and rinsed with warm water.

Pigs were not fed on the morning of exposure. They were sedated by intramuscular injections of xylazine HCl (Rompun®; 2.2 mg/kg) and equal parts of tiletamine HCl and zolazepam HCl (Telazol®; 6 mg/kg), intubated with an appropriate endotracheal tube, and anesthetized to a surgical plane of anesthesia with 0.4-0.6% isoflurane using an anesthesia machine (Narkovet 2, North American Drager, Telford, PA). Oxygen flow was 0.8 L/min. No antibiotics or anticholinergic agents (e.g., atropine) were administered. Six exposure sites were set up on the ventral surface, 3 sites per side parallel to and approximately 2.5 cm lateral to the teat line and located between the axillary and inguinal areas. A plastic template was used for even spacing and consistent anatomical positioning of the sites among animals. Small dots placed at each corner using a permanent marker delineated each site. In addition to the exposure sites, 2 non-exposure control sites were located along the ventral midline, one located near the axillary area and the other near the inguinal area. Tape assemblies (5 cm x 5 cm) were prepared out of double stick carpet tape and duct tape, with a 2.9-cm diameter hole punched through the center of each tape assembly. A circle of Whatman No. 2 glass microfiber filter paper (3.8 cm in diameter) was sandwiched between the carpet tape and the duct tape, centered over the 2.9 cm hole. A small bead of cyanoacrylate adhesive was placed along the periphery of the hole on the duct tape,

and a rubber O-ring (31 mm inner diameter) glued onto the template. Immediately following pre-exposure clinical evaluations and just prior to intubation, the templates were placed onto the ventral surface of the pig, one centered in each of 6 exposure sites. Templates were placed approximately 6 cm apart on center. No templates were placed on the mid-ventral control sites. Following intubation, the pig was placed in the agent hood in dorsal recumbency, supported by a stainless steel pig sling. A therapeutic heating pad (Gaymar Industries, Inc., Orchard Park, NY), with the circulating water temperature set at 41°C, was placed under the animal during the exposure period to minimize hypothermia. Using an Eppendorf repeating pipettor, 400 ul of undiluted SM was placed on each filter paper. SM was slowly applied in a circular motion, starting at the periphery of the high end (e.g., area closest to the ventral midline) and spiraling inward until the entire filter paper was wetted. A solid polytetrafluoroethylene cap liner (PTFE; 0.38 mm thick, sized for a 28 mm cap) was placed over the filter paper, followed by an appropriately sized rubber stopper to occlude the site and ensure complete contact of the wetted filter paper with the skin. The purpose of the O-ring was to keep the PTFE disk and rubber stopper in place. Successive sites were dosed every 2 min. After all 6 sites were dosed and cap liners and rubber stoppers put in place, rubber tile floats (1 per side) were placed on top of the rubber stoppers to ensure even downward pressure on all sites. Vetrap™ bandaging tape (3M Animal Care Products, St. Paul, MN) was then wrapped around the pig to secure the floats in place. All exposures lasted for 2 h, generating deep dermal/full-thickness burns by 48 h post-exposure. At the end of the exposure period, all paraphernalia was removed and the sites damped dry one at a time (in 2-min intervals). Following removal of the dosing templates, each site was damped for 30 seconds with a double layer of absorbent Masslin sports towel. The sites were then air dried for 15 min before the pig was transferred to the holding cage under an adjacent hood. During this drying time, the pig was weaned off of isoflurane. The endotracheal tube was removed upon signs that the pig had regained consiousness (swallow reflex returned), just prior to being placed into the holding cage. Once in the holding cage, water was provided *ad libitum*. Food was provided in the hood within a few hours of recovery from anesthesia on the day of agent exposure (day 0) and early the following morning (day 1). Buprenorphine (0.01 mg/kg i.m.) was administered immediately after exposure and early the following morning, to alleviate any discomfort.

Each pig was kept under the hood for approximately 24 h. The animals were not placed back into their pens until they tested negative for off-gassing. [Off-gassing is an evaporative process whereby an unbound agent or compound evaporates into the local environment from a surface, cavity, orifice or pore.] Off-gassing was conducted at 24 h post-exposure as follows. (1) The pig was anesthetized by intramuscular injections of xylazine HCl (Rompun®; 0.5 mL) and equal parts of tiletamine HCl and zolazepam HCl (Telazol®; 0.3 mL). (2) The animal was placed on its back on thoracic positioners, and a heavy mil plastic bag wrapped around the lower portion of the pig's body (encompassing all 6 exposure sites) and secured to the pig using double stick tape. (3) Off-gassing into the bag was allowed for 15 min, then the air inside the bag was analyzed for SM by a Minicams™ (O.I. Analytical, CMS Field Products Group, Birmingham, AL, a combination pre-concentrator tube and gas chromatograph with a flame photometric detector), via a connector tube which perforated the plastic bag. The

pigs were deemed safe to move out of the exposure hood and back into their pens when the TWA (time weighted average) was at or below 0.5. This level is conservative; a TWA of 1.0 is the U.S. Department of Defense standard for safety (3 ng/L SM = 1 TWA). Once the animals were placed back into their pens, food and water were provided as described above.

III. Treatments

Four treatment regimens were tested and compared for their ability to improve wound healing of severe, deep dermal/full-thickness SM-induced cutaneous burns. The treatments included (1) full-thickness debridement of the burns with a CO_2 laser followed by autologous split-thickness skin grafting, (2) full-thickness sharp surgical tangential excision followed by skin grafting, the "Gold Standard" used in human deep dermal/full-thickness thermal burns management, (3) mid-dermal laser debridement with no grafting, and (4) mid-dermal sharp surgical tangential excision with no grafting. All surgical procedures were performed under standard sterile conditions in a veterinary surgical suite. The treatments were conducted 48 h post-exposure.

In preparation for surgery, animals were sedated by intramuscular injections of xylazine HCl (Rompun®; 2.2 mg/kg) and equal parts of tiletamine HCl and zolazepam HCl (Telazol®; 6 mg/kg), intubated with an appropriate endotracheal tube, and anesthetized to a surgical plane of anesthesia with 1.5-2.0% isoflurane using an anesthesia machine (1 L/min O_2). They were administered atropine (0.05 mg/kg, i.m.) prior to intubation. One mL of sterile extended action penicillin G (150,000 units of penicillin G benzathine + 150,000 units penicillin G procaine in MicroSuspension™) was injected intramuscularly 30 minutes prior to the debridements (G.C. Hanford Mfg. Co., Syracuse, NY). An intravenous catheter (22 gauge, 2.54 cm) was placed in the carpal region of a front limb through a small incision and secured in place with surgical tape (wound was later closed with 4-0 vicryl suture material). A slow 0.9% sodium chloride drip was instituted, through which multiple bolus injections of pancuronium (0.1 mg/kg) were given to stop respirations during the laser debridements. An ambu bag was used to assist with respiration between passes of the laser. Artificial respiration was continued after the laser debridement procedures until spontaneous respirations occurred.

The laser used in this study was the *TX1A Burn Debridement Laser System* (a prototype system developed by the Wellman Laboratories of Photomedicine, Massachusetts General Hospital, Boston, MA). The TX1A is a computer controlled, raster scanned, carbon dioxide laser system. The continuous wave (cw) laser operates at 10.6 um, is RF excited and water-cooled. The system was designed to meet the application needs while maintaining a user-friendly environment. The surgeon can selectively remove necrotic tissue damaged by thermal, chemical, or other means. The system is comprised of a cw CO_2 laser, computer, viewing screen, power measurement and storage devices, a smoke removal system, optical components for beam delivery, custom designed software and a portable enclosure. The optical system was designed to deliver 150 Watts of laser radiation to the target site with a 1.5mm spot size, a depth of focus of +/- 51mm (Rayleigh distance), and an average irradiance of 8.5 kW/cm^2. (The average power measured before each procedure in this study was 164 W.) The

beam is controlled with an x,y-scanner, and the speed is adjusted to keep the fluence constant at 35 J/cm^2. The current system is designed to accommodate a 20X20 cm field of view. The surgeon's interface includes custom designed software that permits the surgeon to enter patient information, modify operating parameters and define the region of debridement to meet the specific procedure requirements. Connected to the TX1A is a smoke evacuator housing, designed in collaboration with Sandia National Laboratories (Albuquerque, NM). Efficient laser ablation of large amounts of tissue creates significant quantities of smoke. The housing is designed to efficiently remove the high volume of smoke generated by the laser. The TX1A has been approved as being safe for human use by the Department of Biomedical Engineering at Massachusetts General Hospital.

Prior to treatment, all SM-exposed sites were centrally biopsied to verify depth of burn using a 4-mm diameter punch. The biopsy wounds were not closed. In addition, non-exposed skin from the medial surface was also biopsied, and the resulting wound closed with 2-0 silk. Two sets of animals were used. Each set of animals was comprised of six SM-exposed pigs. In the first set, two SM-exposed sites on each animal remained untreated (no debridement or grafting), two sites were debrided at 48 h post-exposure using the TX1A laser followed immediately by autologous split-thickness skin grafting, and two sites underwent "Gold Standard" treatment using a dermatome and scalpel. Deep dermal/full-thickness debridement that did not include the investing muscle fascia was conducted. In the second set of animals, two sites on each SM-exposed animal remained untreated, two sites were debrided to mid-dermis using the TX1A laser, and two sites were debrided to mid-dermis by sharp surgical tangential excision. No skin grafting was conducted in this second set of animals. Treatment sites in both sets of animals were rotated to preclude sensitivity biases due to anterior-posterior location. Three additional animals served as negative controls. For the negative control animals (shams), all sites were sham exposed (no SM). These sham pigs were anesthetized at the same frequency and in the same manner as the SM-exposed pigs and were administered the same pharmaceuticals, but there were no debridements or skin grafting procedures conducted.

For the grafted animals, an average of 10 passes of the TX1A were required to debride down to vitalized tissue, at the dermal-subcutus junction. Five passes were used for the non-grafted group, obtaining a debridement to mid-dermal level. The sharp surgical excisions were conducted to comparative levels using 1-2 passes of a compressed nitrogen gas driven dermatome (Zimmer® Air Dermatome, Cat. No. 8801, Zimmer Inc., Columbia, MD) set at 0.75 mm, using a 5.1-cm wide blade guard, supplemented with a #15 scalpel blade used tangentially when necessary.

Immediately following the debridements and just prior to any skin grafting, tattoo dots were placed around the periphery of each lesion using a tattoo gun (AIMS IIIA Tattoo Identification System, Animal Identification and Marking Systems, Inc., Budd Lake, NJ). Four dots were placed within 5 mm of the border between lesional and normal skin, spaced equidistant around the lesions. In addition, tattoo dots were placed at the corners of each mid-ventral control spot on the SM- and sham-exposed animals. A 3.8-cm diameter filter paper was used as a guide for placing tattoos around the periphery of the sham-exposed sites on the sham animals. These tattoo dots were put in place to characterize wound contraction throughout the healing period.

For the first set of animals, the skin on either the right or left paravertebral region was prepared for split-thickness autograft harvest. A total of approximately 120 ml of an epinephrine-saline solution (0.5mg/500 ml normal saline) was infiltrated into the subcutaneous tissue over an area of approximately 200 cm^2 to promote hemostasis prior to skin graft harvest. Mineral oil was applied to the donor site to ensure smooth graft harvest. The grafts were harvested using the dermatome set at 0.50 mm with a 7.6-cm wide blade guard. The harvested skin was placed on a plastic dermacarrier (Cat. No. 7708-000-10, Zimmer Inc., Columbia, MD) and expanded at 1.5:1 through a mesher (Cat. No. 7701-000-000, Zimmer Inc., Columbia, MD). The grafts were cut to fit the debrided burn wounds with minimal expansion of the mesh. The autografts were attached to the skin using 2-0 silk sutures applied every 0.5 cm around the periphery of the wound. The grafted wounds were then covered with a tie-over stent of petrolatum gauze (Xeroform Petrolatum Nonadhering Dressing, Sherwood Medical, St. Louis, MO) and sterile dry cotton roll, which were anchored tightly by the tails of the silk sutures. The untreated SM-exposed sites were not dressed. For those sites debrided but not grafted, petrolatum gauze was sutured in place, followed by sterile cotton gauze to dress the wounds. Donor sites were dressed with Scarlet Red Ointment Dressing (Sherwood Medical, St. Louis, MO) and layers of sterile gauze that were attached to the wound with surgical staples. The pigs were then dressed in 20-cm wide stockinette with holes cut for the legs, stapled in place. An injection of buprenorphine (0.01 mg/kg i.m.) was given for pain, followed by children's oral acetaminophen (160 mg every morning for 7 days, poured over the animal feed). A single person (Graham) performed the surgeries on all of the animals.

The dressings were left in place for 7 days and then removed. The animals were sedated by intramuscular injections of xylazine HCl (Rompun®; 2.2 mg/kg) and equal parts of tiletamine HCl and zolazepam HCl (Telazol®; 6 mg/kg), and all dressings, sutures and staples removed at that time. Skin graft acceptance (graft take) was evaluated on the first set of animals and quantified using image analysis.

IV. Clinical Evaluations

Clinical observations, a variety of non-invasive bioengineering methods, gross digital photography and clinical pathology were conducted throughout the study. All evaluations were conducted immediately before SM exposure, on day 2 prior to the debridement procedures (except for bioengineering methods), and weekly thereafter until euthanasia, on post-surgery (PS) days 8, 15, 22, 29 and 36. Vancouver scar assessments[95-97] were conducted on PS days 22, 29 and 36 by observers blinded to the treatment.

Animals were weighed, body temperatures were determined, blood samples were drawn, the areas around the lesions were clipped of hair, the lesions were gently cleansed, and digital photographs were taken immediately after anesthesia was induced. Non-invasive bioengineering methods were then conducted in the following order: reflectance colorimetry, evaporimetry, laser Doppler perfusion imaging, and ballistometry. A final body temperature measurement was taken before returning the animals to their individual holding pens.

Reflectance colorimetry was conducted to evaluate changes in skin hue, chroma and lightness, using a Minolta Chroma Meter Model CR-300 (Minolta Corporation, Ramsey, NJ). Laser Doppler perfusion imaging was conducted to evaluate cutaneous blood flow, neovascularization and skin graft viability using a moorLDI^{TM} (Moor Instruments, Inc., Wilmington, DE). Ballistometry was conducted to evaluate mechanical properties of the skin (hardness and elasticity) using a Dia-Stron Torsional Ballistometer System (Dia-Stron Ltd., Broomall, PA). Evaporimetry was conducted to measure transepidermal water loss (TEWL) as a way to evaluate barrier function, using a DermaLab® (Cortex Technology, Hadsund, Denmark).[98, 99] Digital pictures of the gross lesions were taken using a Kodak Professional DCS 315 Digital Camera (Eastman Kodak Company, Rochester, NY). The pictures were transferred to an IBM-compatible personal computer via a PCMCIA card, formatted into BMP images using Adobe® Photoshop® 5.0 (Adobe Systems Inc., San Jose, CA), and analyzed for wound size, shape and contraction using Image-Pro® Plus 4.0 (Media Cybernetics, Silver Spring, MD).

All bioengineering methods were conducted in the same environmentally controlled room under similar conditions of lighting, temperature, humidity, and air flow. Animals were housed in rooms under these same conditions prior to being moved into the laboratory for evaluations, so no acclimatization period was necessary. Room temperature and humidity near the work area was periodically recorded on each evaluation day. Animals were under light anesthesia during the measurements and were placed in dorsal recumbency on top of a therapeutic heating pad on an examination table equipped with positioning pillows. A single person (Graham) made all of the measurements throughout the entire study.

The animals were humanely euthanized and the entire wounds excised for histopathological evaluations on PS day 36. A full necropsy was performed to assess systemic SM toxicities and/or infectious disease processes. The following tissues were collected and placed into 10% neutral buffered formalin: liver, gall bladder, kidney, heart, spleen, pancreas, adrenal glands, urinary bladder, lung, thymus, inguinal lymph node, stomach, small intestine, large intestine, brain and bone marrow.

V. Data Analysis

Reflectance Colorimetry

The three-dimensional $L^*a^*b^*$ color system recommended by the Commission Internationale de l'Eclairage in 1976 was utilized. The Minolta Chroma Meter measured the light reflected by the skin surface over an area of an 8-mm diameter circle. Four replicate readings were taken from the center of each experimental site and averaged. For each SM-exposed pig at each time point, the L*, a^* and b* values of similarly treated sites were averaged, resulting in single L*, a^* and b* values for each treatment regimen and the mid-ventral control sites. For the sham-exposed animals, the 2 sites at each of the 3 anterior-posterior positions were averaged (correlating to the paired positioning of treatment sites on the SM-exposed animals), as were the 2 mid-ventral sites. The net changes in lightness ()L*), red/green balance ()a*), and yellow/blue balance ()b*) were calculated for each animal at each time point by subtracting the mid-ventral control site

averages from the treatment site averages. Overall differences in color ()E^*_{ab}) were calculated using the following formula:

$$\Delta E^*_{ab} = \sqrt{\Delta L^{*2} + \Delta a^{*2} + \Delta b^{*2}}$$

Group mean, standard deviation (n-1) and standard error of the mean (SEM) were calculated for each of the treatment groups at each time point. Results of the no treatment sites from both sets of SM-exposed animals were combined. The mean net changes in the L*, a* and b* chromaticity values, as well as overall color differences, were plotted against time for each treatment group.

Evaporimetry

Dual TEWL probes were utilized in a side-by-side fashion, placed centrally over each experimental site. There were 2 rotations of measurements through each of the sites during each measurement session. Using DermaLab® software, each measurement lasted for 90 seconds, with the data collected during the final 30 seconds averaged to arrive at a single TEWL value. The 2 TEWL measurements made on each site by the dual probes during each rotation were averaged. The averages from each of the 2 rotations were then averaged, yielding a single average TEWL rate for each site. All measurements were conducted under a protective hood (constructed from ½" PVC piping and heavy mil plastic) to minimize the effect of air currents in the laboratory.

For each SM-exposed pig at each time point, the values of similarly treated sites were averaged, resulting in a single TEWL rate for each treatment regimen and the mid-ventral control sites. For the sham-exposed animals, the 2 sites at each of the 3 anterior-posterior positions were averaged, as were the 2 mid-ventral sites.

Group mean, standard deviation (n-1) and standard error of the mean (SEM) were calculated for each of the treatment groups and the mid-ventral control group at each time point. Results of the no treatment sites from both sets of SM-exposed animals were combined. The mean TEWL rates (except for mid-ventral control sites) were plotted against time for each treatment group.

Laser Doppler Perfusion Imaging

Operating parameters on the moorLDI were as follows: DC gain= 0, flux gain= 0, conc gain= 2 (gains were set against normal abdominal pig skin), background threshold= 200, distance= 20 cm, scan size= large, scan speed= 10 ms/pixel, DC image resolution= 256 x 256 pixels, blood flux units (arbitrary units) set to "perfusion." No measurements were made on the mid-ventral control sites. All lesions were scanned separately, with a scan area of 4.4 x 5.9 cm (112 x 151 pixel resolution) used before SM exposure, a scan area of 5.7 x 6.8 cm (146 x 174 pixel resolution) used on PS days 8-29, and a scan area of 6.3 x 7.9 cm (162 x 201 pixel resolution) used on PS day 36. Blood flux levels at each of the pixel points within a defined region of interest (ROI) measuring 0.60 cm^2 were measured and averaged, using built-in image analysis software.

Each site was analyzed at each time point as follows. Five ROIs were measured at different spots within the lesion, each generating an average blood flux value. Those 5 values were averaged, arriving at a single flux value (B) within the burn. Similarly, three ROIs were measured at different spots in normal perilesional skin nearest the teat line and averaged, yielding a single flux value (N) for normal skin. A B/N ratio was calculated.

For each SM-exposed pig at each time point, the B/N ratios of similarly treated sites were averaged, resulting in single B/N ratio for each treatment regimen. For the sham-exposed animals, the 2 sites at each of the 3 anterior-posterior positions were averaged.

Group mean, standard deviation (n-1) and standard error of the mean (SEM) were calculated for each of the treatment groups at each time point. Results of the no treatment sites from both sets of SM-exposed animals were combined. The mean burn:normal blood flux ratios were plotted against time for each treatment group.

Ballistometry

The parameters used in this study, as measured by the torsional ballistometer, were indentation (skin hardness) and alpha value (skin elasticity). For the initial indentation measurement (mm), the larger the value, the softer the tissue. This parameter is not related to elasticity (e.g., soft materials can be either elastic or inelastic). Alpha values, representing elasticity, were determined by fitting an exponential decay function to the peaks on the bounce profile generated by oscillations of the probe that were generated following initial contact with the skin. A large alpha value indicated rapid damping (rapid energy loss) thus low elasticity.

The vibrating tip of the ballistometer probe, a spherical ruby ball 2 mm in diameter, was placed over the center of each experimental site. It occasionally needed to be moved off-center to trigger the probe. During each measurement session, 5 rotations of readings through each of the sites were taken, and the 5 individual values for each site averaged. For each SM-exposed pig at each time point, the values of similarly treated sites were averaged, resulting in single indentation and alpha values for each treatment regimen and the mid-ventral control sites. For the sham-exposed animals, the 2 sites at each of the 3 anterior-posterior positions were averaged, as were the 2 mid-ventral sites.

For the SM-exposed animals, group mean, standard deviation (n-1) and standard error of the mean (SEM) were calculated for each of the treatment groups and the mid-ventral control group at each time point. Burn eschar on the non-treated sites would frequently either not trigger the ballistometer or yield a poor bounce profile. As a consequence, the size of the groups for statistics of the non-treated groups was smaller than the treated groups on PS days 15-29. Results of the no treatment sites from both sets of SM-exposed animals were combined.

For the sham-exposed animals, the mean, SD (n-1) and SEM were calculated from the three sets of experimental sites, and separately from the mid-ventral control sites.

The mean indentation and alpha values (except for mid-ventral control sites) were plotted against time for each treatment group.

Image Analysis

Digital photographs of the lesions were used to measure wound size, shape and contraction by image analysis. Prior to making measurements, calibrations were determined via software using the ruler that had been placed in each photograph near the lesions.

The wound size and shape parameters used in this study were area, aspect ratio and roundness. All measurements were made using Image-Pro® Plus 4.0 (Media Cybernetics, Silver Spring, MD) software on an IBM-compatible personal computer. Size and shape measurements were conducted only on SM-exposed sites. Interactively encircling the lesions and allowing the software to automatically fill in the enclosed areas created binary images of the lesions that were used to make the measurements. The parameters used to assess wound contraction were area and percent total body surface area (TBSA) of binary images created by interactively joining the tattoo dots placed at the periphery of each lesion during surgery. Measurements to assess wound contraction were conducted on both SM-exposed and sham-exposed sites. TBSA was calculated using Meeh's formula[100-102] as follows:

$$A = kW^{2/3}$$

where A = surface area in cm^2
W = body weight in gm
k = 9.0 for swine[102]

For each SM-exposed pig at each time point, the values of similarly treated sites were averaged, resulting in single wound area, wound aspect ratio, wound roundness, wound contraction area and % TBSA values for each of the treatments. For the sham-exposed animals, wound contraction area and % TBSA measurements from the 2 sites at each of the 3 anterior-posterior positions were averaged.

Areas of any graft rejection were measured on PS08, with the affected percent of the whole lesion calculated. Additionally, the percentage of each lesion occupied by an ulcerated area on PS29 and 36 was calculated following morphometric evaluation, and plotted for each treatment group.

For the SM-exposed animals, group means, standard deviations (n-1) and standard errors of the means (SEM) were calculated for each of the treatment groups at each time point. Results of the no treatment sites from both sets of SM-exposed animals were combined. For the sham control animals, the means, SDs and SEMs were calculated from the three sets of experimental sites.

The means of each morphometric parameter were plotted against time for each treatment group.

Pathology

The full-thickness biopsies that were collected during surgery at 48 h post-exposure, just prior to the debridement procedures, were placed in 10% neutral buffered formalin, processed through paraffin, and stained with hematoxylin and eosin (H&E).

The following parameters were graded on a scale of 0-3, with 0 being normal, 1 being mild in severity, 2 being moderate, and 3 being severe: muscle necrosis, adipose necrosis, and inflammatory cell infiltration. The following parameters were noted as present or absent: full-thickness epidermal necrosis, microblisters (separation at the dermal-epidermal junction), blood vessel congestion, dermal hemorrhage, dermal coagulation, edema in dermis, edema in adipose, edema in muscle, follicular necrosis, sweat gland necrosis, and sweat gland epithelial cell swelling. Dermal coagulation depth was noted as superficial, mid-dermal or deep dermal. An incidence summary table was prepared, to verify depth of burn as being deep-dermal/full-thickness.

Large tissue sections of each experimental site were collected at necropsy on PS day 36 and prepared in the same manner as were the biopsies. Serial sections were prepared from each paraffin block, with the following stains performed: H&E for routine histopatholgy, Masson's trichrome for collagen morphometry, and Movat's pentachrome for light microscopic evaluation of elastic fibers. Each H&E section was graded as follows. The extent of dermal collagen invading into underlying panniculus carnosa was graded on a scale of 0-3, as described above. The following parameters were noted as present or absent: full reepithelialization, marked epidermal hyperplasia, marked hyperkeratosis, marked parakeratosis, microgranulomas, rete ridge pattern, and hair follicles. Microgranulomas were further noted as being focal or multifocal. Each Movat's pentachrome section was evaluated as follows. Elastic fibers in both the papillary dermis and reticular dermis were noted as being present or absent. When present, general orientation of the fibers was noted (horizontal or vertical to the skin surface, or disorganized), as was thickness (thick, or thin wisps). Thickness of the elastic fibers in the hypodermis was also noted. Each Masson's trichrome-stained section was evaluated on a color image processing and analysis system (Quantimet 600, Leica Inc., Deerfield, IL). Average measurements were made within a 6-mm wide image frame of the fraction of space between the dermal-epidermal junction and underlying muscle that was occupied by collagen, and the fraction of collagen that was new (vs. mature). Mean fractions were plotted for each of the treatment groups for both parameters.

The other tissues collected at necropsy were evaluated for signs of systemic SM toxicity and/or infectious disease processes. Supplemental special stains (Brown-Hopps, Acid-Fast, and Grocott's Methenamine Silver Nitrate method) were performed as needed. An incidence summary table of findings was prepared.

All histopathological evaluations were conducted in a blinded fashion. The primary author (Graham) performed the evaluations of the skin sections. A veterinary pathologist performed evaluations of the other tissues. A board-certified veterinary pathologist reviewed all evaluations in a blinded fashion.

Ten-ml blood samples were collected at each experimental time point and distributed into EDTA tubes and serum separation tubes. Hematology parameters were measured on a Cell-Dyn® 3500 (Abbott Diagnostics, Abbott Park, IL). Clinical chemistry parameters were measured on an Hitachi 704 Automatic Analyzer (Roche Diagnostics Corporation, Indianapolis, IN), and isoenzymes were conducted using Paragon® Electrophoresis Systems and evaluated on an Appraise™ Densitometer (Beckman Instruments Inc., Brea, California). The following clinical pathology parameters were measured: complete blood cell count (CBC), differential white cell counts, hematocrit,

hemoglobin, mean cell volume (RBC), mean cell hemoglobin, mean cell hemoglobin concentration, electrolytes (chloride, sodium, potassium, calcium, phosphorus), blood urea nitrogen (BUN), creatinine, BUN:creatinine ratio, glucose (hexokinase), alanine transaminase (ALT), aspartate transaminase (AST), alkaline phosphatase (ALP), lactate dehydrogenase (LDH), creatine phosphokinase (CPK), amylase, total protein (TP), albumin, globulin and albumin:globulin ratio. Isoenzymes of LDH and CPK were measured on serum samples using classic electrophoretic techniques.

Statistics

For each bioengineering parameter measured, two sample t-tests were performed to ascertain whether there were any differences between the no treatment sites from the 6 SM-exposed animals in the grafting group and the no treatment sites from the 6 SM-exposed animals in the no-grafting group. Only a small number of differences were found, generally attributable to single outliers or measurements that were numerically but not biologically/functionally different. The two no-treatment groups were thus combined in graphical representations of study results. Statements made in the *Results* section below are based upon statistical evaluations that utilized the separate sets of data and were not based upon appearance of the plotted means of the combined no treatment groups.

Two-way repeated measures analysis of variance (ANOVA) tests were performed for each bioengineering and image analysis parameter to look for interactions between grafting procedure (graft/no graft) and method of debridement (sharp surgical/laser). When no interactions were found, the p values of the graft/no graft and sharp/laser comparisons were noted. When interactions were found, (1) two sample t-tests were performed on sharp/grafted vs. sharp/not grafted and on laser/grafted vs. laser/not grafted, and (2) paired t-tests were performed on sharp vs. laser debridement in both the grafted and non-grafted groups.

One-way repeated measures ANOVAs were run on all bioengineering and image analysis data at each time point for both groups of animals (grafted and non-grafted) to ascertain significant differences among the treatment groups. The nonparametric Friedman repeated measures analysis of variance on ranks test was run in those rare instances where normality tests failed. [The Kolmogorov-Smirnov test with Lilliefors' correction was used to test data for normality.] Tukey multiple comparison tests were used to isolate any differences noted among the treatment groups. One-way repeated measures ANOVAs and Tukey multiple comparison tests were run on wound contraction data for each treatment group to examine differences in % TBSA over time.

Comparisons of the sham-exposed animals with the 5 treatment groups were made using a Bonferroni adjusted t-test. Because these were multiple comparisons to the same group, sham-exposed animals, the Bonferroni adjusted t-test was used to control the experiment-wise error rate at alpha = 0.05. The Bonferroni adjusted t-test is based on the Bonferroni inequality, which states that if k statistical tests are performed at the alpha level, the likelihood of observing a test statistic exceeding that alpha level at least once when there is no effect is no greater than k times alpha. The Bonferroni adjusted t-test adjusts for these multiple comparisons to one group by dividing the alpha level by the number of comparisons to be made and therefore maintains the

experiment-wise error rate equal to alpha. For those few instances where the data was not normally distributed or failed the equal variance test (Levene median test), a Mann-Whitney rank sum test was performed.

One-way ANOVAs were conducted on the clinical pathology data, looking for differences among three groups of animals (sham-exposed, SM-exposed and grafted, and SM-exposed and not grafted).

SigmaStat for Windows Version 2.03 (SPSS Inc., Chicago, IL) was used to conduct all statistical evaluations. Statistical significance was defined as $p<0.05$.

RESULTS

I. General Clinical Observations

The average weight of the SM-exposed and grafted animals at the beginning of the experiment was 10.4 kg (SD 1.0 kg) and at the end of the experiment was 27.2 kg (SD 1.8 kg). For the SM-exposed and no-graft animals, the respective weights were 10.6 kg (SD 0.6 kg) and 30.1 kg (SD 2.0 kg). For the sham-exposed animals, the respective weights were 9.8 kg (SD 0.3 kg) and 28.9 kg (SD 2.2 kg). The mean elapsed time under anesthesia during the bioengineering measurements was 1:57 (SD 0:08) for the sham-exposed animals, 2:05 (SD 0:10) for the grafted animals, and 2:05 (SD 0:11) for the no-graft animals. On average, the animals lost 2.86°F (1.59°C), 3.64°F (2.02°C), and 2.32°F (1.29°C), respectively, over that time frame. The average room temperature in the environmentally controlled laboratory during the experiment was 23.2°C (SD 0.4°C) with 41.9% relative humidity (SD 8.7%).

All animals were in good general health during the course of the experiment. No elevated body temperatures were noted. No overt ocular or respiratory problems were noted. The pigs had occasional soft or runny stools, likely caused by excessive dust in the feed. One animal was noted as having a small umbilical hernia with an encapsulated abscess. The skin was normal except for occasional scratches and small areas of dermatitis located on dorsal surfaces.

Hair growth was noted throughout the experiment on the sham-exposed and mid-ventral control sites on the sham animals, as well as on the control sites on the SM-exposed animals. At no time was any hair growth noted in the no treatment sites. Generally, hair growth was not noted on the treated SM-exposed lesions. When hair growth was noted [1 lesion on post-surgery (PS) day 22, 7 lesions on PS day 29, and 11 lesions on PS day 36], it was generally sparse and confined to the periphery of the lesion. This general lack of hair growth is a supportive sign that a deep dermal to full-thickness SM burn was generated. Histopathological evaluation of biopsies taken immediately prior to surgery confirmed this diagnosis (see *Histopathology* section below).

For the SM-exposed sites that were not treated, the burn eschar fell off between PS days 15 and 22 for 20.8% of the lesions, on PS days 22 to 29 for 62.5% of the lesions, and on PS days 29-36 for 16.7% of the lesions. Generally, burn eschar was soft and pliable on PS day 8, semi-hard to hard on PS day 15, and hard with upward cupping on PS days 22 and 29. No burn eschar was noted on any control, sham-exposed, debrided/grafted or debrided/not grafted site.

Signs of an acute inflammatory response (moderate edema) at the burn sites were generally noted only within 48 h of agent exposure, prior to treatment. In a previous study characterizing these lesions in 6 weanling swine using 20 MHz ultrasonography, macroscopic edema accumulation was noted to maximize between 12 and 18 h after SM exposure, and began to subside by 24-48 h. Mean skin thickness at 48 h post-exposure was 4.24 mm (SD 0.56 mm) as determined by high frequency ultrasound (unpublished results). These data were taken into account when planning on the number of required passes of the laser or dermatome used in the mid-dermal debridement (with no grafting) groups.

Observation of gross necrosis of the tissue, as evidenced by white patches seen through the surface of the lesions, was limited to 48 h post-exposure, immediately before surgery. All SM-exposed lesions showed these patchy white areas covering 100% of the sites. No visible signs of necrosis were seen on the control or sham-exposed sites.

There were very few overt signs of infection (suppuration). On PS day 8, one sharp/graft site, one TX1A/graft site, and three sharp/no graft sites showed small areas of suppurative eruptions. On PS day 15, two of the sharp/no graft sites showed eruptions. On PS day 22, one TX1A/graft site showed a single 2 mm diameter eruption along the suture line. At no time were suppurative eruptions noted in the TX1A/no graft group. No cultures were taken of the sites to identify existing pathogens or verify colonization/infection.

For both the TX1A/graft group and the sharp/graft group, 3 sites out of 12 showed signs of focal graft rejection on PS day 8. For the TX1A/graft group, the mean percent of rejected area, as determined by image analysis, was 10.6 (SD 2.2). For the sharp/graft group, the mean percent of rejected area was 6.0 (SD 2.5). These small areas healed by secondary intention and often presented as a thin purplish line on the surface of the healed lesion by PS days 22 to 36. The overall graph acceptance rate appeared to be similar between the sharp surgical debrided and laser debrided groups.

II. Bioengineering Methods

Tables 1-4 show the results of all statistical evaluations.

In general, there were few interactions between grafting procedure (graft/no graft) and method of debridement (sharp surgical/TX1A laser), indicating that for the characteristics measured by the bioengineering methods the effect of different levels of grafting did not depend upon what type of debridement was conducted (Table 1). There were no interactions for erythema or skin elasticity throughout the study. Analyses of the other bioengineering parameters indicated a few interactions toward the end of the study, indicating that at selected times the effect of different levels of grafting depended upon what type of debridement was conducted.

Reflectance Colorimetry

For the reflective colorimetry parameters of lightness ()L*), red/green balance ()a*), yellow/blue balance ()b*) and overall differences in color ()E^*_{ab}), all comparisons were relative to values for the mid-ventral control sites on each animal.

Differences in lightness can be seen in Fig. 2. The no-graft groups were darker than the grafted groups on PS days 8-36. In the no-graft groups, differences were seen on PS days 8 and 15 between both the sharp and TX1A debrided sites and the non-treated (NT) sites, and between the TX1A sites and NT sites on PS day 29. In the grafted groups, differences were seen between the sharp and NT sites on PS day 8, and between both the sharp and TX1A sites and NT sites on PS days 15-36. Significant differences were noted between the sham-exposed sites and all other SM-exposed sites on PS days 8-36.

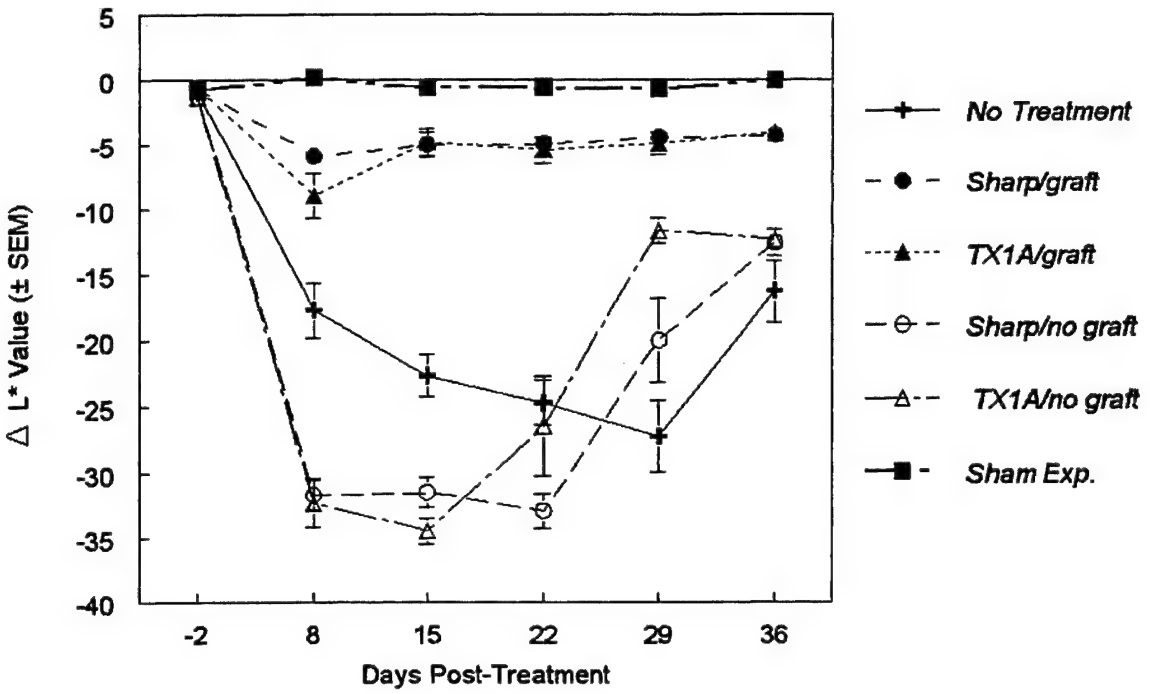

Fig. 2. Mean net change in lightness (L* chromaticity value) vs. time. The no graft sites were darker than the grafted sites throughout the post-surgical observation period. The laser debrided + grafted sites and sharply excised + grafted sites behaved similarly.

Differences in erythema can be seen in Fig. 3. The no-graft sites were redder than the grafted sites on PS days 8, 22 and 29. In the no-graft groups, differences were seen on PS days 8 and 15 between both the sharp and TX1A debrided sites and the NT sites, and between the TX1A sites and NT sites on PS day 29. In the grafted groups, differences were seen between the TX1A debrided and NT sites on PS day 8, and between both the sharp and TX1A debrided sites and NT sites on PS days 15 and 22. Significant differences were noted between the sham-exposed sites and the sharp/graft group only on PS 29, and were never noted between the TX1A/graft and sham sites. Differences were noted at a variety of post-surgical time points between the sham sites and the remaining groups.

Differences in yellow/blue balance can be seen in Fig. 4. The no-graft sites were less blue than the grafted sites on PS days 8-22. This increased yellow component is likely due to the brownish exudative covering on the no-graft sites noted during this time

period. In the no-graft groups, differences were seen on PS day 29 between TX1A debrided sites and the NT sites. In the grafted groups, differences were seen between both the sharp and TX1A debrided sites and NT sites on PS days 8-29, and between the sharp sites and NT sites on PS day 36. Significant differences were noted between the sham-exposed sites and the SM-exposed sites throughout most of the post-surgical observation period.

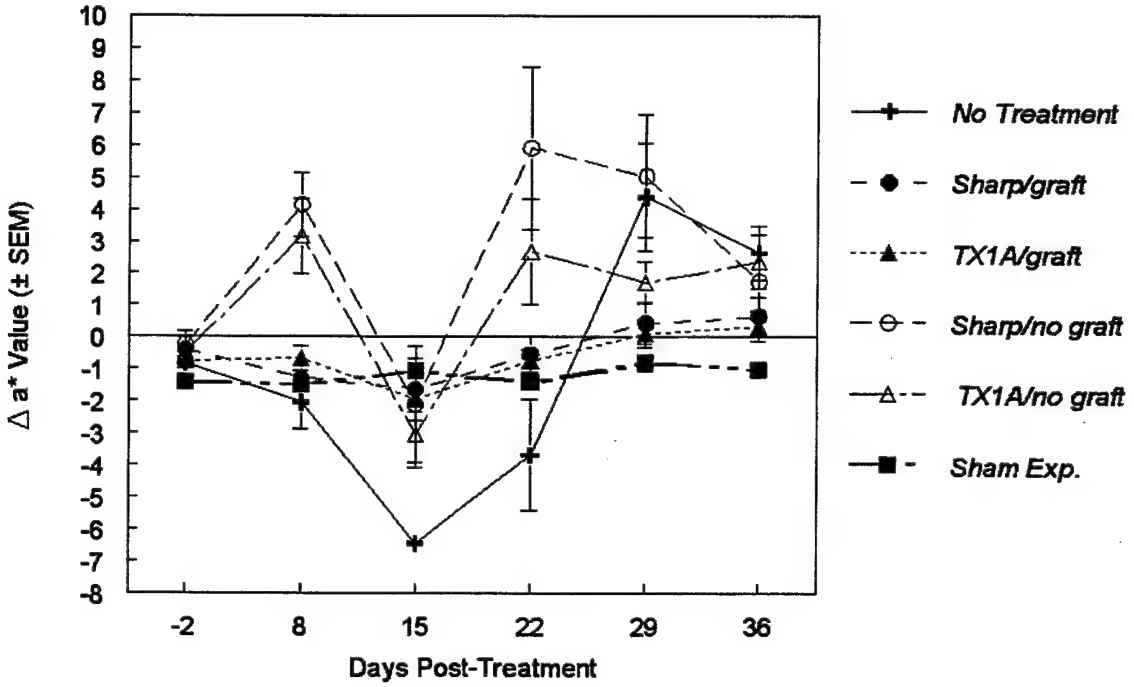

Fig. 3. Mean net change in red/green balance (a* chromaticity value) vs. time. The no-graft sites were redder than the grafted sites through most of the post-surgical observation period. The laser debrided + grafted sites and sharply excised + grafted sites behaved similarly.

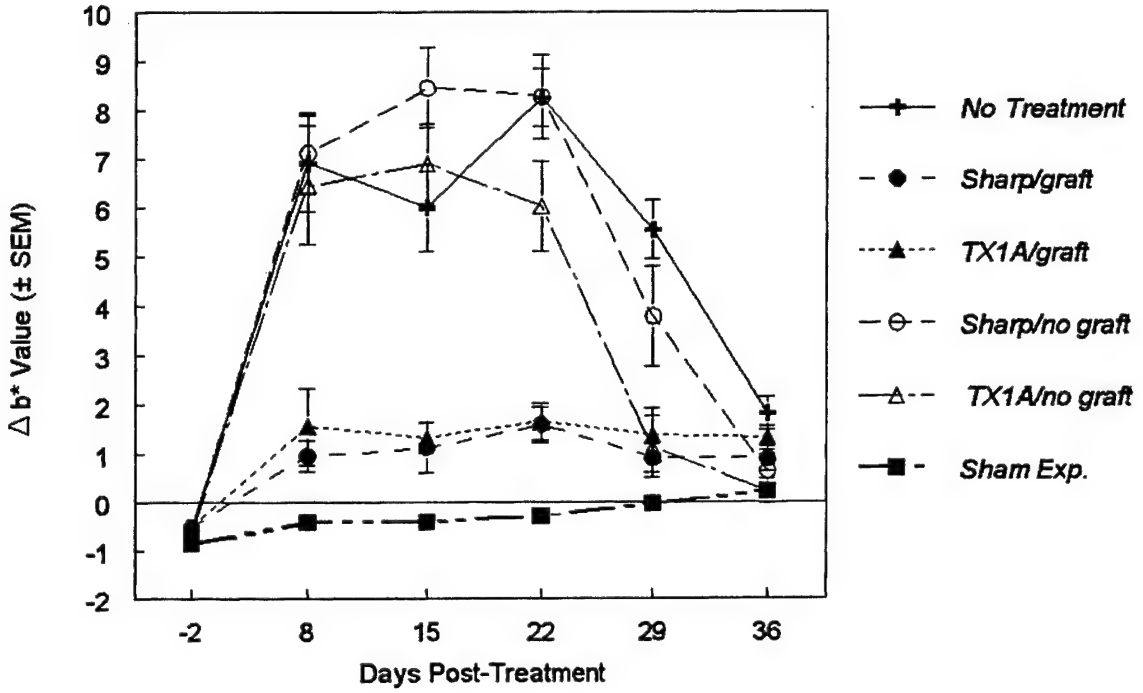

Fig. 4. Mean net change in yellow/blue balance (b* chromaticity value) vs. time. The no graft sites were less blue than the grafted sites on post-surgical days 8-22. This increased yellow component was likely due to the brownish exudative covering on the non-grafted sites during this time. The laser debrided + grafted sites and sharply excised + grafted sites behaved similarly.

Overall color differences can be seen in Fig. 5. The no-graft sites showed greater color change than the grafted sites on PS days 8-36. In the no-graft groups, differences were seen on PS days 8 and 15 between both the sharp and TX1A debrided sites and the NT sites, and between the TX1A and NT sites on PS day 29. In the grafted groups, differences were seen between both the sharp and TX1A debrided sites and NT sites on PS days 8-36. Significant differences were noted between the sham-exposed sites and the SM-exposed sites throughout the entire post-surgical observation period.

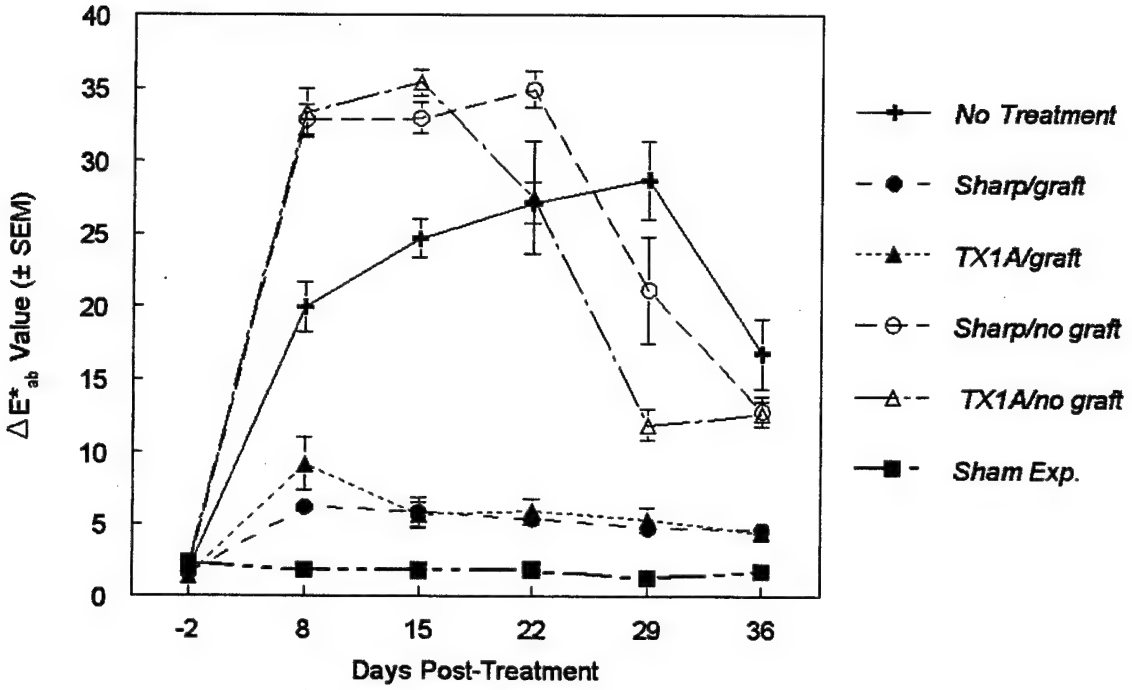

Fig. 5. Mean net change in overall color vs. time. Overall, the no-graft sites showed greater color change than the grafted sites throughout the post-surgical observation period. The laser debrided + grafted sites and sharply excised + grafted sites behaved similarly.

Evaporimetry

Transepidermal water loss (TEWL) rates are plotted in Fig. 6. The no-graft sites had considerably higher TEWL rates than the grafted sites on PS days 8-36. In the no-graft groups, no differences were seen on PS days 8-36 between both the sharp and TX1A debrided sites and the NT sites, or between the sharp sites and TX1A sites. Differences were noted, however, between these SM-exposed sites and the mid-ventral control sites. In the grafted groups, differences were seen between both the sharp and TX1A debrided sites and NT sites on PS days 8-29. While a one-way repeated measures ANOVA showed significant differences between both the sharp and TX1A sites and the NT sites on PS day 36, the Friedman statistic, run because of a failed normality test, found significant differences ($p<0.001$) that pinpointed only a difference

between mid-ventral control sites and the NT sites. Some differences were noted between these SM-exposed sites and mid-ventral control sites throughout the study. Significant differences were noted between the sham-exposed sites and the no-graft or NT sites throughout the post-surgical observation period. Significant differences were noted between the sharp/graft group and the sham group only on PS day 8. Significant differences were found between the TX1A/graft sites and the sham sites on PS days 8, 22, 29 and 36. While these latter differences were of statistical significance, they were likely of no biological significance on PS days 22-36 (e.g., they did not represent any functional difference based upon the relatively low TEWL rates noted at those time points).

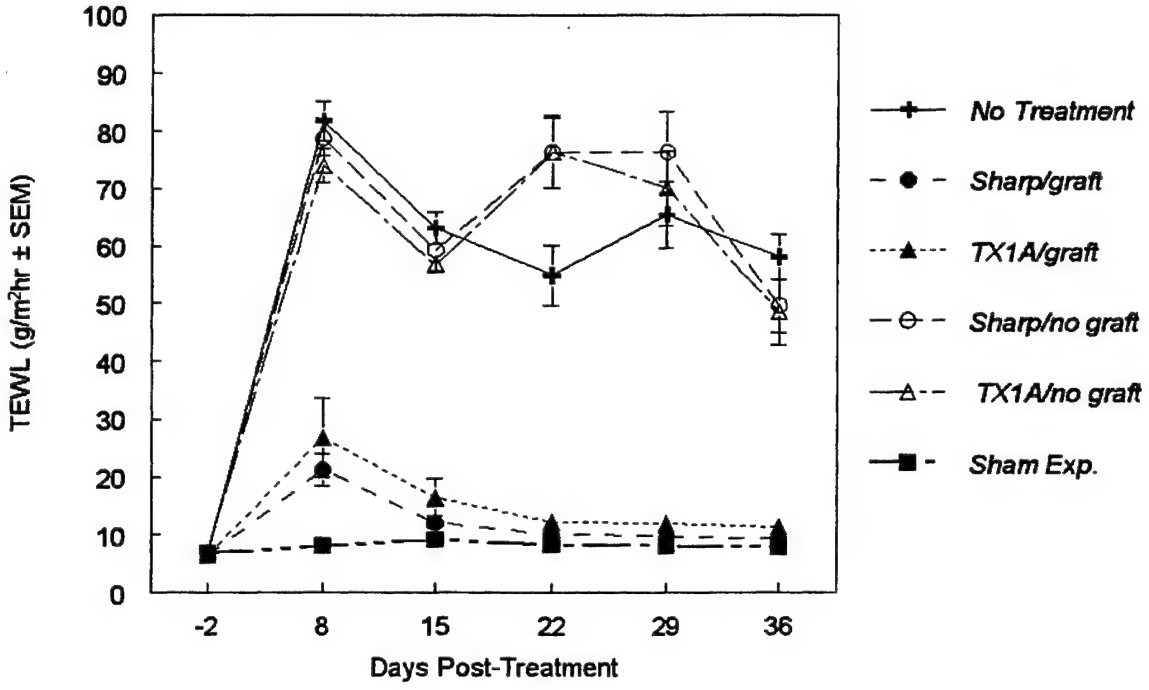

Fig. 6. Transepidermal water loss (TEWL) rates vs. time. The no graft sites had considerably higher transepidermal water loss rates than the grafted sites throughout the 36-day post-surgical observation period. The laser debrided + grafted sites and sharply excised + grafted sites behaved similarly. Barrier function of these two groups approached normal levels within 15 days of treatment.

Laser Doppler Perfusion Imaging

Blood flux levels in the cutaneous microcirculation are plotted in Fig. 7. The no-graft sites had lower B:N ratios (poorer perfusion rates) than the grafted sites on PS day 8, but higher ratios on PS days 22 and 29. In the no-graft groups, differences were seen on PS day 8 between both the sharp and TX1A debrided sites and the NT sites, and between the sharp and TX1A sites on PS day 29. Graphically using combined NT groups, it appeared that there was no difference between the TX1A/no-graft sites and the NT sites on PS day 29. However, a one way repeated measures ANOVA using only the NT sites from the no-graft group indicated that there was a significant difference at that time point. In the grafted groups, differences were seen between both the sharp and TX1A sites and NT sites on PS days 8-22. Significant differences were noted between the sham-exposed sites and other groups throughout most of the experiment. Generally, all SM-exposed sites remained at about 50-60% of normal blood flux. It should be noted that the measurements made on the NT sites between PS days 15 and 29 may not be a true reflection of tissue perfusion, since penetration of the laser beam through hardened eschar is attenuated. This phenomenon was clearly seen in those cases where eschar had only partially fallen off. In those instances, much higher perfusion rates were noted in the areas not covered by eschar compared with those areas covered by eschar.

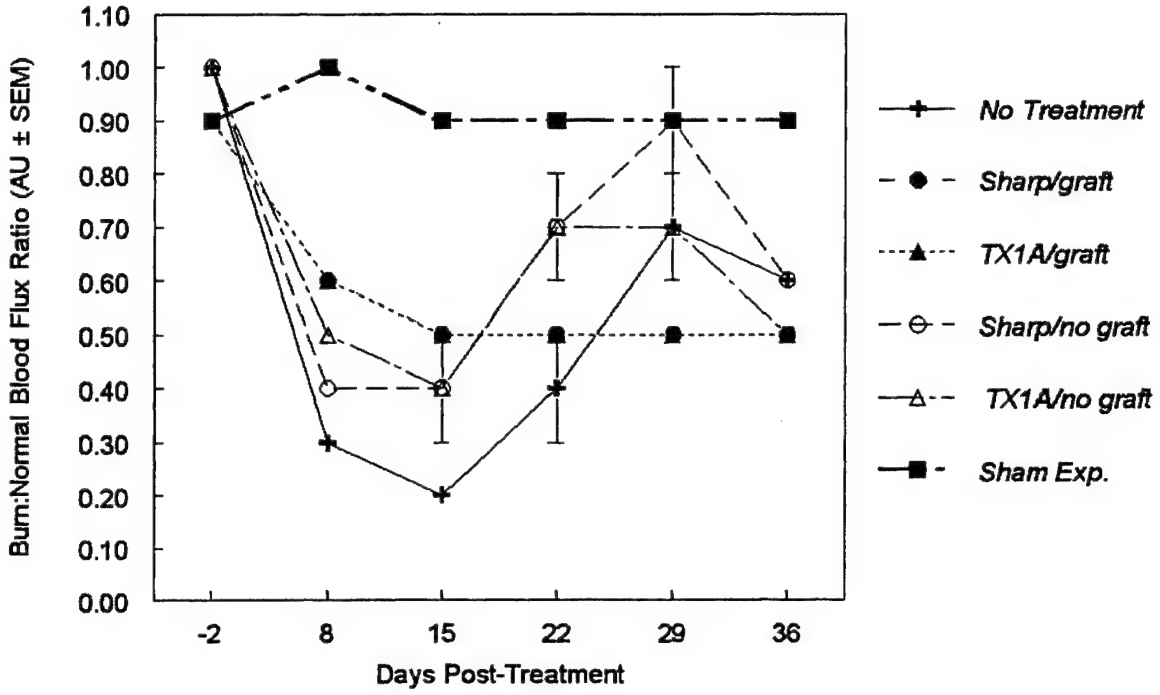

Fig. 7. Laser Doppler perfusion imaging, mean burn:normal blood flux ratios vs. time. Generally, all sulfur mustard-exposed sites remained at about 50-60% of normal blood flux, indicating that while the tissues were still being adequately perfused to ensure viability, there were larger and/or more blood vessels in unexposed skin. This likely represents a loss of patency of larger blood vessels following liquid SM insult, with subsequent neovascularization providing smaller vessels.

Ballistometry

The hardened eschar on the NT sites would frequently fail to trigger the ballistometer, making statistical comparisons with the NT group difficult to attain at times, as noted below.

Skin hardness is plotted in Fig. 8. The no-graft sites showed increased hardness over the grafted sites before exposure and on PS days 8-36, although the differences were smaller before exposure. The statistical differences noted before exposure were likely of no biological significance due to the narrow range of measurements and would likely not have appeared given a larger group of animals. In the no-graft groups, no

differences were seen between both the sharp and TX1A debrided sites and the NT sites (no comparisons with the NT group could be made on PS day 15), or between the sharp sites and TX1A sites. Differences were noted, however, between these SM-exposed sites and the softer mid-ventral controls throughout the post-surgical observation period. In the grafted groups, differences were seen between the sharp sites and NT sites on PS day 8, and between both the sharp and TX1A sites and NT sites on PS day 36 (no comparisons with the NT group could be made on PS days 15-29). Differences were again noted between these SM-exposed sites and the softer mid-ventral control sites throughout the post-surgical observation period. Significant differences were noted between the sham-exposed sites and the other sites throughout most of post-surgical observation period.

Skin elasticity is plotted in Fig. 9. The no-graft sites showed decreased elasticity over the grafted sites throughout the post-surgical observation period. In the no-graft groups, differences were seen between the sharply debrided sites and the NT sites on PS day 8 (no comparisons with the NT group could be made on PS day 15), and between the sharp sites and TX1A sites on PS day 29 and 36. A difference between sharp sites and TX1A sites before SM-exposure was also noted using the Friedman statistic, run because of a failed normality test, although this difference was likely of no biological/functional significance. Mid-ventral control sites were more elastic than the SM-exposed sites throughout the post-surgical observation period. In the grafted groups, differences were seen between both the sharp and TX1A sites and NT sites on PS days 8 and 36 (no comparisons with the NT group could be made on PS days 15-29). Differences were occasionally noted between these SM-exposed sites and the mid-ventral control sites. No significant differences in elasticity were noted between the sham-exposed sites and the grafted sites throughout the experiment. Differences were noted, however, between the sham sites and both the NT and no-graft sites throughout the post-surgery observation period.

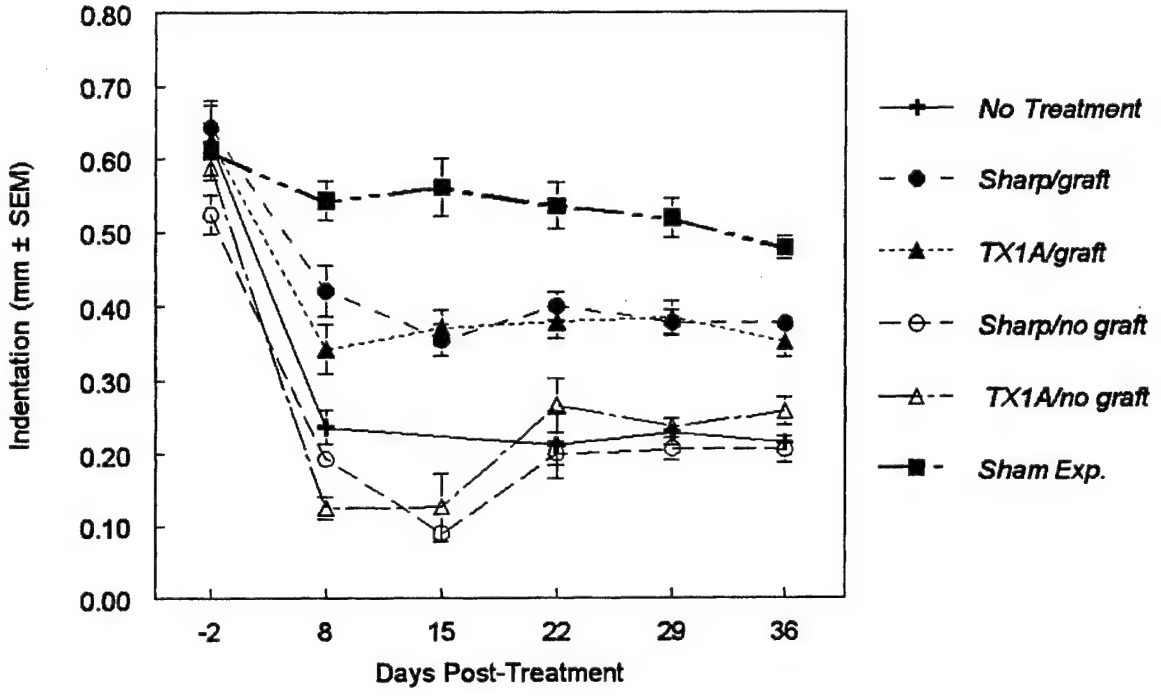

Fig. 8. Mean indentation (hardness) vs. time. The no-graft sites showed increased hardness over the grafted sites, which were harder than the sham sites. The laser debrided + grafted sites and sharply excised + grafted sites behaved similarly.

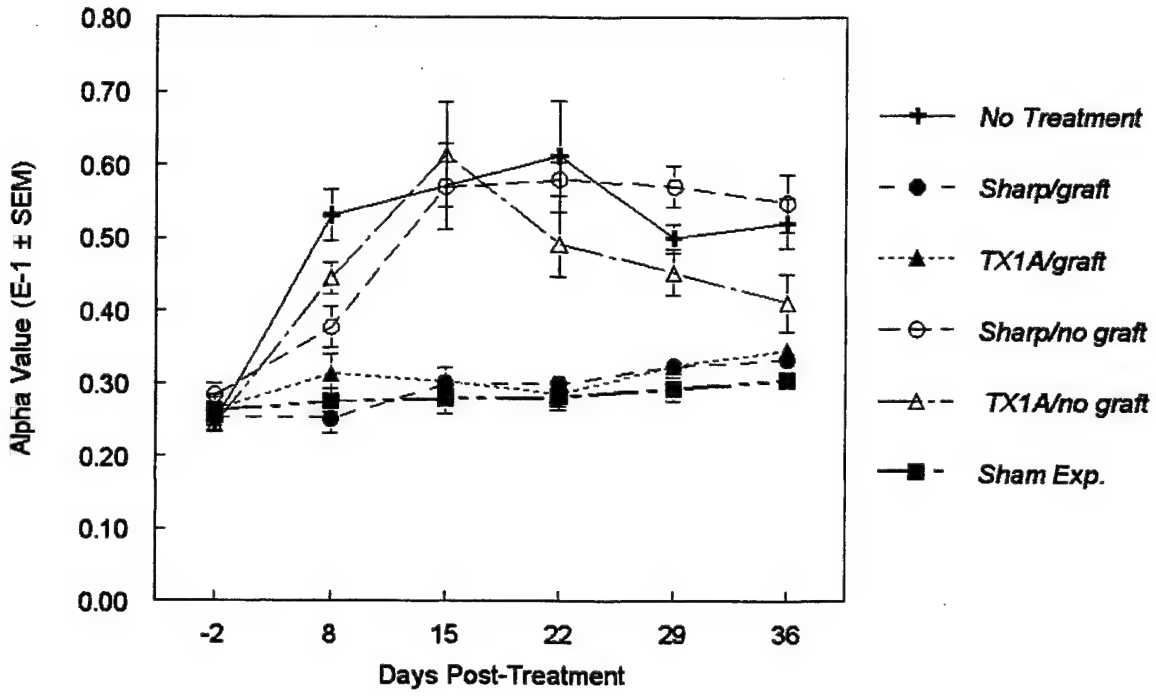

Fig. 9. Mean alpha value (elasticity) vs. time. The no-graft sites had decreased elasticity compared with the grafted sites. No significant differences in elasticity were noted between the sham-exposed sites and the grafted sites throughout the experiment.

III. Image Analysis for Wound Size, Shape, and Contraction

In general, there were interactions between grafting procedure (graft/no graft) and method of debridement (sharp surgical/TX1A laser), indicating that the effect of different levels of grafting on wound size and shape depended upon what type of debridement was conducted (Table 1). There was an interaction noted for wound contraction only on PS 29.

The debrided/grafted lesions grew in size as the animals grew, whereas the NT and no-graft sites did not (Fig. 10). The no-graft sites were significantly smaller than the grafted sites following surgery. In the no-graft groups, differences were seen between TX1A debrided sites and the NT sites on PS days 15-36, and between the sharp sites and TX1A sites on PS days 8-36. The TX1A debrided sites remained larger than the sharply excised sites at the end of the study. In the grafted groups, differences were

seen between both the sharp and TX1A sites and NT sites on PS days 8-36. Since there were no lesions on sham-exposed sites, no Bonferroni adjusted t-tests comparing sham sites with other sites were performed.

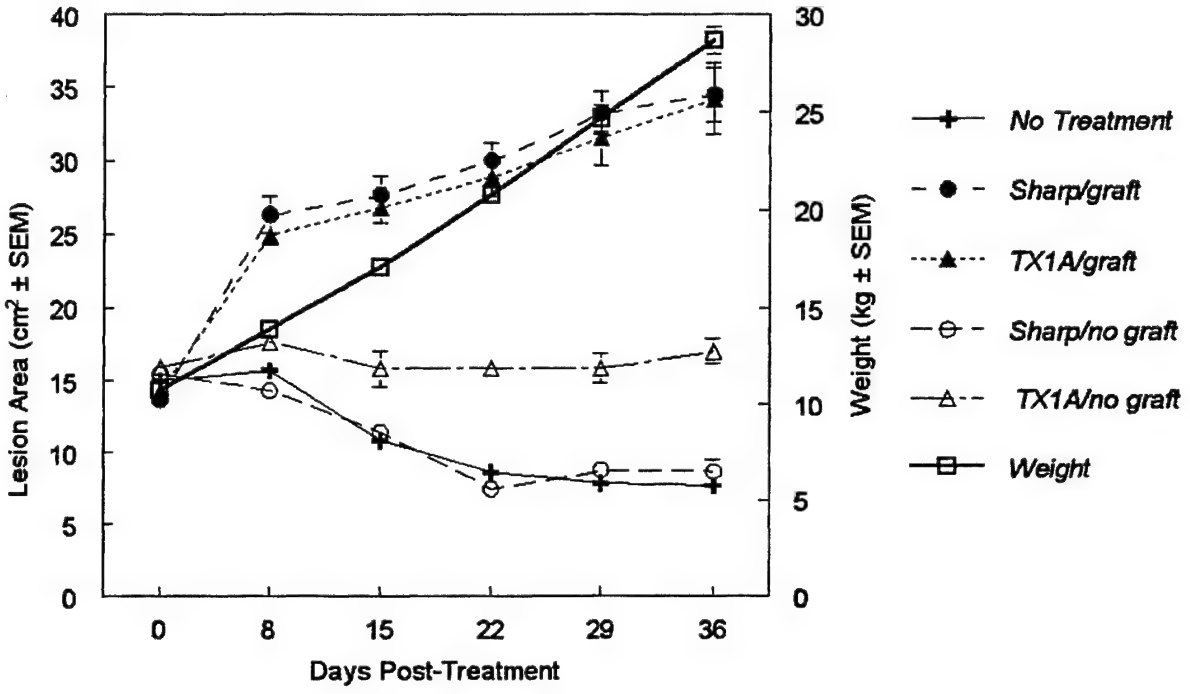

Fig. 10. Mean lesion area and weight vs. time. The grafted lesions appeared to grow with the animals, whereas the no treatment and non-grafted sites did not. The no-graft sites were significantly smaller than the grafted sites, with the laser/no graft sites remaining larger than the sharp excision/no graft sites.

By the end of the study, the laser debrided/grafted sites retained their circular figures (Fig. 11), whereas the other SM-exposed sites did not. In the no-graft groups, no differences in lesion roundness were noted among any of the SM-exposed sites throughout the post-surgical observation period. In the grafted groups, differences were seen between the sharp sites and NT sites on PS days 8-29, between the TX1A sites and NT sites on PS day 36, and between the sharp and TX1A sites on PS days 8-36.

As with lesion roundness, the aspect ratio of the laser debrided/grafted sites showed very little change throughout the post-surgical observation period (Fig. 12). In

the no-graft groups, no differences were noted among any of the SM-exposed sites throughout the post-surgical observation period. In the grafted groups, differences were seen between the sharp sites and NT sites on PS days 8, 22 and 29, and between the sharp and TX1A sites on PS days 8, 22, 29 and 36.

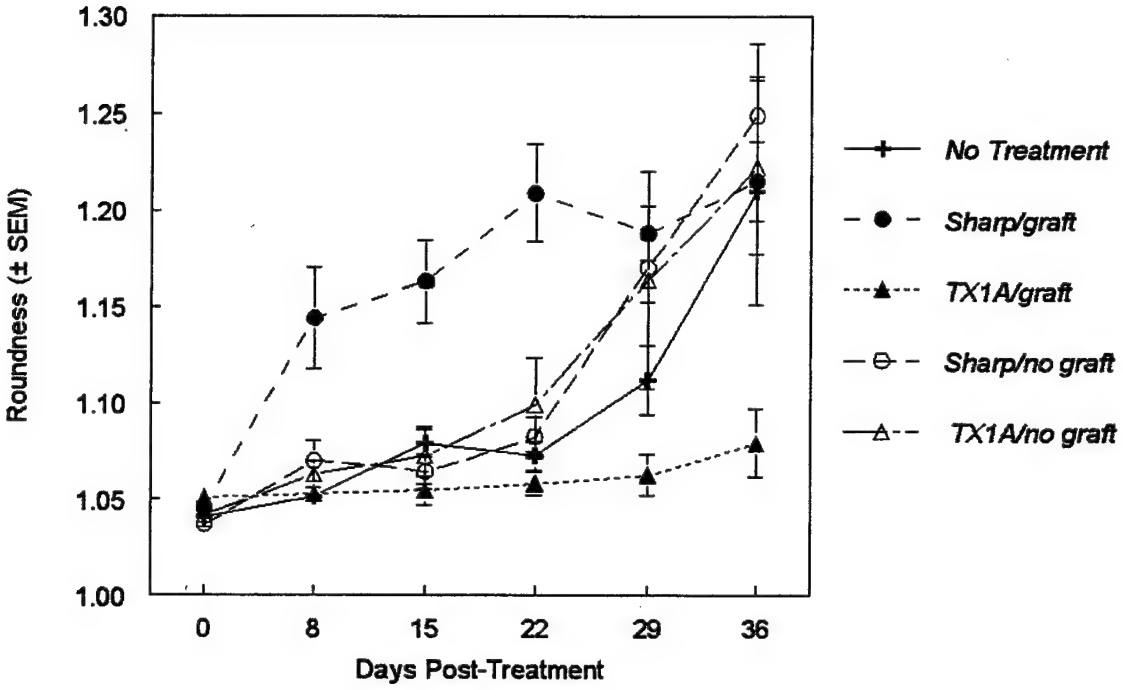

Fig. 11. Lesion roundness vs. time. By the end of the study, the laser debrided + grafted sites retained their circular figures, whereas the other sulfur mustard-exposed sites did not.

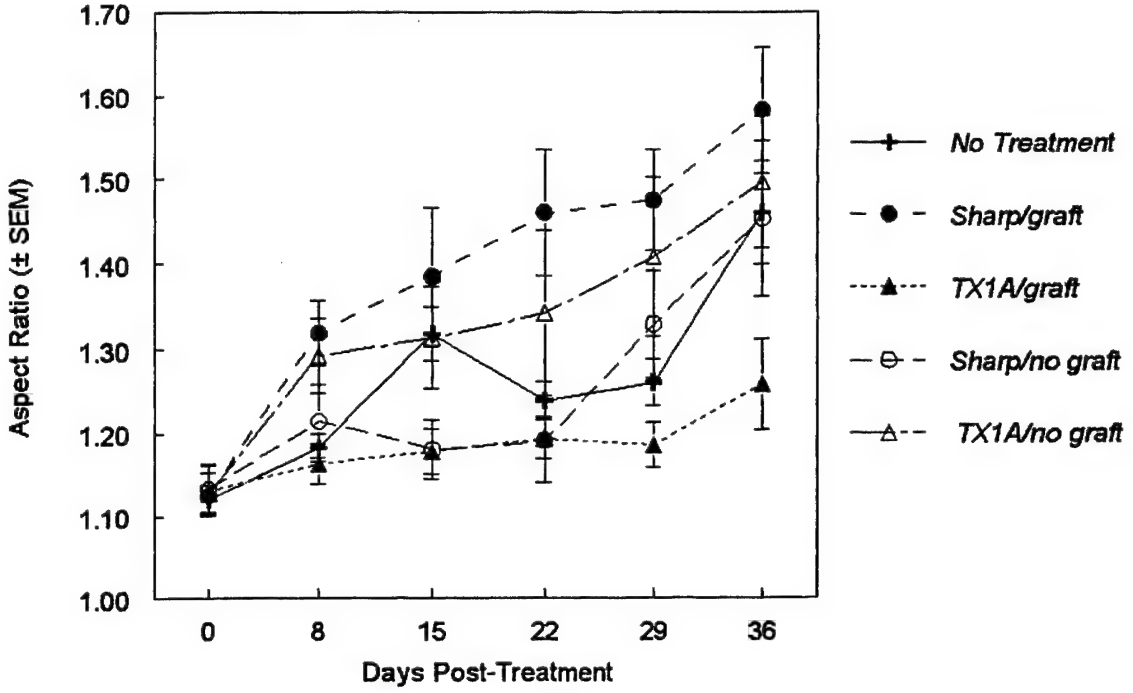

Fig. 12. Lesion aspect ratio vs. time. The laser debrided + grafted sites appeared to retain their aspect ratios better than the other sites.

Representative gross lesions on PS day 36 can be seen in Fig. 13, showing contraction of an untreated, ulcerated SM lesion on the far left. Fig. 14 depicts changes in areas over time of quadrilateral binary images created by connecting the tattoo spots around each site using image analysis software. The areas of these images from the grafted sites and sham sites grew at about the same rate as the mean animal weights, whereas the other SM-exposed sites grew at a lower rate (TX1A/no-graft sites) or not at all (sharp/no-graft sites and NT sites). To assess degree of wound contraction over time, these areas were normalized to total body surface area (TBSA) using the Meeh formula.[100-102] The grafted lesions retained a larger % TBSA than the no-graft group throughout the study (Fig. 15). In the no-graft groups, differences were noted between the TX1A sites and the NT sites, and between the sharp sites and TX1A sites throughout the post-surgery observation period. In the grafted groups, differences were seen between both the sharp and TX1A sites and the NT sites throughout the post-surgery observation period. For all groups except the TX1A/no-graft, differences

between the sham sites and SM-exposed sites were noted during most of the study. Wound contraction over time was assessed statistically by performing a one-way repeated measures ANOVA on each treatment group, with time as the repeating factor. Graphically, those groups whose lines were horizontal over the time span of the experiment did not undergo contraction, as the size of the lesions remained proportional to body size as the animals grew. Table 5 (Appendix 1) shows the differences that were noted. The only groups to show no change in %TBSA over time, thus little-to-no contraction, were the sharp/graft, TX1A/graft, and sham groups. The TX1A/no-graft group did not contract as much as the sharp/no-graft group.

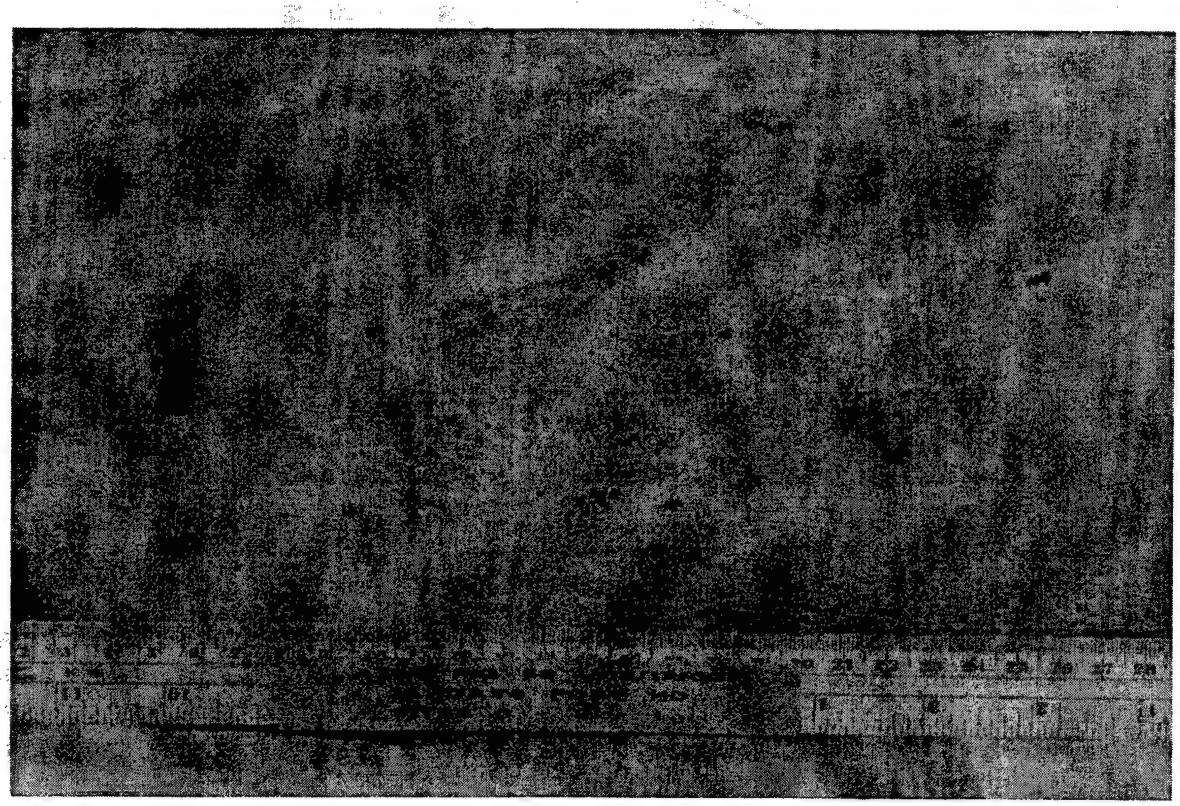

Fig. 13. Gross photograph of sulfur mustard-exposed lesions 36 days following surgery. The lesion on the far left was untreated. The lesion in the center underwent sharp surgical tangential excision followed by autologous split-thickness skin grafting. The lesion on the far right underwent laser debridement followed by skin grafting. The grafted sites grew with the animal, whereas the untreated site contracted. Note the ulcer still present on the untreated site and the retained circular shape of the laser debrided site.

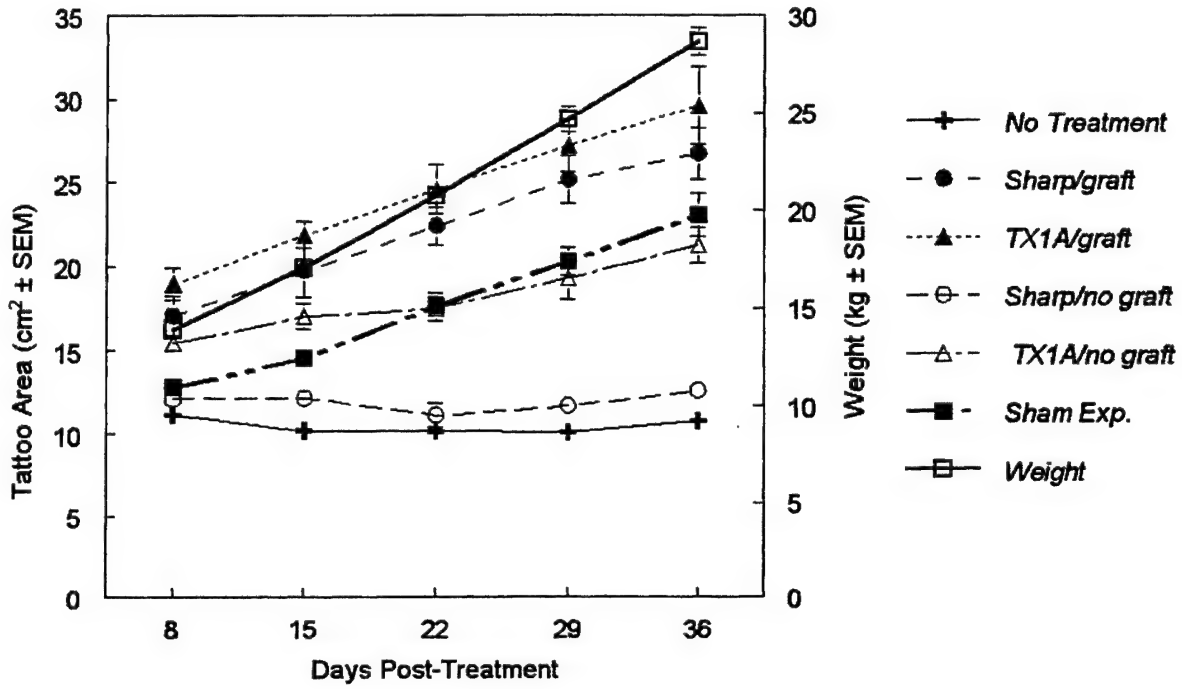

Fig. 14. Changes over time in weight and areas of quadrilateral binary images created by connecting the tattoo spots using image analysis software. The areas of these images over the grafted sites and sham sites grew at about the same rate as the animal weights, whereas the other SM-exposed sites grew at a lower rate (TX1A/no-graft sites) or not at all (sharp/no-graft sites and NT sites).

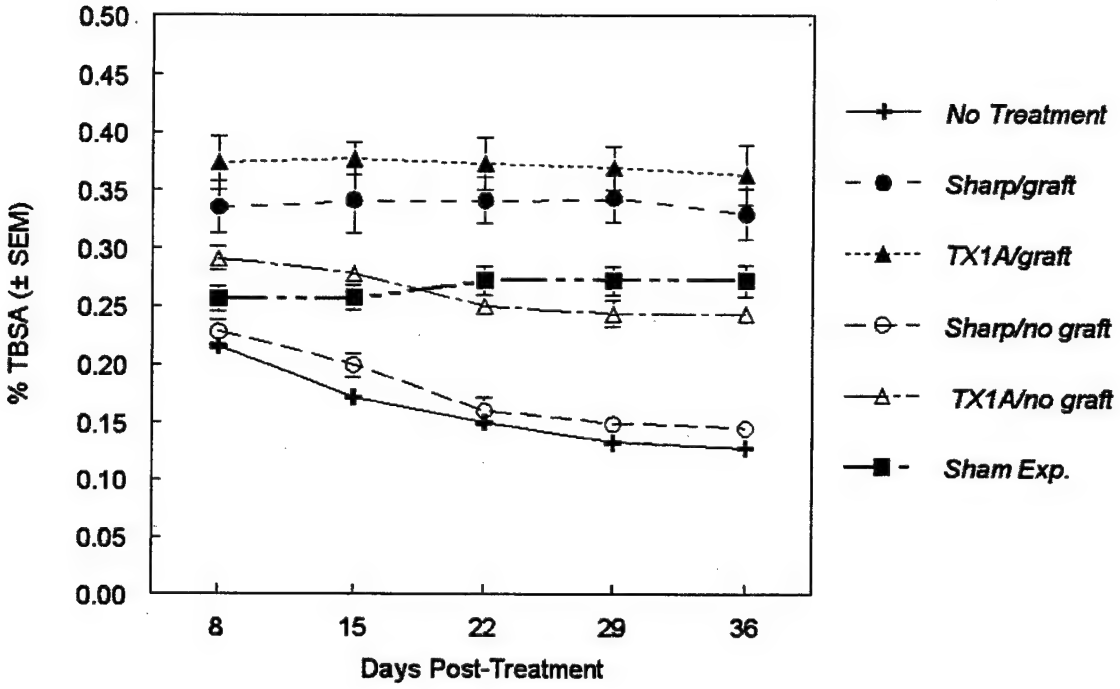

Fig. 15. Percent total body surface area (TBSA) vs. time of quadrilateral binary images created by connecting the tattoo spots using image analysis software. The only groups to show no change in %TBSA over time, thus little-to-no contraction, were the sharp excision + grafted group, the laser debrided + grafted group, and the sham–exposed group. The laser debrided + no graft lesions did not contract as much as the sharp excision + no graft lesions.

IV. Histopathology

To verify burn depth, full thickness 4-mm punch biopsies were taken from the center of each site immediately before the debridement procedure. Table 6 is an incidence summary table of the changes noted. The histological evidence that supports the burns being deep/dermal full thickness is full thickness epithelial necrosis (Fig. 16), follicular necrosis (Fig. 17), and sweat gland necrosis (Fig. 18). Full thickness epithelial necrosis was noted in 100% of the SM-exposed tissues. Follicular necrosis was noted in 98% of the SM-exposed sections that had hair follicles. Sweat gland necrosis was noted in 67% of the SM-exposed sections that had sweat glands. Sweat gland

epithelial cell swelling, a likely precursor to cell death, was noted in 42% of sections containing sweat glands. Supportive gross clinical findings included general lack of hair growth by PS day 36, and lack of healing by 21 days in the SM-exposed, untreated sites. Other findings noted included edema throughout the dermis and hypodermis, and occasionally into muscle; a mild inflammatory cell infiltrate in the dermis; dermal blood vessel congestion; and dermal hemorrhage. The edema noted in the adipose tissue followed the tracks of connective tissue, occasionally following those tracks into underlying muscle. Edema in the adipose tissue was noted as full thickness. Microblisters, a finding in guinea pig and pig models exposed to SM vapor, were not noted in any of these sections. Dermal coagulation was noted in 15% of the sections, with depths typically mid- to deep dermal. Arrector pili muscles appeared to be unaffected at this time point. Sham-exposed sites and mid-ventral control sites on SM-exposed pigs were normal histologically.

Table 7 shows the incidence of findings of the skin sections taken at necropsy, 36 days following surgery. Full reepithelialization was noted in 50% of the sites that underwent sharp surgical excision but were not grafted, in 67% of the laser debrided/no-graft sites, in 100% of the sharp or laser debrided and grafted sites, and in 54% of the SM-exposed sites that were not treated. Fig. 19 is a graphical representation of the percent surface area of the gross lesions that were ulcerated on PS days 29 and 36. An improvement in healing was noted between those two time points, with the NT sites showing, on average, a larger portion of unhealed surface area than either of the debrided sites. Histologically, the epidermis was similar in non-ulcerated areas of SM-exposed sites that were either not treated or debrided but not grafted. In these sections, marked epidermal hyperplasia (acanthosis), marked hyperkeratosis, and marked parakeratosis were noted (Fig. 20). The epidermis in the grafted sites was essentially normal. Microgranulomas were noted in most SM-exposed tissue sections and were generally eosinophilic. Many of those noted in the grafted sections were noted at the periphery, a likely reaction to suture material. Microgranulomas had a tendency towards being multifocal. They were likely a reaction to a ruptured hair follicle, ruptured fat cell, or bacteria. A rete ridge pattern, normally found in porcine skin, was noted in all sections. Hair follicles were noted in 100% of the grafted sites throughout the graft and noted in many of the other SM-exposed sections, typically limited to the periphery of the lesion. Arrector pili muscles were missing from all SM-exposed, no-graft sections. Sham-exposed sites and mid-ventral control sites on the SM-exposed animals were essentially normal.

The dermal collagen was frequently found to be invading the underlying muscle in the SM-exposed sites. It occurred in 75% of the sharp/no graft sections with a tendency toward being moderate in severity, in 67% of the TX1A/no graft sections (moderate to severe), in 17% of the sharp/graft sections (mild to moderate), in 33% of the TX1A/graft sections (severe), and in 54% of the NT sites (mild to severe). Image analysis was conducted on Masson's trichrome-stained sections to determine the fraction of the space between the dermal-epidermal junction (DEJ) and underlying muscle that was occupied by collagen fibers (Fig. 21) and the fraction of the collagen layer that was new (vs. mature) collagen (Fig. 22). Two-way repeated measures ANOVAs conducted on the data of both parameters did not indicate any interaction between grafting procedure (graft/no graft) and method of debridement (sharp

surgical/TX1A laser). In the no-graft groups, no differences were noted among any of the SM-exposed sites for either parameter. In the grafted groups, no differences were noted among any of the SM-exposed sites for fraction of space occupied by collagen. Differences were noted between both the sharp and TX1A sites and NT sites for the fraction of dermal collagen that was new. There were significant differences in both parameters between the sham-exposed sites and all SM-exposed sites. All SM-exposed sections showed an increased fraction of the space between the DEJ and muscle taken up by collagen (Fig. 21). The entire amount of collagen in the NT sites and those SM-exposed sites that were not grafted was entirely made up of new collagen (Fig. 22). Mature collagen was only noted in the grafted sections, sham sections, and mid-ventral control sites. Generally, the amount of new collagen below the grafts was minimal.

Movat's pentachrome-stained sections were evaluated for the presence/absence and orientation of elastic fibers in the papillary and reticular dermis (Table 8). In normal weanling pig skin, these fibers are generally oriented perpendicular to the skin surface in the papillary dermis and appear thin and wispy. In the lower reticular dermis they run parallel to the skin surface and are thicker. The fibers in the papillary dermis were absent in the SM-exposed NT and no-graft sites, but were present with proper orientation and thickness in the grafted sites (Fig. 23). The reticular dermis of most SM-exposed sites showed fibers that had a tendency toward being disorganized and wispy in appearance (Fig. 24), with occasional multifocal areas of thicker, horizontally oriented fibers. Fibers were always present in the connective tissue of the hypodermis, and showed no clear pattern of thickness in any of the sections examined. Incidence summary results of the general histopathological examination for systemic toxicities and/or infectious processes are shown in Table 9. The changes noted in the thymus, lung, and lymph node of all animals, including sham-exposed, were indicative of a systemic viral infection. Probable causes include Porcine Reproductive and Respiratory Syndrome Virus (PRRSV) and/or circovirus. Diagnostic testing at the Iowa State University Veterinary Diagnostic Laboratory to confirm presence of either of these viruses by immunohistochemistry failed to identify any evidence of viral protein. This finding did not rule out the possibility of a latent, non-productive infection, or infection by another yet unidentified virus. The few brain and dorsal skin lesions that were noted were consistent with this diagnosis. Special histological stains have ruled out bacterial or fungal causes. Specialists at Purdue University reviewed several cases, and concluded that the lesions were most consistent with a viral etiology, most likely porcine circovirus type 2. Much remains to be learned about this virus.[103] The lesions noted were most likely of little to no clinical or experimental significance; however, the possibility of a deficiency of the general immune system must be considered. The other tissues examined, including bone marrow, did not reveal any SM-induced systemic toxicities.

In general, clinical pathology did not indicate any SM-induced toxicities or infectious processes. Hematology results are presented in Table 10. Very few statistical differences among the three groups (sham-exposed, SM-exposed/grafted, and SM-exposed/not grafted) were noted. In those instances where differences were noted, the changes were not biologically significant because the mean values were within normal ranges for swine. Hematocrits were uniformly below values reported for adult swine.

Clinical chemistry results are presented in Table 11. Very few statistical differences among the three groups (sham-exposed, SM-exposed/grafted, and SM-exposed/not grafted) were noted. In most of those instances, the changes were not biologically significant because the mean values were within normal ranges for swine. A single animal from the no-graft group showed a slightly depressed sodium level on PS day 29. Several animals in the grafted group showed very slight elevations of ALT and ALP on PS day 36. Increases in ALT alone would have been indicative of skeletal muscle damage due to multiple intramuscular injections. Increases in ALP alone would have been indicative of stress. Increases in both ALP and ALT in the same animals on the same day indicated mild portal hepatitis that was not picked up on histopathology due to the limited sampling that was conducted.

V. Vancouver Scar Assessments

The burn scars were rated according to the method described by Baryza and Baryza[97] and utilized at the Shriners Burns Institute, Boston, MA. Mean ratings for vascularity, pigmentation, pliability and height can be found in Table 12. Scars were rated only on PS days 22, 29 and 36. Most of the SM-exposed non-treated lesions could not be evaluated on PS day 22 due to the continued presence of burn eschar, with several lesions still not available for rating on PS day 29. By the end of the study, the grafted sites were normal to pink, while the non-grafted and NT sites were visually noted as being red to purple. These differences in perceived color can be noted in the reflectance colorimetry data seen in Fig. 2 (lightness), Fig. 3 (red/green balance), and Fig. 5 (overall color difference). There was never any hyper- or hypopigmentation noted in these white pigs. Pliability of all of the treated sites appeared to be between normal and supple, whereas the NT sites were graded between supple and yielding. Mean scar heights were 0-1 mm.

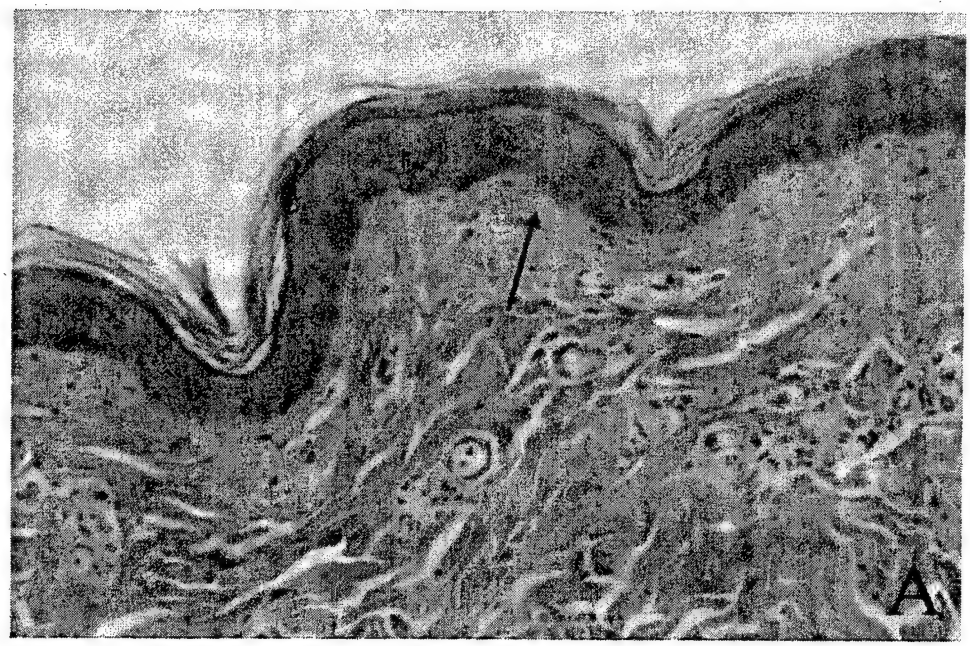

Fig. 16. Epithelium from biopsies taken during surgery. Fig. 16A represents normal epidermis from an unexposed site (arrow). Fig. 16B depicts full thickness epithelial cell necrosis (arrow) and blood vessel congestion with dermal hemorrhage (arrowheads). [25X]

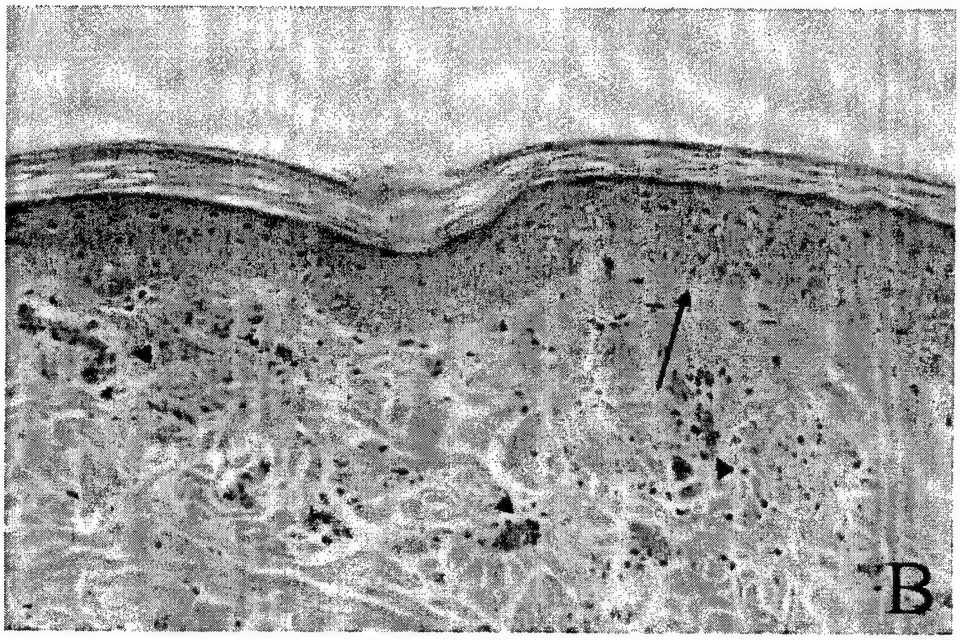

Fig. 17. A normal follicle is seen in an unexposed site in Fig. 17A (arrow). Follicular necrosis was noted in sulfur mustard-exposed sites (arrow, Fig. 17B). [25X]

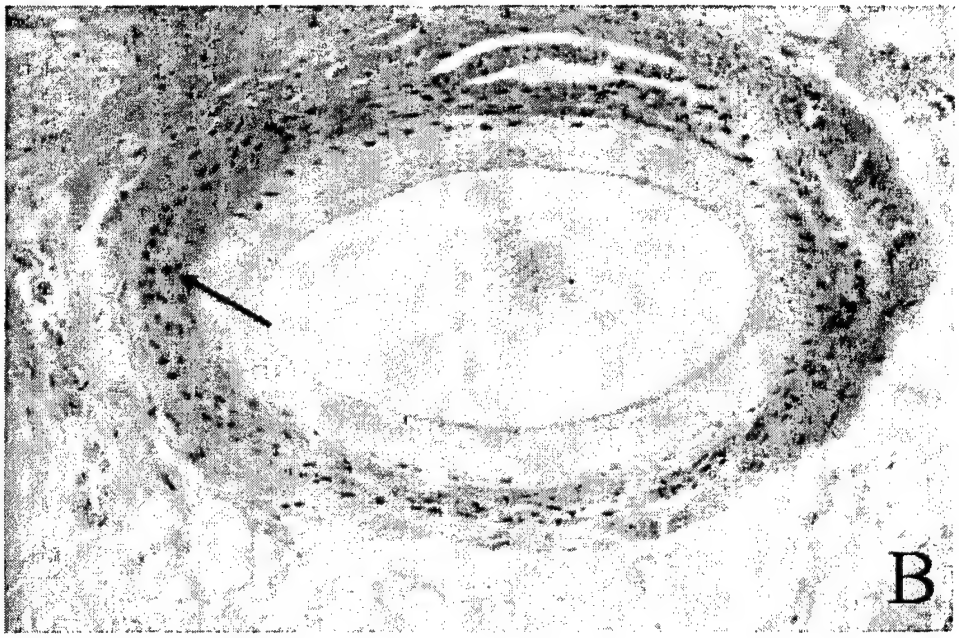

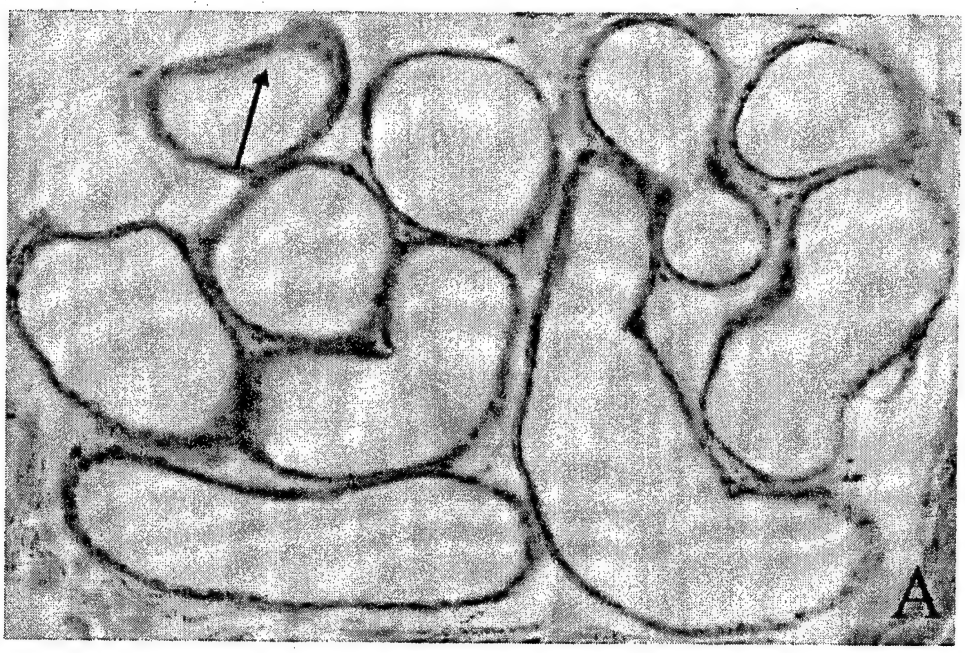

Fig. 18. Fig. 18A shows normal sweat glands from an unexposed site (arrow). Sweat gland necrosis can be seen in sulfur mustard-exposed sites, with cellular debris in the duct lumen (arrow) as well as denuded epithelial surfaces (arrowhead) in Fig. 18B. [25X]

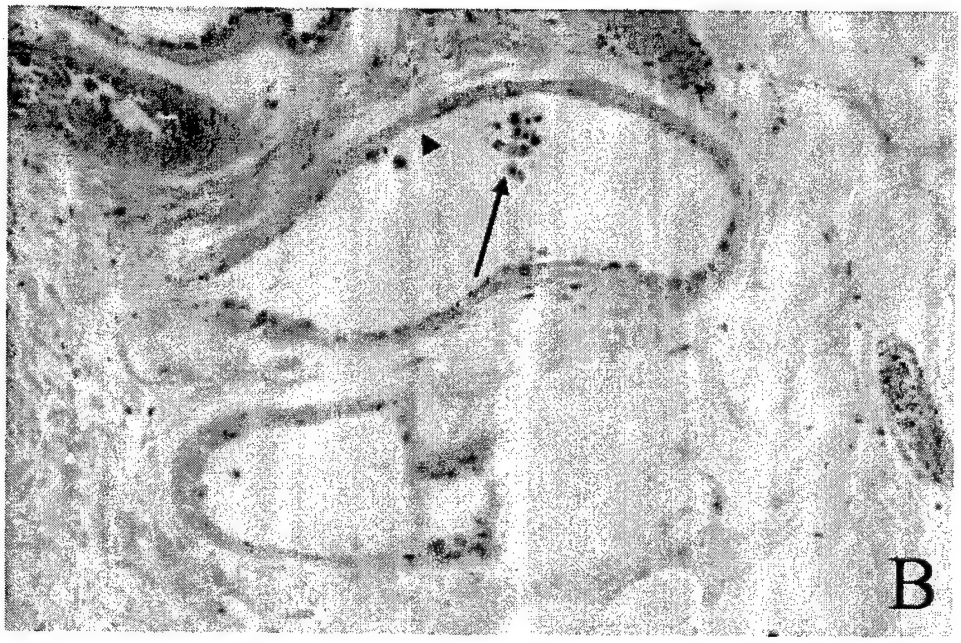

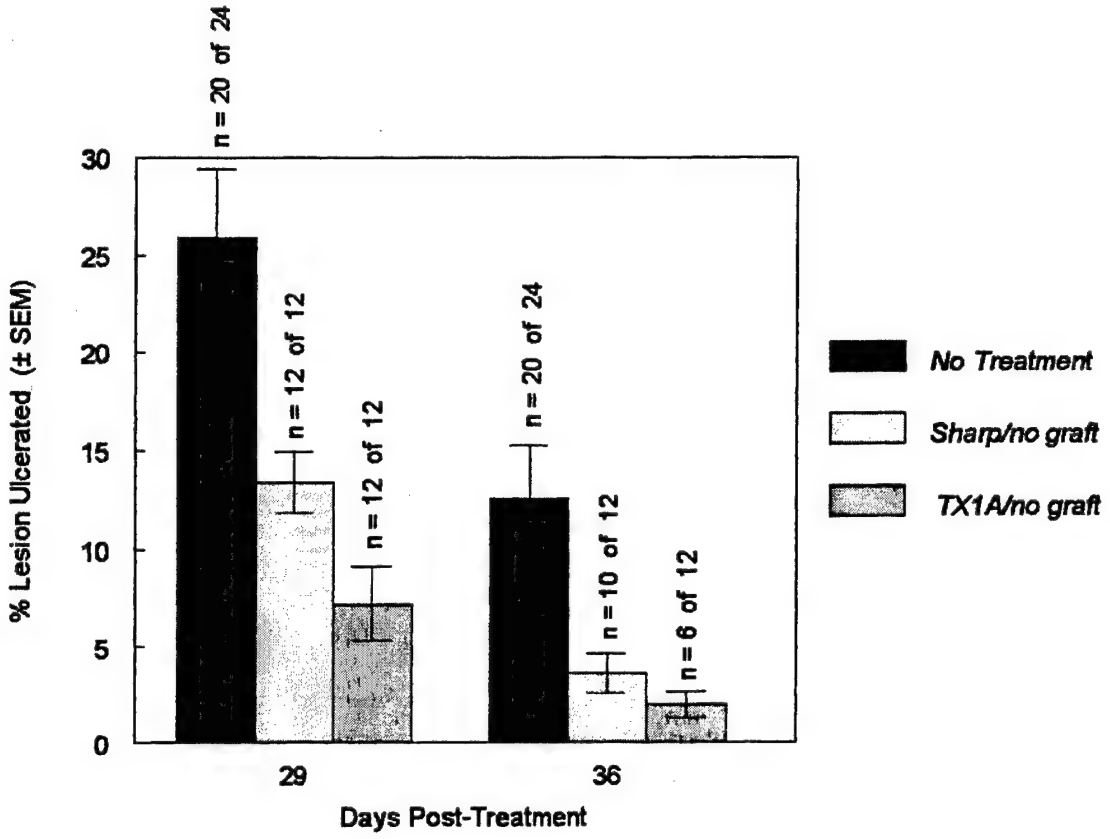

Fig. 19. Graphic representation of the percent surface area of non-treated and debrided but not grafted sites that remained ulcerated on post-surgery days 29 and 36. An improvement in healing was noted between days 29 and 36, with the no treatment sites having significantly larger percentages of the sites ulcerated at both time points.

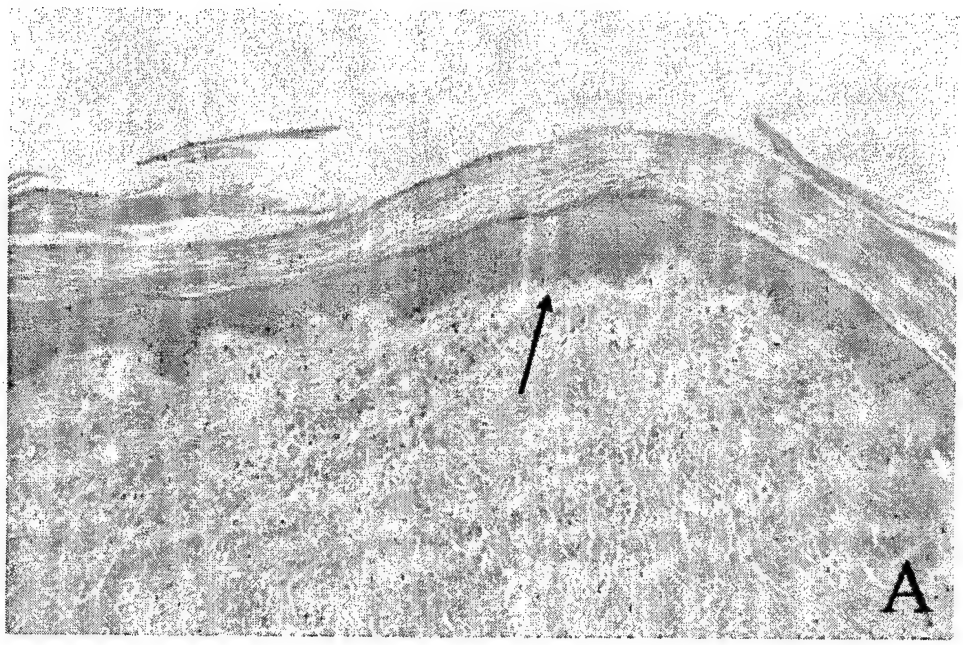

Fig. 20. The epidermides of debrided + grafted sites (Fig. 20A) were relatively normal. Sulfur mustard-exposed sites that were either not treated or debrided but not grafted exhibited marked epidermal hyperplasia (acanthosis, arrows), hyperkeratosis (arrowhead) and parakeratosis (Fig. 20B). These changes would likely subside with time. [25X]

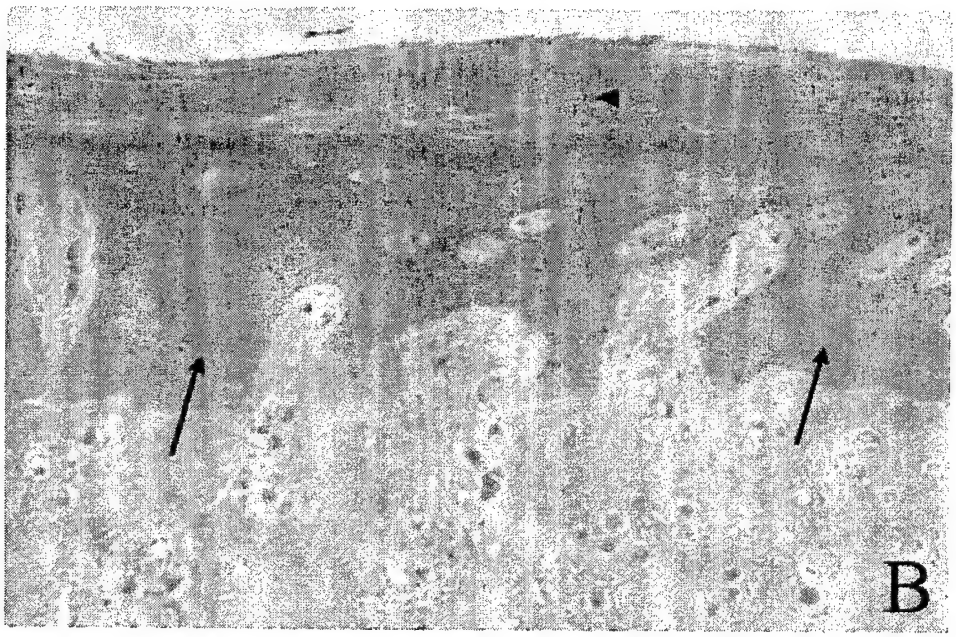

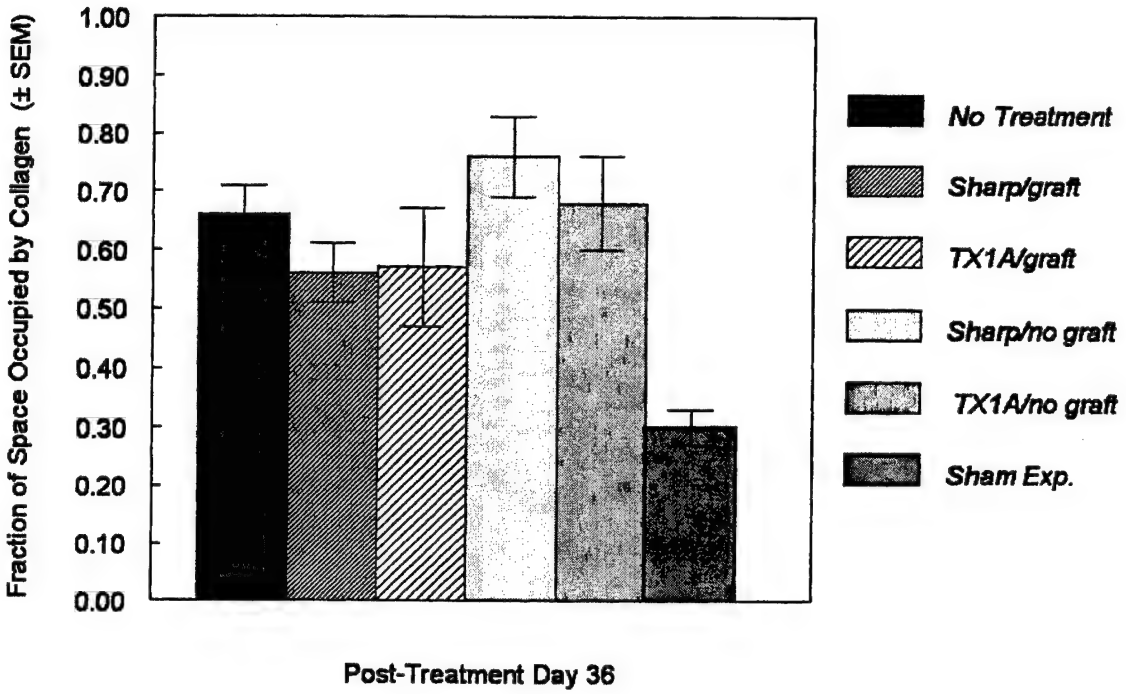

Fig. 21. Graphical representation of the amount of space between the dermal-epidermal junction and underlying panniculus carnosa that was occupied by collagen fibers. There were no differences among any of the treatment groups, all of which occupied significantly more space than the sham-exposed sites.

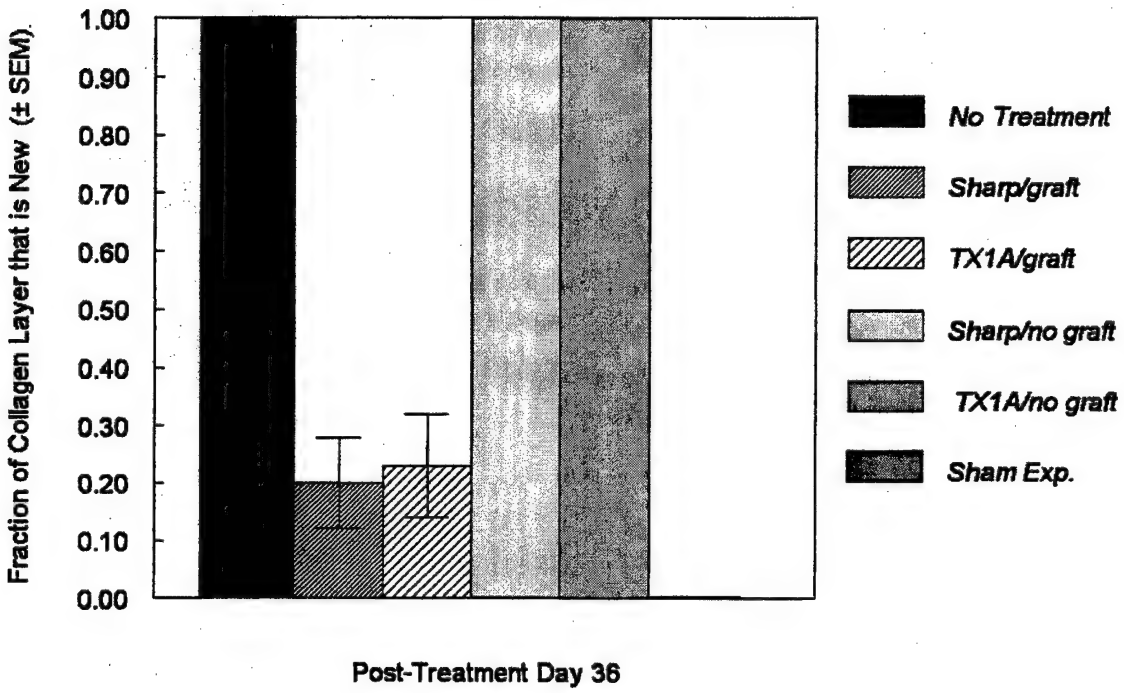

Fig. 22. Graphical representation of the fraction of dermal collagen that was new (vs. mature). All of the collagen was new in sites that were either not treated or debrided but not grafted. There was minimal new collagen below the skin grafts.

Fig. 23. Elastic fibers can be seen in the papillary dermis of unexposed or grafted skin collected 36 days following surgery. The fibers are generally thin and oriented perpendicular to the skin surface (arrows, Fig. 23A). There was a total absence of these fibers in sulfur mustard-exposed, not-grafted skin (arrows, Fig. 23B). [Movat's pentachrome stain, 25X]

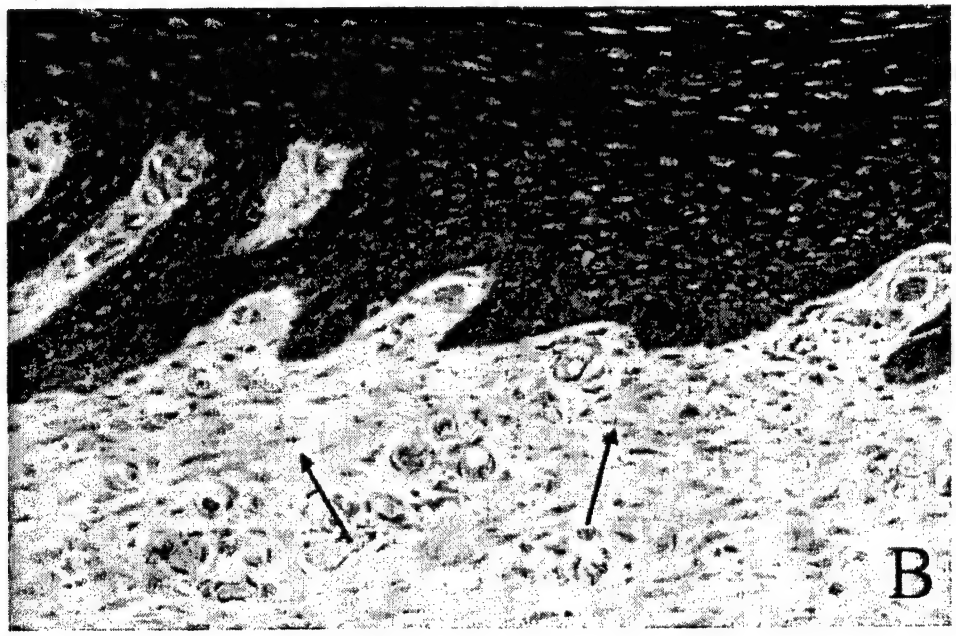

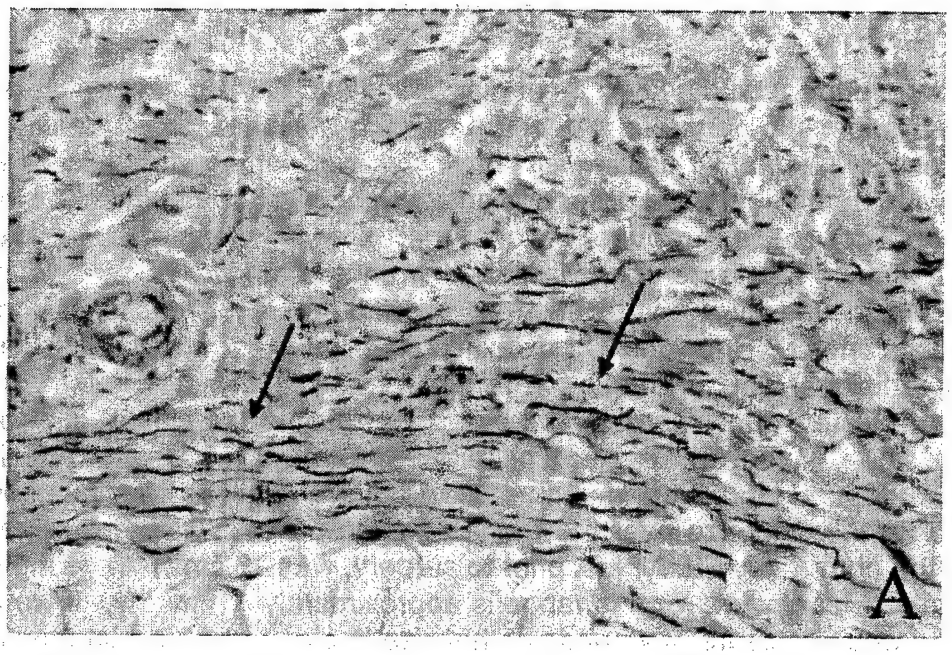

Fig. 24. Elastic fibers can be seen in the reticular dermis of unexposed skin collected 36 days following surgery (arrows, Fig. 24A). The fibers are generally thick and oriented parallel to the skin surface. The elastic fibers seen in the reticular dermis of all sulfur-mustard exposed sites, no matter the treatment they received, were thin and disorganized (arrows, Fig 24B). [Movat's pentachrome stain, 25X]

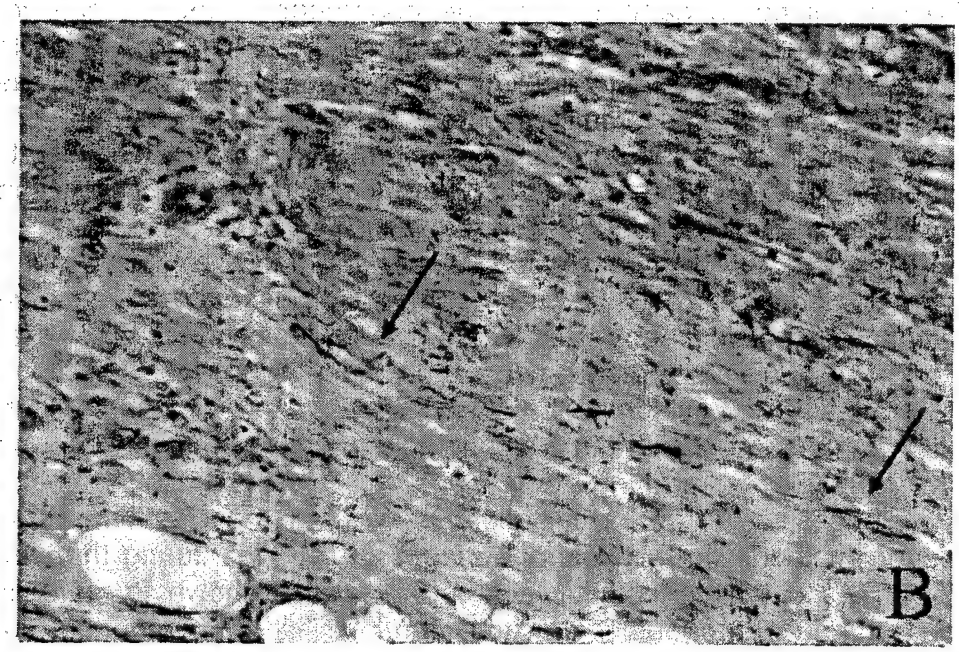

DISCUSSION

In the current study, large 4-cm diameter liquid SM burns were generated on the ventrum of pigs. To generate 6 deep burns of this size, a large quantity of liquid SM was necessary (2.4 ml). This is much larger than war fighters are anticipated to come in contact with on the battlefield or for civilians caught in a terrorist attack. However, good wound healing studies require lesions that are large enough to prevent quick, spontaneous, complete re-epithelialization from the edges of the wound. Wound closure is achieved by a combination of two independent processes: contraction and epithelialization.[104] Snowden[104] examined the rate of movement (contraction) of dressed excisional wound margins in a number of species. He found a linear rate of movement of the wound margins and noted that the rate of closure can be calculated from the slope of the area$^{1/2}$ vs. time plot. He found these rates of closure to be relatively independent of wound shape. With both rabbits and humans, this rate varies very little with wound size over the range of 10 to 50 cm^2. (The average area of the burns in the current SM study, just prior to surgery, was 15 cm^2.) In young humans (av. 20 yr) the rate of closure for this range is approximately 1 mm/day. If we approximate the rate of wound closure of wounds of this size in pigs to that in humans, it would take 21 days for a 2-cm diameter excisional wound to close. Lawrence[105] states that prompt and satisfactory closure of full-thickness burns that are greater than 3 cm in diameter can best be achieved by skin grafting. Our animal model was created such that candidate treatment regimens would be evaluated on burns that could not heal quickly from the edges by 21 days without efficacious treatment. Promising treatment regimens that show improved healing of burns smaller than 3 cm in diameter may not be very efficacious with deep burns covering a larger surface area. Caution is needed when interpreting results of healing efficacy studies when small lesions are being treated.

The six SM burns generated on the abdomens of the animals in this study covered approximately 2% of the total body surface area. The rate of healing found in this study may not be representative of wounds involving larger surface areas due to the onset of shock and other systemic effects. In addition, the benefit of hemostatic excision offered by laser debridement may not be fully realized in this study because the amount of blood loss due to sharp excision was small and blood transfusions were not necessary. Further studies are needed to resolve these issues.

Graham et al.[106] have described clinical pathology findings and the urinary excretion profile of a major SM metabolite (thiodiglycol) over a 7-day observation period in this animal model. Results revealed subtle SM-related changes that were suggestive of a mild hemolytic episode that likely occurred within the skin lesions. No other signs of clinically significant systemic toxicities were noted, including bone marrow suppression. In agreement with our previous findings, no systemic toxicities were noted in the current debridement/grafting study.

It was necessary to periodically lightly anesthetize each animal to conduct the bioengineering methods on the ventral surfaces of the pigs during the weekly clinical observations. As certain anesthetic agents have been shown to have an effect on cardiac output and cutaneous microcirculation,[107-109] it was important to select an anesthetic regimen that produced minimal effects or at least consistent vascular effects on dermal dose sites. Prior to the current study, a short study was conducted on 6 pigs

to examine the effects of various anesthetic regimens on several bioengineering methods conducted on ventral pig skin (unpublished results). The regimens tested were (1) Telazol® (tiletamine + zolazepam) with xylazine in repeated intramuscular injections, (2) Telazol®/xylazine solution as a pre-anesthetic and inhalation of isoflurane to maintain anesthesia, (3) isoflurane inhalation via mask induction followed by intubated delivery, (4) and repeated i.m. injections of ketamine + xylazine. Multiple iterations of each regimen were performed on each animal within a week time span, with a minimum one-week washout period before the next regimen was tested. On each day of testing, each of 6 unexposed (no SM) sites per animal was evaluated in 4 successive testing rounds using LDPI, reflectance colorimetry and evaporimetry. No regimen was clearly preferable for LDPI since they all affected cutaneous blood flow. The Telazol®/xylazine combination or Telazol®/xylazine with isoflurane was preferable for the TEWL measurements. For the reflectance colorimeter, either Telazol®/xylazine or ketamine/xylazine was suitable; Telazol®/xylazine preferred due to a lesser blanching effect. Overall, Telazol®/xylazine was the recommended anesthetic regimen for use with these bioengineering techniques. It was also recommended that reflectance colorimetry and evaporimetry readings be taken first since they were the most sensitive to time following induction of anesthesia. This order was followed on each clinical observation day in the current laser debridement study. Relating several of the bioengineering parameters to data collected from control sites or normal perilesional skin helped to further minimize effects of anesthesia. Detailed results of the short anesthetics study will be published in the future.

A number of bioengineering methods were used on a weekly basis throughout the study to non-invasively monitor wound healing. Reflectance colorimetry, evaporimetry, laser Doppler perfusion imaging, and ballistometry all proved useful.

We routinely use a reflectance colorimeter in our laboratory to assess erythema (a*) response following sulfur mustard exposure.[10, 16, 17] Carvalho et al.[110] examined the color of restored skin (RS) of healed partial thickness burns using a portable spectrophotometer. They found RS became darker (L*) one year after the burn occurred, in subjects with sun exposure, and in older subjects. RS became redder (a*) in subjects who had been exposed to the sun, in older subjects, and within the first 6 months after the burn. Finally, RS was bluer (b*) than healthy skin within one year after the burn. Our results on L* and a* parameters measured on the SM-exposed no treatment sites are in general agreement with their observations. Skin tone is cosmetically important to the patient, and any treatment that is rendered should leave the pigmentation level and skin tone of healed lesional skin as close to that of surrounding perilesional skin as possible. Reflectance colorimetry can play an important role in objectively measuring skin color parameters in wound healing studies.

Preliminary data from our laboratory indicated that barrier function is severely disrupted in ventral pig skin by 3-7 days after exposure to liquid SM for 30-120 minutes and does not return to baseline values until 63-70 days post-exposure (unpublished results). Chilcott et al.[59] found that TEWL mirrored the progression of the macroscopic injury after 12 hours, following exposure of dorsal pig skin to SM and Lewisite vapors. They found that maximal TEWL rates of skin exposed to SM occurred at 1 week compared with 24 hr for Lewisite-exposed skin. Our findings are in general agreement with theirs and can be explained by the *in situ* existence of an intact stratum corneum in

SM burns for the first few days following exposure.

Direct comparisons in the literature between SM and thermal burns are scarce. Papirmeister noted that disintegration of the basal cell layer caused by thermal burns has been shown to produce an intraepidermal blister that contains fragments of the basal cell layer attached to the basal lamina, unlike the almost totally denuded basement membrane in SM lesions.[1] An argument against the adage "a burn is a burn" is that SM initially targets a specific cell type (epithelial basal cells), unlike a thermal burn that begins damage at the stratum corneum then works its way downward. Since stratum corneum is the structure largely responsible for barrier function, water loss rates are very high immediately after a thermal burn (140-180 $g/m^2/h$ in humans).[111] The stratum corneum remains intact for 2-3 days after a SM burn, after which barrier function becomes compromised by loss of sloughing epidermis or deroofing of the blister. In the current study, the histopathology conducted on the biopsies taken during surgery, 48 h after SM exposure, showed an intact stratum corneum. By the end of the current study (36 days post-surgery), high evaporative water loss rates were still noted in sites that did not undergo grafting. Histologically, a hyperkeratotic stratum corneum was noted in those sites. Poor barrier function is generally attributed to an imbalance in water content, and/or lack of proper organization and/or adhesion of the corneocytes that make up the stratum corneum. In the future, looking at the stratum corneum in these healing lesions using scanning electron microscopy, transmission electron microscopy, and freeze-fracture or freeze-etch electron microscopy techniques may provide a better idea of how the stratum corneum, hence barrier function, is being restored. Sorption-desorption tests, moisture accumulation tests, and plastic occlusion stress tests may also prove useful.[112, 113] Information gleaned from these techniques may help in choosing an appropriate treatment that targets stratum corneum organization/structure, thereby improving barrier function. Using a term coined by dermatologist Dr. Albert Kligman, there are many "cosmoceuticals" on the market that specifically target the stratum corneum.

The delay in increased evaporative water loss that we noted has direct implication for the need for early replacement fluid therapy, considered essential in early thermal burn treatment.[114] Thermal burn patients often require excessive fluid replacement, which is detrimental if given to patients who do not need it. An instrumented, large total body surface area (20%) SM burn model in swine will be developed in the future that will allow us to examine (1) hemodynamic and other physiological changes over time, (2) hematocrit and electrolyte balance, (3) transepidermal water loss, and (4) the need and/or timing for fluid replacement therapy following significant SM exposure.

Generally, blood flux in all SM-exposed sites in this study remained at about 50-60% of normal levels, indicating that while the tissues were still being adequately perfused to ensure viability, there were larger and/or more blood vessels in the unexposed perilesional skin. This likely represents a loss of patency of existing blood vessels following liquid SM insult, with subsequent neovascularization providing smaller vessels. The blood vessel congestion and dermal hemorrhage noted histologically at 48 h post-exposure supports this conclusion. Image analysis of immunohistochemically localized blood vessels throughout the healing phase should yield a better understanding of the neovascularization process in healing SM burns.

While adequate blood flow into damaged tissues is vitally important in the healing process, we do not recommend routine use of LDPI in cutaneous wound healing studies. LDPI is currently rather time consuming if there are multiple sites to be evaluated and/or large images to be collected at high resolution. LDPI is not necessary for evaluating graft acceptance, because devitalized tissue is readily assessed visually. We will limit use of this methodology in the future to burn depth estimation prior to treatment and for evaluation of pharmaceuticals specifically designed to improve or sustain blood flow into damaged areas.

Mechanical properties of the skin are important from both a functional and cosmetic point of view, especially in areas that undergo tension or flexion. The SM-exposed sites that had undergone debridement with grafting were much closer to normal hardness and elasticity than SM-exposed sites either not treated or partially debrided but not grafted. These mechanical characteristics, as measured by a torsional ballistometer, were likely a reflection of dermal collagen structure/organization, viscous ground substance, and the subcutis rather than elastic fibers, as the skin was being compressed downward rather than twisted, stretched horizontally or pulled upward. The differences noted are likely attributable to the thick layers of immature (new) collagen seen histologically in those SM-exposed sites that had not been grafted. The grafted sites retained the mature collagen present in the donor sites, with small amounts of additional new collagen below the grafts. Immunohistochemical identification of type I and type III collagen remains to be conducted in these lesions. Other methods of measuring mechanical properties of the skin such as twistometry, suction chamber methods, levarometry, indentometry, and dynometry may help to break down the contribution of each of the viscoelastic skin components (collagen fibers, elastin fibers and ground substance) on the hardness and elasticity characteristics of healing SM lesions.

Hinrichsen et al.[115] showed in a minipig model that the extent of wound contraction of excisional full-thickness skin wounds is dependent upon anatomical location of the wound and that circular wounds do heal with contraction. They also found, as shown in the current study, that grafted wounds contracted significantly less than those allowed to heal by secondary intention. Medial wounds located close to the abdomen were found to heal faster than areas located laterally, close to the back, with medial sites contracting more than lateral ones. The idea that different anatomical sites possess specific characteristics was first suggested in 1861 by Langer.[116] The experimental ventral sites on the pigs in the current laser debridement study were rotated cranial to caudal to take into account any site specific biases that may have been present.

McGrath and Simon[117] described contraction of an excisional wound as a decaying exponential with a non-zero asymptote between days 6 and 39 after wounding, and that regardless of size or shape, the contraction-rate constant is invariant with age- and species-matched animals (differently shaped wounds of the same size contract at the same rate during the exponential period). They stated that shape exerted its effect prior to the onset of contraction, during the first 48 hours, by defining the size of the wound entering the exponential period. Tranquillo and Murray[118] found similar results using a mathematical model. Madison and Gronwall[119] found that the rate of wound contraction on the dorsum of the metacarpus of horses followed an

exponential model better than a linear one, and that wound shape did not influence the rate of wound healing. Snowden et al.[120] found that scab formation over undressed excision wounds in rabbits and rats had little or no effect on the overall rate of wound contraction. In the current study, we noted scab formation over those SM-exposed sites that had undergone partial-thickness debridement with no grafting, and surmise that the presence of the scabs had little effect on the rate of wound contraction in those lesions.

Wound contraction benefits surgeons by reducing the ultimate size of a defect.[121] In burns medicine, however, excessive wound contraction can lead to contractures that result in functional deficits and cosmetic deformities. These abnormalities, especially when they occur over joints, can limit mobility or dexterity and usually require further surgical intervention. Wound contraction is not easily quantified in humans; however in animal studies orientation marks (tattoos) can be placed near the wound edges and followed by image analysis.[115, 122] Using this procedure, we noted that grafting of deep cutaneous SM burns appeared to be beneficial in minimizing or preventing wound contraction in this animal model. In the absence of grafting, mid-dermal laser debridement appeared to result in less contraction than that which resulted from partial-thickness sharp surgical excision or no debridement at all. It is not understood why laser debridement resulted in less contraction than sharp surgical tangential excision in those SM-exposed sites that had not undergone grafting. Studies in CO_2 laser skin resurfacing have noted significant shrinkage of the tissue, especially once the epidermis has been removed, that has appeared to persist throughout healing.[83, 84] The dermal remodeling process noted in our healing tissues likely replaced the shrunken collagen fibers that existed immediately after the laser debridement procedures. Further study is needed to examine the effect of laser and sharp surgical debridement on SM-exposed and unexposed ventral pig skin. Image analysis of collagen fiber thickness and length, morphometry of immunohistochemically localized fibroblasts/myofibroblasts, and differentiation of viable and devitalized structures using a vital stain such as nitroblue tetrazolium chloride will likely provide explanations for the differences in wound contraction among treatment groups seen in this study.

The marked epidermal hyperplasia (acanthosis, often representing increased mitotic activity), hyperkeratosis and parakeratosis noted in our healing tissues would likely have subsided with time until a histologically normal epidermis resulted. It is not known how long this would take to occur, and a longer-term histopathological study is required to make this determination. Application of topical lactate-containing formulations, used extensively for the treatment of hyperkeratosis and dry skin conditions in humans, may be of benefit in quickly returning the skin to normal architecture.[123]

Glatter et al.[93] utilized the TX1A laser in a thermal burn model in pigs, and found that long-term scarring, based upon Vancouver scar assessments, was equivalent at 6 months post-surgery in both laser-ablated + grafted and sharply excised + grafted burns. Additionally, he noted no significant difference in engraftment rates between the two methods of debridement. This study revealed similar findings.

Routine manipulation of those SM-exposed lesions that histologically showed an investment of dermal collagen into the underlying muscle may have proven beneficial in reducing the severity of those adhesions. Those investments did not result in significant pliability limitations, however, as reflected in the Vancouver scar assessment scores.

The scars of our treated and untreated SM burns were relatively mild, and may have worsened or improved with time. The occurrence of hypertrophic scars in thermal burn patients is fairly normal and will typically reach maximum prominence at around 3 months following injury. Much of the treatment of human burn victims involves preventing or treating scar hypertrophy.[121] Grafting is utilized to prevent or minimize scar hypertrophy of deep dermal or full-thickness thermal burns that would inevitably occur if these wounds are allowed to heal by secondary intention. This scarring has been noted to develop not only in untreated sites but also in both grafted and donor sites, and can lead to contractures, deformity, functional deficits in movement or dexterity, and cosmetic disfigurement. Pressure garments have been extensively used to prevent and control hypertrophic scarring, lessening the need for future treatment.[121] Radiation treatments, steroid injections (e.g., triamcinalone) and reconstructive surgery are often utilized to reduce these deficits, and may prove useful in minimizing SM-related hypertrophic scarring.

The question arises as to why severe cutaneous SM lesions often take several months to heal. The evaporimetry data along with the histopathology conducted at 48 h post-exposure and 36 days post-surgery in this study offer some insights into lesion development and wound healing of these burns. In this study it was noted histologically that deeper structures such as sweat glands were affected, while other structures less deep, such as stratum corneum, arrector pili muscles, and dermal collagen, mostly appeared to be unaffected at an early stage (i.e., 48 h post-exposure). In a thermal burn, if the sweat glands are damaged, all structures above them are damaged as well. Ultimately, however, the collagen in these deep SM burns became functionally affected. In those sites that did not undergo grafting, there were no histological signs of mature collagen at 36 days post-surgery. If the collagen had not been damaged in some manner, either through SM alkylation or protease action, it would not have all been broken down and then replaced by new collagen. These histopathological results do provide support for the supposition that even though keratinocytes are a primary target, collagen is ultimately affected by SM exposure, either directly or indirectly. A study looking at histological endpoints throughout the healing process, to examine the pathology of the healing SM burn and the time line of when noted changes occur, would be of value. Invasive procedures, rather than the non-invasive methods used in the current study, need to be exhaustively conducted to fully understand the healing processes of SM burns. That, of course, would require a set of animals for each post-treatment day examined, as multiple/serial biopsy punches cannot be taken from the same site on the same animal. Doing that would, in itself, negatively affect healing.

In addition to signs that the dermal matrix was affected and had to undergo remodeling, the keratinocytes that feed new growth had obviously been affected. Damage is clearly noted at the periphery of such lesions and has been reported previously.[10, 124, 125] During reepithelialization, growth comes not only from the margins but also residual hair follicles and sebaceous glands. The hair follicles in the SM-exposed sites of this study have been affected, as supported by four observations. First, signs of severe nuclear damage were seen in the follicles in the 48-h biopsies. Second, there was little to no visible hair growth at 36 days, indicating that severe damage was inflicted to the follicles. Third, there were multifocal microgranulomas in all SM-exposed sections. The ones located at surgical margins in the grafted animals were likely a

result of the body's reaction to the suture material. The ones scattered throughout the sections were likely due to ruptured hair follicles. Fourth, when noted histologically, follicles were typically limited to the periphery in sites that were either not treated or had been debrided to mid-dermis and not grafted. So without actively dividing keratinocytes in healthy hair follicles, new growth can only come from the margins. While non-treated wounds underwent severe wound contraction that brought the edges closer together, large ulcerated (not fully reepithelialized) areas remained. With new collagen already in place, this slowness to heal may be primarily a consequence of damaged keratinocytes at the periphery of the lesion that cannot replicate normally, and/or are unable to produce the proteins necessary for translocation (e.g., integrins, and basement membrane components such as fibronectin, collagen and laminin). The slowness to reepithelialize may also be due to decreased or abnormal production of necessary growth factors secreted by macrophages, fibroblasts and epithelial cells, or faulty/absent growth factor receptors on the surface of the migrating, proliferating and differentiating keratinocytes. In the absence of treatment, the reepithelialization process is likely stalled until autolytic debridement occurs to rid the body of dead or malfunctioning keratinocytes at the wound margins. Non-grafted sites in this experiment that were debrided well into normal tissue showed fewer and far smaller ulcers by the end of the study than did non-treated sites, indicating that lateral debridement into healthy tissue was able to speed up the reepithelialization process. Without hair follicles participating in this process, healing was not as quick as that attained in the meshed graft sites that, histologically, showed healthy hair follicles throughout the skin sections at 36 days post-surgery. To further elucidate the slow reepithelialization process in healing SM lesions, a characterization (present/absent) of the pertinent proteins in skin samples is necessary (see discussion below).

Laser debridement offers significant advantages over other methods of physical debridement: (1) hemostatic control during surgery, (2) minimal debridement of normal perilesional skin, (3) minimal risk of exposure to aerosolized pathogens [as one may get with powered dermabrasion], and (4) improvement in cosmetic result. Eldad et al.[74] noted that it is technically difficult to control the amount of tissue to be removed by surgical tangential excision, and that laser ablation of nitrogen mustard burns in a guinea pig model enabled both control of the amount of tissue to be removed and minimal blood loss. As lasers become more efficient at debriding large burns, hemostatic control without the use of electrocauteries, epinephrine, triglycyl-lysine-vasopressin,[50] fibrin sealants,[126] or other hemostatic agents will be advantageous to the patient. Laser debridement of burn eschar has previously been shown to control blood loss.[74, 89, 90, 93]

In his initial clinical trials of laser ablation of thermal burns in children using a scanning, high-powered CO_2 laser similar to the TX1A used in this study, Sheridan[94] demonstrated the feasibility of laser vaporization of burn eschar with immediate autografting. Several concerns were raised regarding the use of lasers in burns medicine, listed as follows. (1) Laser ablation of very large wounds may be more time consuming than sharp excision. (2) Overheating of the laser with extended use in a single operation may pose a problem, should the cooling system prove inadequate in long operations. (3) Laser ablation works well on planar surfaces, but will likely be more time consuming on circumferential extremities. (4) The adequacy of excision needs to

be judged in the absence of diffuse capillary bleeding from the wound bed, a sign that normally tells burn surgeons they have debrided down into vitalized tissue. Thus, deeper debridement than required may be conducted unnecessarily. (5) High-powered laser systems could become unwanted, powerful excisional tools should the scanning mirrors malfunction during operation. (6) There is a possibility that flammable materials or gasses might be ignited in the operating room by a misdirected laser beam. Most of these concerns can be overcome with time and experience. Laser facial resurfacing (albeit at a lower power) has shown an excellent safety record. Routine maintenance of the equipment and periodic refresher training of personnel in its proper use will also make this technique more acceptable, efficient, and widespread in civilian burn clinics and military hospitals.

Whether or not burn surgeons accept the use of lasers in the operating room, this study should turn attention to the need for early aggressive treatment of deep SM burns. The results of this study should alter the thinking of how aggressive treatment needs to be if the desired outcomes are (1) speedy recovery, (2) close-to-normal function, (3) close-to-normal cosmetic appearance, and (4) minimal wound contraction. Current therapies for SM burns are often not aggressive enough to prevent unwanted cosmetic and functional deficits. The depth of a SM burn will frequently get worse between 2 and 7 days post-exposure.[124] Failure to properly diagnose the depth of these burns early on may have dire cosmetic and functional consequences for the patient. Hyper- and hypopigmentation are noted complications, and on visible body parts might be quite bothersome.[32] Hypertrophic scar formation and wound contraction in areas around joints could limit mobility or dexterity. Follow-up care and the use of pressure garments to minimize hypertrophic scarring should become routine after a sulfur mustard burn, as it is for thermal burns.[121]

In the future, both superficial and superficial dermal (partial thickness) SM burns will be incorporated into our weanling pig model, since these depths may have greater clinical relevance on the battlefield. As in human thermal burns medicine, the depth of the SM burn will likely determine the treatment regimen needed, thereby focusing attention to the further development of methods that can accurately diagnose wound depth. Perhaps the key to a successful outcome for the SM casualty is proper burn depth diagnosis starting as early as 24 hours following insult, and lasting at least a week to assure the burn has not deepened by the latter time point. Laser Doppler perfusion imaging is a viable option. Another promising technology that is capable of being miniaturized (therefore portable onto battlefield medical facilities) is indocyanine green fluorescence imaging. The fluorescence of intravenous indocyanine green (ICG) has been shown to estimate burn depth in small animals.[127] In contrast to fluorescein fluorescence,[128] ICG fluorescence is capable of distinguishing superficial and deep partial thickness burns from full thickness burns. The fluorescence intensity of ICG decreases exponentially with burn depth for burns of similar age.[129] ICG fluorescence was used to estimate burn depth in a porcine model using healing as an endpoint.[130] At the Wellman Laboratories of Photomedicine, an imaging system with a diagnostic algorithm was developed that accurately distinguished burns that healed within 21 days with minimal scarring from those that took longer to heal by secondary means. Measurements were made on burns created 2, 24, 48, and 72 hours prior to imaging. The algorithm was shown to be dependent on the age of the burn and independent on

the location of the burn. This technology showed promise in accurate determination of thermal burn depth in humans.[131] The system has already been miniaturized with the use of night vision goggles equipped with the proper filters, along with a small hand-held diode laser to excite the dye. This is a minimally invasive procedure that requires the placement of an intravenous line. ICG is FDA approved for use in humans to determine cardiac output, hepatic function and liver blood flow, and for ophthalmic angiography.

Studies remain to be conducted that will ultimately help us develop better treatment regimens, by offering insights into the mechanisms of lesion development and wound healing at the molecular level. Collaborative research projects involving molecular biology are in the planning stages, to look at mRNA transcript and protein expression profiles in the pig model. At various points throughout lesion development and healing, total cellular RNA will be isolated from skin samples, purified, and analyzed using a standard polymerase chain reaction-subtraction library technique. This technique includes reverse transcription of mRNA, hybridization reactions, PCR amplification of double-stranded cDNA, and sequence identity using the NIH cDNA databank. For select, highly expressed transcripts, mRNA levels will be quantified by competitive or quantitative PCR from total RNA isolates. Protein expression determination will be conducted following identification of specific dysregulated genes using standard ELISA techniques. Other techniques that are available to help us better understand the molecular mechanisms involved in SM lesion development and healing include ribonuclease protection assays (RPAs) and proteolytic enzyme activity assays. Immunohistochemistry, immunoelectron microscopy, and *in situ* hybridization can be utilized to localize tissue components and mediators in skin samples. Mediators of specific interest include growth factors, angiogenic inducers, degradative proteases, and inflammatory mediators involved in all stages of wound healing (coagulation/hemostasis, inflammation, cell migration and proliferation/fibroplasia, and remodeling). A list of the mediators of interest can be found in Table 13.

Laser debridement may not be the only efficacious treatment regimen for SM burns and will certainly not prove to be the least expensive. We fully intend to explore other potential treatments. There is a plethora of information and techniques that have been applied in patients suffering from pressure ulcers, venous and arterial leg ulcers, and diabetic foot ulcers that may be useful in treating ulcerated (not fully reepithelialized) SM lesions. There are many pharmacological approaches and wound dressings on the market to potentiate the healing of these wounds.

Table 14 lists a number of potential therapies that can be examined. The list remains to be prioritized according to military and civilian medical preferences, as well as by likelihood of success. Our focus will be on testing pharmaceuticals already approved by the FDA for use in humans, and on off-the-shelf products. Molecular biology techniques may provide clues that point us toward the use of particular therapies most likely to be of benefit (see discussion above).

It is not likely that a single silver bullet will be the "cure all" answer for the speedy recovery from SM burns. We foresee that combination therapies for superficial or superficial dermal SM burns will include the early use of anti-inflammatory agents, wound debridement, topical or systemic antibacterial agents, and growth factor cocktails applied with concomitant antiproteases, sequestered beneath occlusive or moisture-retentive dressings. The use of temporary skin substitutes may also be efficacious.

Skin substitutes[132] can be (1) permanent or temporary, (2) epidermal, dermal or composite, and (3) biologic or synthetic. An effective combination therapy seen for deep dermal/full-thickness SM burns includes early anti-inflammatory agents, wound debridement, antibacterial agents, and either autologous split-thickness skin grafts or permanent skin substitutes.

As there are no current animal models that inflict both thermal burns and SM burns of similar depth on the same animal at the same time, it is difficult to compare healing of these two types of burns. In the future, we will be incorporating thermal burns into our swine model. Not only will it afford the ability to compare the healing of untreated SM burns with that of thermal burns of similar depth, it will also make it easier to see whether the two types of burns respond to the same treatment regimen in the same way. Differing responses may result in a better understanding of SM-specific healing processes.

CONCLUSIONS

The consequences of receiving a cutaneous sulfur mustard burn are a prolonged healing phase and secondary infection. The reason for undertaking the current study was to find a treatment regimen that promotes speedier healing with fewer complications and less disfigurement.

Laser debridement followed by autologous split-thickness skin grafting was as efficacious in improving the wound healing of deep dermal/full thickness cutaneous sulfur mustard burns in weanling swine as full thickness sharp surgical tangential excision followed by skin grafting, the "Gold Standard" used in human deep dermal/full-thickness thermal burns management. Engraftment rates and Vancouver scar assessments were similar between both methods of debridement. The use of a computer controlled, raster scanned continuous wave CO_2 laser offered additional benefits that included hemostatic control during surgery and minimal debridement of normal perilesional skin, resulting in significantly less blood loss and an improved cosmetic result. Mid-dermal debridement by sharp surgical tangential excision or laser ablation without the use of skin grafts did not produce results that were as good as those attained through the use of grafts, but was better than no surgical treatment of the wounds at all.

There are a number of characteristics of healed wounds that are important to the patient from both a functional and cosmetic point of view. These characteristics include full reepithelialization, no detrimental wound contraction, normal color, a functional epidermal barrier, adequate blood flow, and normal skin hardness and elasticity. Image analysis of digital images was useful in determining the size of ulcers and general wound size, shape and contraction. Bioengineering methods were useful in evaluating multiple characteristics during wound healing: (1) reflectance colorimetry for skin color, (2) evaporimetry to measure transepidermal water loss as an indicator of barrier function, (3) laser Doppler perfusion imaging to assess cutaneous blood flow, and (4) ballistometry to measure the mechanical properties of hardness and elasticity. The image analysis and bioengineering methods not only were useful in providing important measurements, but also allowed us to non-invasively examine several parameters without having to perform multiple, invasive procedures. Histopathological evaluations conducted at the end of the study were important for making morphological correlates to changes noted by the non-invasive methods. Perhaps the most useful of the non-invasive methods were image analysis and evaporimetry, since reepithelialization, wound contraction, and barrier function were the best indicators of healed wounds. The use of reflectance colorimetry and ballistometry will continue in future wound healing studies for their added contributions in judging cosmetic and functional outcomes. While useful, laser Doppler perfusion imaging was found to be rather time consuming. This methodology will be limited in the future to burn depth estimation prior to treatment, and for evaluation of pharmaceuticals specifically designed to improve or sustain blood flow into damaged areas.

REFERENCES

1. Papirmeister B, Feister AJ, Robinson SI, Ford RD. Medical defense against mustard gas: toxic mechanisms and pharmacological implications. Boston: CRC Press, 1991. pp. 2-3, 14-32, 49, 61, 69, 79-86, 100-115, 174-199.

2. Somani SM, Babu SR. Toxicodynamics of sulfur mustard. Int J Clin Pharmacol Ther Toxicol 1989; 27(9):419-435.

3. Petrali JP, Oglesby SB, Mills KR. Ultrastructural correlates of sulfur mustard toxicity. J Toxicol-Cut & Ocular Toxicol 1990; 9(3):193-214.

4. Petrali JP, Oglesby SB, Hamilton TA, Mills KR. Ultrastructural pathology and immunohistochemistry of mustard gas lesion. Proceedings of the 1993 Medical Defense Bioscience Review, USAMRICD, APG, MD. pp. 15-20. AD A275667

5. Vogt RF, Dannenberg AM, Schofield BH, Hynes NA, Papirmeister B. Pathogenesis of skin lesions caused by sulfur mustard. Fund Appl Toxicol 1984; 4:S71-S83.

6. Monteiro-Riviere NA, King JR, Riviere JE. Mustard induced vesication in isolated perfused skin: biochemical, physiological, and morphological studies. Proceedings of the 1991 Medical Defense Bioscience Review, USAMRICD, APG, MD. pp. 159-162. AD-B158588.

7. Monteiro-Riviere NA, Inman AO. Histochemical localization of three basement membrane epitopes with sulfur mustard induced toxicity in porcine skin. Toxicologist 1993; 13:58.

8. Zhang Z, Peters BP, Monteiro-Riviere NA. Assessment of sulfur mustard interaction with basement membrane components. Cell Biol Toxicol 1995; 11(2):89-101.

9. Mitcheltree LW, Mershon MM, Wall HG, Pulliam JD, Manthei JH. Microblister formation in vesicant-exposed pig skin. J Toxicol-Cut & Ocular Toxicol 1989; 8(3):309-319.

10. Graham JS, Martin JL, Zallnick JE, Nalls CR, Mitcheltree LW, Lee RB, Logan TP, Braue EH. Assessment of cutaneous sulfur mustard injury in the weanling pig. Skin Res Technol 1999; 5(1):56-67.

11. Mellor SG, Rice P, Cooper GJ. Vesicant burns. Br J Plast Surg 1991; 44(6):434-437.

12. Requena L, Requena C, Sanchez M et al. Chemical warfare. J Am Acad Dermatol 1988; 19(3):529-536.

13. Borak J, Sidell FR. Agents of chemical warfare: sulfur mustard. Ann Emerg Med 1992; 21(3):303-308.

14. Orrenius S, Nicotera P. On the role of calcium in chemical toxicity. Arch Toxicol 1987; Suppl. 11:11-19.

15. Papirmeister B. Does apoptosis (programmed cell death) play a role in sulfur mustard injury? Medical Chemical Defense 1994; 7(1):1-12.

16. Braue EH, Mershon MM, Wade JV, Litchfield MR. In vivo assessment of vesicant skin injury using a Minolta Chroma Meter. J Soc Cosmet Chem 1990; 41:259-265.

17. Braue EH, Koplovitz I, Mitcheltree LW, Clayson ET, Litchfield MR, Bangledorf CR. Characterization of the sulfur mustard vapor induced cutaneous lesions on hairless guinea pigs. Toxicology Methods 1992; 2(4):242-254.

18. Dannenberg AM. Sulfur mustard (SM) lesions in organ-cultured human skin: markers of injury and inflammatory mediators. Final Report, U.S. Army Medical Research and Development Command, Fort Detrick, Frederick, MD, Contract No. DAMD17-87-C-7040, 1990. AD A227358

19. Graham JS, Bryant MA, Braue EH. Effect of sulfur mustard on mast cells in hairless guinea pig skin. J Toxicol-Cut & Ocular Toxicol 1994; 13(1):47-54.

20. Marlow DD, Mershon MM, Mitcheltree LW, Petrali JP, Jaax GP. Evaluation of euthymic hairless guinea pigs [crl:IAF(HA)BR] as an animal model for vesicant injury. J Toxicol-Cut & Ocular Toxicol 1990; 9(3):179-192.

21. Mershon MM, Mitcheltree LW, Petrali JP, Braue EH, Wade JV. Hairless guinea pig bioassay model for vesicant vapor exposures. Fund Appl Toxicol 1990; 15:622-630.

22. Moore KG, Schofield BH, Higuchi K et al. Two sensitive *in vitro* monitors of chemical toxicity to human and animal skin (in short-term organ culture): I. paranuclear vacuolization in glycol methacrylate tissue sections II. interference with [^{14}C]leucine incorporation. J Toxicol-Cut & Ocular Toxicol 1986; 5(4):285-302.

23. Papirmeister B, Gross CL, Petrali JP, Hixson CJ. Pathology produced by sulfur mustard in human skin grafts on athymic nude mice. I. Gross and light microscopic changes. J Toxicol-Cut & Ocular Toxicol 1984; 3(4):371-391.

24. Yourick JJ, Clark CR, Mitcheltree LW. Niacinamide pretreatment reduces microvesicle formation in sulfur mustard cutaneously exposed hairless guinea pigs. Fund Appl Toxicol 1991; 17:533-542.

25. Petrali JP, Oglesby SB, Justus TA. Morphologic effects of sulfur mustard on a human skin equivalent. J Toxicol-Cut & Ocular Toxicol 1991; 10(4): 315-324.

26. Petrali JP, Oglesby SB, Hamilton TA, Mills KR. Comparative morphology of sulfur mustard effects in the hairless guinea pig and a human skin equivalent. J Submicrosc Cytol Pathol 1993; 25(1):113-118.

27. King JR, Monteiro-Riviere NA. Cutaneous toxicity of 2-chloroethyl methyl sulfide in isolated perfused porcine skin. Toxicol Appl Pharmacol 1990; 104(1):167-179.

28. Petrali JP, Oglesby SB, Hamilton TA, Mills KR. Ultrastructural pathology and immunohistochemistry of mustard gas lesion. Proceedings of the 50th Annual Meeting of the Electron Microscopy Society of America, Aug 16-21, 1992, Boston, MA.

29. Henriques FC, Moritz AR, Breyfogle HS, Patterson LA. The mechanism of cutaneous injury by mustard gas. An experimental study using mustard prepared with radioactive sulfur. Washington, D.C.: Division 9, National Defense Research Committee of the Office of Scientific Research and Development, Contract No. NDCrc 169, Formal Progress Report, 1943. DTIC No. ATI 30343.

30. Ruhl CM, Park SJ, Danisa O et al. A serious skin sulfur mustard burn from an artillery shell. J Emerg Med 1994; 12(2):159-166.

31. Kadivar H, Adams SC. Treatment of chemical and biological warfare injuries: insights derived from the 1984 Iraqi attack on Majnoon Island. Military Medicine 1991; 156(4):171-177.

32. Sidell FR, Urbanetti JS, Smith WJ, Hurst CG. Vesicants. In: Sidell FR, Takafuji ET, Franz DR, editors. Textbook of Military Medicine, Part I: Warfare, Weaponry, and the Casualty - Medical Aspects of Chemical and Biological Warfare. Washington, D.C.: Office of the Surgeon General at TMM Publications, Borden Institute, Walter Reed Army Medical Center, 1997. pp. 197-228.

33. Kerstein MD, Bensing KA, Brill LR et al. The physiology of wound healing. Philadelphia: Oxford Institute for Continuing Education, 1998.

34. Stevens A, Lowe J, editors. Pathology. Baltimore: Mosby, 1995. pp. 69-71.

35. Hunt TK, Hopf H, Hussain Z. Physiology of wound healing. Adv Wound Care 2000; 13 (S2):6-11.

36. Schaefer H, Redelmeier TE. Skin barrier: principles of percutaneous absorption. New York: Karger, 1996. p. 22.

37. Nilsson GE. Measurement of water exchange through skin. Med Biol Eng. Comput 1977; 15(3):209-218.

38. Pinnagoda J, Tupker RA. Measurement of transepidermal water loss. In: Serup J, Jemec GBE, editors. Handbook of Non-Invasive Methods and the Skin. Boca Raton: CRC Press, 1995. pp. 173-178.

39. Barel AO, Clarys P. Comparison of methods for measurement of transepidermal water loss. In: Serup J, Jemec GBE, editors. Handbook of Non-Invasive Methods and the Skin. Boca Raton: CRC Press, 1995. pp. 179-184.

40. Gabard B, Elsner P, Treffel P. Barrier function of the skin in a repetitive irritation model and influence of 2 different treatments. Skin Res Technol 1996; 2(2):78-82.

41. Pinnagoda J, Tupker RA, Agner T, Serup J. Guidelines for transepidermal water loss (TEWL) measurement. Contact Dermatitis 1990; 22:164-178.

42. Bircher AJ. Laser Doppler measurement of skin blood flux: variation and validation. In: Serup J, Jemec GBE, editors. Handbook of Non-Invasive Methods and the Skin. Boca Raton: CRC Press, 1995. pp. 399-403.

43. Belcaro G, Nicolaides AN. Laser-Doppler flowmetry: principles of technology and clinical applications. In: Serup J, Jemec GBE, editors. Handbook of Non-Invasive Methods and the Skin. Boca Raton: CRC Press, 1995. pp. 405-410.

44. Wardell K, Andersson T, Anderson C. Analysis of laser Doppler perfusion images of experimental irritant skin reactions. Skin Res Technol 1996; 2(4):149-157.

45. Linden M, Wardell K, Andersson T, Anderson C. High resolution laser Doppler perfusion imaging for the investigation of blood circulatory changes after microdialysis probe insertion. Skin Res Technol 1997; 3(4):227-232.

46. Krogstad A-L, Pegenius G, Elam M. Visual scoring and laser Doppler perfusion imaging of skin irritancy induced by different nicotine patches. Skin Res Technol 1996; 2(4):158-163.

47. Wardell K, Nilsson G. Laser Doppler imaging of skin. In: Serup J, Jemec GBE, editors. Handbook of Non-Invasive Methods and the Skin. Boca Raton: CRC Press, 1995. pp. 421-428.

48. Alsbjorn B, Micheels J, Sorensen B. Laser Doppler flowmetry measurements of superficial dermal, deep dermal and subdermal burns. Scand J of Plast Reconstr Surgery 1984; 18:75-79.

49. Blomgren I, Bagge U. Postburn blood flow, edema, and survival of the hairy mouse ear after injury at different temperatures. Scand J of Plast Reconstr Surgery 1984; 18:269-275.

50. Garner WL, Thomson PD, Moore NP, Rodriguez JL, Smith DJ. Effect of triglycyl-lysine-vasopressin on skin blood flow and blood loss during wound excision in patients with burns. J Burn Care Rehabil 1993; 14(4):458-460.

51. Micheels J, Alsbjorn B, Sorensen B. Clinical use of laser Doppler flowmetry in a burns unit. Scand J of Plast Reconstr Surgery 1984; 18:65-73.

52. Niazi ZBM, Essex TJH, Papini R, Scott D, McLean NR, Black MJM. New laser Doppler scanner, a valuable adjunct in burn depth assessment. Burns 1993; 19(6):485-489.

53. O'Reilly TJ, Spence RJ, Taylor RM, Scheulen JJ. Laser Doppler flowmetry evaluation of burn wound depth. J Burn Care Rehabil 1989; Jan:1-6.

54. Regas FC, Ehrlich HP. Elucidating the vascular response to burns with a new rat model. J Trauma 1992; 32(5):557-563.

55. Shakespeare PG. Looking at burn wounds: the A.B. Wallace memorial lecture 1991. Burns 1992; 18(4):287-295.

56. Waxman K. Heated laser Doppler flow measurements to determine depth of burn injury. Am Surg 1989; June:541-543.

57. Heimbach D, Engrav L, Grube B, Marvin J. Burn depth: a review. World J. Surg. 1992; 16:10-15.

58. Brown RFR, Rice P, Bennett NJ. The use of laser Doppler imaging as an aid in clinical management decision making in the treatment of vesicant burns. Burns 1998; 24(8):692-698.

59. Chilcott RP, Brown RFR, Rice P. Non-invasive quantification of skin injury resulting from exposure to sulphur mustard and Lewisite vapours. Burns 2000; 26(3):245-250.

60. Hargens CW, Ballistometry. In: Serup J, Jemec GBE, editors. Handbook of Non-Invasive Methods and the Skin. Boca Raton: CRC Press, 1995. pp. 359-364.

61. Stender I-M, Nakagawa H, Shimozuma M, Søndergard J. Differentiation of inflicted burns by high-frequency ultrasound scanning: an animal experiment. Skin Res Technol 1996; 2(1):27-31.

62. Whipple TL, Caspari RB, Meyers JF. Laser subtotal meniscectomy in rabbits. Lasers Surg Med 1984; 3:297-304.

63. Hebda PA, Klingbeil CK, Abraham JA, Fiddes JC. Basic fibroblast growth factor stimulation of epidermal wound healing in pigs. J Invest Dermatol 1990; 95(6):626-631.

64. Montagna W, Yun JS. The skin of the domestic pig. J Invest Dermatol 1964; 43:11-21.

65. Swindle MM. Porcine models in surgical research: an overview. In: Tumbleson ME, editor. Swine in Biomedical Research. New York: Plenum Press, 1986. pp. 235-251.

66. Dick IP, Scott RC. Pig ear skin as an in-vitro model for human skin permeability. J Pharm Pharmacol 1992; 44:640-645.

67. EPA Research and Development-Interim Guidance for Dermal Exposure Assessment, Jan 1992. EPA/600/8-91/011B.

68. Klain GJ, Bonner SJ, Bell WG. The distribution of selected metabolic processes in the pig and human skin. In: Tumbleson ME, editor. Swine in Biomedical Research. New York: Plenum Press, 1986. pp. 667-671.

69. Meyer W, Schwarz R, Neurand K. Current problems in dermatology. Basel: Karger, 1978. Vol 7, pp. 39-52.

70. Rice P. The use of dermabrasion to accelerate the naturally slow rate of epidermal healing mustard injuries in pigs. Proceedings of the 1995 NATO Research Study Group - 3 Meeting on Prophylaxis and Therapy Against Chemical Agents, Chemical and Biological Defence Establishment, Porton Down, Salisbury, England.

71. Rice P, Brown RFR, Lam DGK, Chilcott RP, Bennett NJ. Dermabrasion – a novel concept in the surgical management of sulphur mustard injuries. Burns 2000; 26(1):34-40.

72. Kjellstr m BT, Persson JKE, Runn P. Surgical treatment of skin lesions induced by sulfur mustard ("mustard gas") – an experimental study in the guinea pig. Ann Acad Med Singapore 1997; 26(1):30-36.

73. Rice P, Bennett NJ, Lam DGK, Brown RFR. The role of dermabrasion in lewisite-induced skin injury. Proceedings of the 2000 Medical Defense Bioscience Review, USAMRICD, Hunt Valley, MD. p. 214.

74. Eldad A, Weinberg A, Breiterman S, Chaouat M, Palanker D, Ben-Bassat H. Early nonsurgical removal of chemically injured tissue enhances wound healing in partial thickness burns. Burns 1998; 24(2):166-172.

75. Graham JS, Smith KJ, Braue EH, Martin JL, Matterson PA, Tucker FS, Hurst CG, Hackley BE. Improved healing of sulfur mustard-induced cutaneous lesions in the weanling pig by pulsed CO_2 laser debridement. J Toxicol-Cut & Ocular Toxicol 1997; 16(4):275-295.

76. Acland KM, Barlow RJ. Lasers for the dermatologist. Br J Dermatol 2000; 143:244-255.

77. Walsh JT, Flotte TJ, Anderson RR, Deutsch TF. Pulsed CO_2 laser tissue ablation: Effect of tissue type and pulse duration on thermal damage. Lasers Surg Med 1988; 8:108-118.

78. Green HA, Burd EE, Nishioka NS, Compton CC. Skin graft take and healing following 193-nm excimer, continuous-wave carbon dioxide (CO_2), pulsed CO_2, or pulsed holmium:YAG laser ablation of the graft bed. Arch Dermatol 1993; 129:979-988.

79. Schoenrock LD, Chernoff WG, Rubach BW. Cutaneous UltraPulse® laser resurfacing of the eyelids. Int J Aesth Restor Surg 1995; 3(1):31-36.

80. Fitzpatrick RE, Goldman MP. Advances in carbon dioxide laser surgery. Clin Dermatol 1995; 13:35-47.

81. Fitzpatrick RE, Goldman MP, Ruiz-Esparza J. Clinical advantage of the CO_2 laser superpulsed mode. J Dermatol Surg Oncol 1994; 20:449-456.

82. Hobbs ER, Bailin PL, Wheeland RG, Ratz JL. Superpulsed lasers: minimizing thermal damage with short duration, high irradiance pulses. J Dermatol Surg Oncol 1987; 13:9.

83. Fitzpatrick RE, Goldman MP, Satur NM, Tope WD. Pulsed carbon dioxide laser resurfacing of photoaged facial skin. Arch Dermatol 1996; 132:395-402.

84. Hruza GJ. Laser skin resurfacing. Arch Dermatol 1996; 132:451-455.

85. Chernoff WG, Schoenrock LD, Cramer H, Wand J. Cutaneous laser resurfacing. Int J Aesth Restor Surg 1995; 3(1):57-58.

86. Stellar S, Levine N, Ger R, Levenson SM. Laser excision of acute third degree burns followed by immediate autograft replacement: an experimental study in the pig. J Trauma 1973; 13(1):45-53.

87. Fidler JP, Low E, Rockwell J et al. Carbon dioxide laser excision of acute burns with immediate autografting. J Surg Res 1974; 17:1-11.

88. Levine N, Ger R, Stellar S et al. Use of a carbon dioxide laser for the debridement of third degree burns. Ann Surg 1974; 179:246-259.

89. Levine NS, Salisbury RE, Peterson SM, Pruitt BA. Clinical evaluation of the carbon dioxide laser for burn wound excisions: a comparison of the laser, scalpel, and electrocautery. J Trauma 1975; 15(9):800-807.

90. Green HA, Burd E, Nishioka NS, Brŋggemann U, Compton CC. Middermal wound healing. Arch Dermatol 1992; 128:639-645.

91. Schomacker KT, Walsh JT, Flotte TJ, Deutsch TF. Thermal damage produced by high irradiance continuous wave CO_2 laser cutting of tissue. Lasers Surg Med 1990; 10:74-84.

92. Domankevitz Y, Nishioka NS. Effects of a rapidly scanned carbon dioxide laser on porcine dermis. J Burn Care Rehabil 1997; 18:206-209.

93. Glatter RD, Goldberg JS, Schomacker KT, Compton CC, Flotte TJ, Bua DP, Greaves KW, Nishioka NS, Sheridan RL. Carbon dioxide laser ablation with immediate autografting in a full-thickness porcine burn model. Annals of Surgery 1998; 228(2):257-265.

94. Sheridan RL, Lydon MM, Petras LM, Schomacker KT, Tompkins RG, Glatter RD, Parrish JA. Laser ablation of burns: initial clinical trial. Surgery 1999; 125(1):92-95.

95. Sullivan T, Smith J, Kermode J, McIver E, Courtemanche DJ. Rating the burn scar. J Burn Care Rehabil 1990; 11:256-260.

96. Nedelec B, Shankowsky HA, Tredget EE. Rating the resolving hypertrophic scar: comparison of the Vancouver Scar Scale and scar volume. J Burn Care Rehabil 2000; 21(3):205-212.

97. Baryza MJ, Baryza GA. The Vancouver Scar Scale: an administration tool and its interrater reliability. J Burn Care Rehabil 1995; 16(5):535-538.

98. Grove GL, Grove MJ, Zerweck C, Pierce E. Comparative metrology of the evaporimeter and the DermaLab® TEWL probe. Skin Res Technol 1999; 5(1):1-8.

99. Grove GL, Grove MJ, Zerweck C, Pierce E. Computerized evaporimetry using the DermaLab® TEWL probe. Skin Res Technol 1999; 5(1):9-13.

100. Walker HL, Mason AD. A standard animal burn. J Trauma 1968; 8(6):1049-1051.

101. Kleiber M. The fire of life: an introduction to animal energetics. New York: John Wiley & Sons, Inc., 1961. pp. 181-184.

102. Quiring DP. Surface-area determination. In: Glasser O, editor. Medical Physics, Vol. 1. Chicago: Yearbook, 1955. pp. 1490-1494.

103. Allan GM, Ellis, JA. Porcine circoviruses: a review. J Vet Diagn Invest 2000; 12:3-14.

104. Snowden JM. Wound contraction: a quantitative interpretation. Aust J Exp Biol Med Sci 1981; 59(Pt. 2):203-217.

105. Lawrence JC. Dressings for burns. In: Settle JAD, editor. Principles and Practice of Burns Management. New York: Churchill Livingstone, 1996. pp. 259-269.

106. Graham JS, Reid FM, Smith JR, Stotts RR, Tucker FS, Shumaker SM, Niemuth NA, Janny SJ. A cutaneous full-thickness liquid sulfur mustard burn model in weanling swine: clinical pathology and urinary excretion of thiodiglycol. J Appl Toxicol 2000; 20:S161-S172.

107. Rang HP, Dale MM, Ritter JM, Gardner P. Pharmacology. New York: Churchchill Livingstone, 1995. pp. 532-547.

108. Swindle MM. Surgery, anesthesia, and experimental techniques in swine. Ames: Iowa State University Press, 1998. pp.33-63.

109. Bollen PJ, Hansen AK, Rasmussen HJ. The laboratory swine. Boca Raton: CRC Press, 2000. pp. 61-82.

110. Carvalho DA, Mariani U, Gomez DS, Gemperli R, Ferreira MC. A study of the postburned restored skin. Burns 1999; 25(5):385-394.

111. Arturson G. Local effects. In: Settle JAD, editor. Principles and Practice of Burns Management. New York: Churchill Livingstone, 1996. pp. 83-94.

112. Tagami H, Kanamuru Y, Inoue KM, Suheisa S. Water sorption-desorption test of the skin *in vivo* for functional assessment of the stratum corneum. J Invest Dermatol 1992; 78:425-428.

113. Rodrigues L, Pinto P, Pereira LM. The quantitative assessment of the in vivo "barrier function." Skin Res Technol 2000; 6(3):171-172.

114. Settle JAD, Principles of replacement fluid therapy. In: Settle JAD, editor. Principles and Practice of Burns Management. New York: Churchill Livingstone, 1996. pp. 217-222.

115. Hinrichsen N, Birk-Sprensen L, Gottrup F, Hjortdal V. Wound contraction in an experimental porcine model. Scand J Plast Reconstr Hand Surg 1998; 32:243-248.

116. Langer C. On the anatomy and physiology of the skin. I. The cleavability of the cutis (translation). Br J Plast Surg 1978; 31:3-8.

117. McGrath MH, Simon RH. Wound geometry and the kinetics of wound contraction. Plast Reconstr Surg 1983; 72(1):66-72.

118. Tranquillo RT, Murray JD. Mechanistic model of wound contraction. J Surg Res 1993; 55(2):233-247.

119. Madison JB, Gronwall RR. Influence of wound shape on wound contraction in horses. Am J Vet Res 1992; 53(9):1575-1578.

120. Snowden JM, Kennedy DF, Cliff WJ. Wound contraction: the effects of scab formation and the nature of the wound bed. Aust J Exp Biol Med Sci 1982; 60(Pt. 1):73-82.

121. Fenton RCO. Disfigurement and disablement. In: Settle JAD, editor. Principles and Practice of Burns Management. New York: Churchill Livingstone, 1996. pp. 465-482.

122. Mekkes JR, Westerhof W. Image processing in the study of wound healing. Clin Dermatol 1995; 13(4):401-407.

123. Dykes P. Techniques for the localization of sweat glands. In: Serup J, Jemec GBE, editors. Handbook of Non-Invasive Methods and the Skin. Boca Raton: CRC Press, 1995. pp. 497-501.

124. Reid FM, Graham JS, Niemuth NA, Singer AW, Janny SJ. Sulfur mustard-induced skin burns in weanling swine evaluated clinically and histopathologically. J Appl Toxicol 2000; 20:S153-160.

125. Braue EH, Nalls CR, Way RA, Zallnick JE, Reider RG, Mitcheltree LW. Nikolsky's sign: a novel way to evaluate damage at the dermal-epidermal junction. Skin Res Technol 1997; 3(4): 245-251.

126. Greenhalgh DG, Gamelli RL, Lee M et al. Multicenter trial to evaluate the safety and potential efficacy of pooled human fibrin sealant for the treatment of burn wounds. J Trauma 1999; 46(3):433-440.

127. Green HA, Bua D, Anderson RR, Nishioka NS. Burn depth estimation using indocyanine green fluorescence. Arch Dermatol 1992; 128: 43-49.

128. Black KS, Hewitt CW, Miller DM et al. Burn depth evaluation with fluorometry: is it really definitive? J Burn Care Rehab 1986; 7:313-317.

129. Schomacker KT, Torri A, Sandison DR, Sheridan RL, Nishioka NS. Biodistribution of indocyanine green in a porcine burn model: light and fluorescence microscopy. J Trauma 1997; 43: 813-819.

130. Jerath MR, Schomacker KT, Sheridan RL, Nishioka NS. Burn wound assessment in porcine skin using indocyanine green fluorescence. J Trauma 1999; 46(6):1085-1088.

131. Sheridan RL, Schomacker KT, Lucchina LC et al. Burn depth estimation by use of indocyanine green fluorescence: initial human trial. J Burn Care Rehabil 1995: 16(6):602-604.

132. Sheridan RL, Tompkins RG. Skin substitutes in burns. Burns 1999; 25(2):97-103.

LIST OF ABBREVIATIONS

CODE	HEMATOLOGY TEST	UNITS
WBC	white blood cell count	thousands/uL
RBC	red blood cell count	millions/uL
HGB	hemoglobin	g/dL
HCT	hematocrit	percent
MCV	mean corpuscular volume	fL
MCH	mean corpuscular hemoglobin	pg
MCHC	mean corpuscular Hb concentration	g/dL
RDW	relative distribution size of platelets	%
PLT	platelet count	thousands/uL
MPV	mean platelet volume	fL
PCT	% platelets	percent
NEU %	neutrophils	% of WBC
LYM %	lymphocytes	% of WBC
MONO %	monocytes	% of WBC
EOS %	eosinophils	% of WBC
BASO %	basophils	% of WBC

CODE	CLINICAL CHEMISTRY TEST	UNITS
CPK	creatine phosphokinase	U/L
LDH	lactate dehydrogenase	U/L
AST	aspartate transaminase	U/L
ALT	alanine transaminase	U/L
ALP	alkaline phosphatase	U/L
AMY	amylase	U/L
BUN	blood urea nitrogen	mg/dL
CRE	creatinine	mg/dL
B/C	BUN:CRE ratio	-
TP	total protein	g/dL
ALB	albumin	g/dL
GLOB	globulin (TP-ALB)	g/dL
A/G	ALB:GLOB ratio	-
TBIL	total bilirubin	mg/dL
CAL	calcium	mg/dL
PHOS	phosphorus	mg/dL
GLU	glucose (hexokinase)	mg/dL
NA	sodium	mEq/L
K	potassium	mEq/L
CHLOR	chloride	mEq/L
MAG	magnesium	MEq/L

HISTOPATHOLOGY ABBREVIATIONS

0 = normal
1 = mild
2 = moderate
3 = severe
NA = not applicable
p = present
a = absent
s = superficial (super)
m = mid-dermal (mid)
d = deep dermal (deep)
F = focal
MF = multifocal
H = horizontal
V = vertical
D = disorganized
w = thin wisps
t = thick
nsl = no significant lesions

GENERAL ABBREVIATIONS

b:n = burn:normal
BSM = before sulfur mustard
BSURG = before surgery
F = fail (statistical tables)
FEV = failed equal variance test
FN = failed normality test
n = no
NT = non-treated
p = pass (statistical tables)
PS = post-surgical
sharp = sharp surgical tangential excision
SM = sulfur mustard
TBSA = total body surface area
TEWL = transepidermal water loss
Tx = treatment
TX1A = TX1A Burn Debridement Laser System
y = yes

Notes:

U = international unit; one U represents the enzyme activity that converts 1 umol substrate in one minute at 25 degrees Celsius.
mEq = milliequivalent (10^{-3} mole dividend by valence).

Preceding Page Blank

APPENDIX

Table 1. Two-Way Repeated Measures ANOVA Results, Grafting (graft/no graft) vs. Debridement (sharp/laser)

								Two Sample t-test				Paired t-test			
		Grafted		Debridement				TX1A/graft vs.		Sharp/graft vs.		Sharp vs. TX1A		Sharp vs. TX1A	
Parameter	Time	Difference?	P value	Difference?	P Value	Interaction?	P value	TX1A/no graft	P value	Sharp/no graft	P value	No graft group	P value	Grafted group	P value
Lightness	BSM	n	0.092	n	0.969	n	0.879								
	PS08	y	<0.001	n	0.211	n	0.397								
	PS15	y	<0.001	n	0.108	n	0.084								
	PS22	y	<0.001	n	0.109	n	0.064								
	PS29	y	<0.001	n	0.055	y	0.035	y	<0.001	y	<0.001	n	0.066	n	0.467
	PS36	y	<0.001	n	0.692	n	0.942								
Red/Green Balance	BSM	n	0.663	n	0.262	n	0.627								
	PS08	y	<0.001	n	0.839	n	0.348								
	PS15	n	0.622	n	0.361	n	0.648								
	PS22	y	<0.001	n	0.410	n	0.467								
	PS29	y	0.012	n	0.138	n	0.218								
	PS36	n	0.128	n	0.756	n	0.307								
Yellow/Blue Balance	BSM	n	0.515	n	0.996	n	0.975								
	PS08	y	<0.001	n	0.967	n	0.405								
	PS15	y	<0.001	n	0.220	n	0.122								
	PS22	y	<0.001	n	0.094	n	0.077								
	PS29	n	0.091	n	0.119	y	0.033	n	0.753	y	0.021	n	0.074	n	0.368
	PS36	n	0.086	n	0.992	y	0.033	y	0.012	n	0.575	n	0.206	n	0.065
"Color" Difference	BSM	n	0.109	n	0.983	n	0.391								
	PS08	y	<0.001	n	0.199	n	0.342								
	PS15	y	<0.001	n	0.138	n	0.092								
	PS22	y	<0.001	n	0.069	y	0.040	y	<0.001	y	<0.001	n	0.075	n	0.446
	PS29	y	<0.001	n	0.062	y	0.038	y	<0.001	y	0.001	n	0.072	n	0.436
	PS36	y	<0.001	n	0.728	n	0.976								
TEWL	BSM	n	0.143	n	0.602	n	0.490								
	PS08	y	<0.001	n	0.907	n	0.181								
	PS15	y	<0.001	n	0.666	n	0.100								
	PS22	y	<0.001	n	0.830	n	0.814								
	PS29	y	<0.001	n	0.169	y	0.009	y	<0.001	y (FN)	0.002	n (FN)	0.063	n	0.117
	PS36	y	<0.001	n	0.848	n	0.530								
B/N ratio	BSM	n	0.111	n	0.256	n	0.529								
	PS08	y	0.035	n	0.657	n	0.717								
	PS15	n	0.175	n	0.873	n	0.709								
	PS22	y	0.012	n	0.775	n	0.990								
	PS29	y	0.004	y	0.002	y	0.003	y	0.018	y	0.002	y	0.004	n	0.794
	PS36	n	0.104	n	0.147	n	0.403								

Table 1. Two-Way Repeated Measures ANOVA Results, Grafting (graft/no graft) vs. Debridement (sharp/laser)

								Two Sample t-test				Paired t-test			
		Grafted		Debridement				TX1A/graft vs.		Sharp/graft vs.		Sharp vs. TX1A		Sharp vs. TX1A	
Parameter	Time	Difference?	P value	Difference?	P Value	Interaction?	P value	TX1A/no graft	P value	Sharp/no graft	P value	No graft group	P value	Grafted group	P value
Indentation	BSM	y	0.049	n	0.492	n	0.247								
	PS08	y	<0.001	y	0.031	n	0.852								
	PS15	NA	NA	NA	NA	NA	NA								
	PS22	y	<0.001	n	0.394	n	0.104								
	PS29	y	<0.001	n	0.250	n	0.459								
	PS36	y	<0.001	n	0.401	y	0.044	y	0.007	y	<0.001	n	0.076	n	0.354
Elasticity	BSM	n	0.759	n	0.352	n	0.140								
	PS08	y	<0.001	n	0.052	n	0.930								
	PS15	NA	NA	NA	NA	NA	NA								
	PS22	y	<0.001	n	0.135	n	0.259								
	PS29	y	<0.001	n	0.052	n	0.052								
	PS36	y	<0.001	n	0.090	n	0.051								
Lesion Area	BSURG	y	0.013	n	0.192	n	0.904								
	PS08	y	<0.001	n	0.249	y	0.012	y	<0.001	y	<0.001	y	0.006	n	0.340
	PS15	y	<0.001	n	0.066	y	0.011	y	<0.001	y	<0.001	y	0.010	n	0.539
	PS22	y	<0.001	y	0.006	y	0.001	y	<0.001	y	<0.001	y	<0.001	n	0.581
	PS29	y	<0.001	n	0.072	y	0.007	y	<0.001	y	<0.001	y	0.008	n	0.433
	PS36	y	<0.001	y	0.018	y	0.012	y	<0.001	y	<0.001	y	0.002	n	0.913
Lesion Aspect Ratio	BSURG	n	0.934	n	0.982	n	0.802								
	PS08	n	0.797	n	0.174	y	0.001	y	0.028	n	0.102	y	0.039	y	0.020
	PS15	n	0.562	n	0.509	y	0.010	n	0.066	y	0.045	n	0.061	n	0.073
	PS22	n	0.467	n	0.291	y	0.002	n	0.171	y (FN)	0.009	n	0.067	y	0.021
	PS29	n	0.512	n	0.185	y	0.031	y	0.046	n	0.124	n	0.568	y	0.008
	PS36	n	0.411	n	0.140	n	0.062								
Lesion Roundness	BSURG	n	0.073	n	0.279	n	0.947								
	PS08	n	0.067	y	0.005	y	0.012	n	0.239	y	0.025	n	0.370	y	0.019
	PS15	y	0.017	y	0.006	y	0.002	n	0.301	y	0.002	n	0.632	y	0.006
	PS22	n	0.056	y	0.003	y	<0.001	n	0.134	y (FEV)	0.002	n	0.510	y	0.002
	PS29	n	0.099	n	0.107	n	0.140								
	PS36	y	0.018	y	0.032	n	0.125								
% TBSA (Contraction)	PS08	y	<0.001	y	0.014	n	0.484								
	PS15	y	<0.001	y	0.005	n	0.219								
	PS22	y	<0.001	y	0.006	n	0.125								
	PS29	y	<0.001	y	0.003	y	0.046	y	<0.001	y	<0.001	y	0.002	n	0.363
	PS36	y	<0.001	y	0.003	n	0.085								
Total Collagen Fraction	PS36	y	0.014	n	0.752	n	0.652								
New Collagen Fraction	PS36	y	<0.001	n	0.786	n	0.786								

Table 2. One-Way Repeated Measures ANOVA Results, no treatment vs. sharp/grafted vs. TX1A/grafted

Day	Parameter	Normality Test	Equal Variance	Statistical Difference?	P value	P < 0.050? sharp/graft vs. none	sharp/graft vs. TX1A/graft	TX1A/graft vs. none	ctrl vs TX1A/graft	ctrl vs. sharp/graft	ctrl vs. none
-2	lightness	p	p	n	0.981						
8	lightness	p	p	y	0.015	y	n	n			
15	lightness	p	p	y	< 0.001	y	n	y			
22	lightness	p	p	y	< 0.001	y	n	y			
29	lightness	p	p	y	< 0.001	y	n	y			
36	lightness	p	p	y	0.008	y	n	y			
-2	red/green	p	p	n	0.538						
8	red/green	p	p	y	0.021	n	n	y			
15	red/green	p	p	y	< 0.001	y	n	y			
22	red/green	p	p	y	< 0.001	y	n	y			
29	red/green	p	p	n	0.817						
36	red/green	p	p	n	0.481						
-2	yellow/blue	p	p	n	0.843						
8	yellow/blue	p	p	y	< 0.001	y	n	y			
15	yellow/blue	p	p	y	< 0.001	y	n	y			
22	yellow/blue	p	p	y	< 0.001	y	n	y			
29	yellow/blue	p	p	y	< 0.001	y	n	y			
36	yellow/blue	p	p	y	0.033	y	n	n			
-2	color difference	p	p	n	0.693						
8	color difference	p	p	y	0.001	y	n	y			
15	color difference	p	p	y	< 0.001	y	n	y			
22	color difference	p	p	y	< 0.001	y	n	y			
29	color difference	p	p	y	< 0.001	y	n	y			
36	color difference	p	p	y	0.009	y	n	y			
-2	b:n flux	p	p	n	0.579						
8	b:n flux	p	p	y	< 0.001	y	n	y			
15	b:n flux	p	p	y	< 0.001	y	n	y			
22	b:n flux	p	p	y	0.001	y	n	y			
29	b:n flux	p	p	n	0.871						
36	b:n flux	p	p	n	0.118						

Table 2. One-Way Repeated Measures ANOVA Results, no treatment vs. sharp/grafted vs. TX1A/grafted

Day	Parameter	Normality Test	Equal Variance	Statistical Difference?	P value	P < 0.050? sharp/graft vs. none	sharp/graft vs. TX1A/graft	TX1A/graft vs. none	ctrl vs TX1A/graft	ctrl vs. sharp/graft	ctrl vs. none
0	lesion area	p	p	n	0.573						
8	lesion area	p	p	y	< 0.001	y	n	y			
15	lesion area	p	p	y	< 0.001	y	n	y			
22	lesion area	p	p	y	< 0.001	y	n	y			
29	lesion area	p	p	y	< 0.001	y	n	y			
36	lesion area	p	p	y	< 0.001	y	n	y			
0	roundness	p	p	n	0.230						
8	roundness	p	p	y	0.002	y	y	n			
15	roundness	p	p	y	< 0.001	y	y	n			
22	roundness	p	p	y	< 0.001	y	y	n			
29	roundness	p	p	y	< 0.001	y	y	n			
36	roundness	p	p	y	< 0.001	n	y	y			
0	aspect ratio	p	p	n	0.317						
8	aspect ratio	p	p	y	0.002	y	y	n			
15	aspect ratio	p	p	n	0.074						
22	aspect ratio	p	p	y	0.014	y	y	n			
29	aspect ratio	p	p	y	0.003	y	y	n			
36	aspect ratio	p	p	y	0.020	n	y	n			
8	% TBSA	p	p	y	< 0.001	y	n	y			
15	% TBSA	p	p	y	< 0.001	y	n	y			
22	% TBSA	p	p	y	< 0.001	y	n	y			
29	% TBSA	p	p	y	< 0.001	y	n	y			
36	% TBSA	p	p	y	< 0.001	y	n	y			
-2	TEWL	p	p	y	< 0.001	n	n	n	y	y	y
8	TEWL	p	p	y	< 0.001	y	n	y	y	n	y
15	TEWL	p	p	y	< 0.001	y	n	y	y	n	y
22	TEWL	p	p	y	< 0.001	y	n	y	n	n	y
29	TEWL	p	p	y	< 0.001	y	n	y	n	n	y
36	TEWL	F	p	y	< 0.001	y	n	y	n	n	y

Table 2. One-Way Repeated Measures ANOVA Results, no treatment vs. sharp/grafted vs. TX1A/grafted

						P < 0.050?					
Day	Parameter	Normality Test	Equal Variance	Statistical Difference?	P value	sharp/graft vs. none	sharp/graft vs. TX1A/graft	TX1A/graft vs. none	ctrl vs TX1A/graft	ctrl vs. sharp/graft	ctrl vs. none
-2	elasticity	p	p	n	0.171						
8	elasticity	p	p	y	< 0.001	y	n	y	n	n	y
15	elasticity	p	p	y	0.040	NA	n	NA	n	n	NA
22	elasticity	p	p	y	0.036	NA	n	NA	n	y	NA
29	elasticity	p	p	y	0.002	NA	n	NA	y	y	NA
36	elasticity	p	p	y	< 0.001	y	n	y	n	n	y
-2	hardness	p	p	n	0.751						
8	hardness	p	p	y	< 0.001	y	n	n	y	y	y
15	hardness	p	p	y	< 0.001	NA	n	NA	y	y	NA
22	hardness	p	p	y	< 0.001	NA	n	NA	y	y	NA
29	hardness	p	p	y	< 0.001	NA	n	NA	y	y	NA
36	hardness	p	p	y	< 0.001	y	n	y	y	y	y
36	% collagen	F	p	n	0.834						
36	new:old collagen	p	p	y	<0.001	y	n	y			

Table 3. One-Way Repeated Measures ANOVA Results, no treatment vs. sharp/not grafted vs. TX1A/not grafted

Day	Parameter	Normality Test	Equal Variance	Statistical Difference?	P value	P < 0.050? sharp vs. none	sharp vs. TX1A	TX1A vs. none	ctrl vs TX1A	ctrl vs. sharp	ctrl vs. none
-2	lightness	p	p	n	0.986						
8	lightness	p	p	y	0.004	y	n	y			
15	lightness	p	p	y	0.001	y	n	y			
22	lightness	p	p	n	0.270						
29	lightness	p	p	y	0.018	n	n	y			
36	lightness	p	p	n	0.152						
-2	red/green	p	p	n	0.097						
8	red/green	p	p	y	0.011	y	n	y			
15	red/green	p	p	y	0.007	y	n	y			
22	red/green	p	p	n	0.201						
29	red/green	p	p	y	0.040	n	n	y			
36	red/green	p	p	n	0.108						
-2	yellow/blue	p	p	n	0.883						
8	yellow/blue	p	p	n	0.762						
15	yellow/blue	p	p	n	0.139						
22	yellow/blue	p	p	n	0.200						
29	yellow/blue	p	p	y	0.007	n	n	y			
36	yellow/blue	p	p	n	0.056						
-2	color difference	p	p	n	0.814						
8	color difference	p	p	y	0.002	y	n	y			
15	color difference	p	p	y	<0.001	y	n	y			
22	color difference	p	p	n	0.176						
29	color difference	p	p	y	0.016	n	n	y			
36	color difference	p	p	n	0.127						
-2	b:n flux	p	p	n	0.423						
8	b:n flux	p	p	y	<0.001	y	n	y			
15	b:n flux	p	p	n	0.126						
22	b:n flux	p	p	n	0.151						
29	b:n flux	p	p	y	0.002	n	y	y			
36	b:n flux	p	p	n	0.217						

Table 3. One-Way Repeated Measures ANOVA Results, no treatment vs. sharp/not grafted vs. TX1A/not grafted

Day	Parameter	Normality Test	Equal Variance	Statistical Difference?	P value	P < 0.050? sharp vs. none	sharp vs. TX1A	TX1A vs. none	ctrl vs TX1A	ctrl vs. sharp	ctrl vs. none
0	lesion area	p	p	n	0.638						
8	lesion area	p	p	y	0.017	n	y	n			
15	lesion area	p	p	y	0.003	n	y	y			
22	lesion area	p	p	y	<0.001	n	y	y			
29	lesion area	p	p	y	<0.001	n	y	y			
36	lesion area	p	p	y	<0.001	n	y	y			
0	roundness	p	p	n	0.776						
8	roundness	p	p	n	0.361						
15	roundness	p	p	n	0.602						
22	roundness	p	p	n	0.222						
29	roundness	p	p	n	0.645						
36	roundness	p	p	n	0.973						
0	aspect ratio	p	p	n	0.806						
8	aspect ratio	p	p	n	0.122						
15	aspect ratio	p	p	n	0.050						
22	aspect ratio	p	p	n	0.138						
29	aspect ratio	p	p	n	0.427						
36	aspect ratio	p	p	n	0.754						
8	% TBSA	p	p	y	0.001	n	y	y			
15	% TBSA	p	p	y	<0.001	n	y	y			
22	% TBSA	p	p	y	<0.001	n	y	y			
29	% TBSA	p	p	y	<0.001	n	y	y			
36	% TBSA	p	p	y	<0.001	n	y	y			
-2	TEWL	p	p	y	0.004	n	n	n	y	y	y
8	TEWL	p	p	y	<0.001	n	n	n	y	y	y
15	TEWL	p	p	y	<0.001	n	n	n	y	y	y
22	TEWL	p	p	y	<0.001	n	n	n	y	y	y
29	TEWL	p	p	y	<0.001	n	n	n	y	y	y
36	TEWL	p	p	y	<0.001	n	n	n	y	y	y

Table 3. One-Way Repeated Measures ANOVA Results, no treatment vs. sharp/not grafted vs. TX1A/not grafted

Day	Parameter	Normality Test	Equal Variance	Statistical Difference?	P value	P < 0.050? sharp vs. none	sharp vs. TX1A	TX1A vs. none	ctrl vs TX1A	ctrl vs. sharp	ctrl vs. none
-2	elasticity	F	p	y	0.019	n	n	n	n	y	n
8	elasticity	p	p	y	<0.001	y	n	n	y	y	y
15	elasticity	p	p	y	0.011	NA	n	NA	y	y	NA
22	elasticity	p	p	y	<0.001	n	n	n	y	y	y
29	elasticity	p	p	y	<0.001	n	y	n	y	y	y
36	elasticity	p	p	y	<0.001	n	y	n	y	y	y
-2	hardness	p	p	n	0.209						
8	hardness	p	p	y	<0.001	n	n	n	y	y	y
15	hardness	p	p	y	<0.001	NA	n	NA	y	y	NA
22	hardness	p	p	y	<0.001	n	n	n	y	y	y
29	hardness	p	p	y	<0.001	n	n	n	y	y	y
36	hardness	p	p	y	<0.001	n	n	n	y	y	y
36	% collagen	p	p	n	0.796						
36	new:old collagen	F	p	n	<0.001	n	n	n			

Table 4. Bonferroni Adjusted t-Test Results, sham vs. other treatment groups

		Sharp/graft					
		Normality	Equal	Statistical		M-W RS	
Day	Parameter	Test	Variance	Difference?	P value	Difference?	P value
-2	lightness	p	p	n	0.920		
8	lightness	p	p	y	<0.001		
15	lightness	p	p	y	<0.001		
22	lightness	p	p	y	<0.001		
29	lightness	p	p	y	<0.001		
36	lightness	p	p	y	<0.001		
-2	red/green	p	p	n	0.034		
8	red/green	p	p	n	0.650		
15	red/green	F	p	n	0.514	n	0.068
22	red/green	F	p	n	0.104	n	0.263
29	red/green	F	p	n	0.036	y	0.008
36	red/green	p	p	n	0.012		
-2	yellow/blue	p	p	n	0.268		
8	yellow/blue	p	p	y	<0.001		
15	yellow/blue	p	p	y	0.005		
22	yellow/blue	p	p	y	<0.001		
29	yellow/blue	p	p	y	0.005		
36	yellow/blue	p	p	n	0.034		
-2	color difference	p	p	n	0.035		
8	color difference	p	p	y	<0.001		
15	color difference	p	p	y	<0.001		
22	color difference	p	p	y	<0.001		
29	color difference	p	p	y	<0.001		
36	color difference	p	p	y	<0.001		
-2	b:n flux	F	p	n	0.788	n	0.517
8	b:n flux	p	p	y	<0.001		
15	b:n flux	p	p	y	<0.001		
22	b:n flux	F	p	y	<0.001	y	0.002
29	b:n flux	p	p	y	<0.001		
36	b:n flux	p	p	y	<0.001		
8	% TBSA	p	p	y	0.003		
15	% TBSA	p	p	y	0.007		
22	% TBSA	p	p	y	0.008		
29	% TBSA	p	p	y	0.008		
36	% TBSA	p	p	n	0.032		
-2	TEWL	p	p	n	0.369		
8	TEWL	p	p	y	<0.001		
15	TEWL	p	F	n	0.025	n	0.087
22	TEWL	p	p	n	0.031		
29	TEWL	p	p	n	0.015		
36	TEWL	p	p	n	0.027		
-2	hardness	p	p	n	0.587		
8	hardness	p	p	n	0.012		
15	hardness	p	p	y	0.001		
22	hardness	p	p	y	0.007		
29	hardness	p	p	y	0.002		
36	hardness	p	p	y	<0.001		
-2	elasticity	p	p	n	0.801		
8	elasticity	p	p	n	0.353		
15	elasticity	p	p	n	0.454		
22	elasticity	p	p	n	0.517		
29	elasticity	p	p	n	0.162		
36	elasticity	p	p	n	0.076		
36	% collagen	p	p	y	<0.001		
36	new:old collagen	F	p	y	0.007	n	0.037

Table 4. Bonferroni Adjusted t-Test Results, sham vs. other treatment groups

		TX1A/graft					
		Normality	Equal	Statistical		M-W RS	
Day	Parameter	Test	Variance	Difference?	P value	Difference?	P value
-2	lightness	p	p	n	0.820		
8	lightness	F	p	y	<0.001	y	0.002
15	lightness	p	p	y	<0.001		
22	lightness	p	p	y	<0.001		
29	lightness	p	p	y	<0.001		
36	lightness	p	p	y	<0.001		
-2	red/green	p	p	n	0.049		
8	red/green	p	p	n	0.048		
15	red/green	p	p	n	0.064		
22	red/green	p	p	n	0.080		
29	red/green	p	p	n	0.023		
36	red/green	p	p	n	0.018		
-2	yellow/blue	p	p	n	0.235		
8	yellow/blue	p	p	y	0.009		
15	yellow/blue	p	p	y	<0.001		
22	yellow/blue	p	p	y	<0.001		
29	yellow/blue	p	p	y	0.006		
36	yellow/blue	F	p	y	0.002	y	0.006
-2	color difference	p	p	n	0.015		
8	color difference	F	p	y	<0.001	y	0.002
15	color difference	p	F	y	<0.001	y	0.002
22	color difference	p	F	y	<0.001	y	0.002
29	color difference	p	F	y	<0.001	y	0.002
36	color difference	p	p	y	0.002		
-2	b:n flux	p	p	n	0.979		
8	b:n flux	p	p	y	<0.001		
15	b:n flux	p	p	y	<0.001		
22	b:n flux	F	p	y	<0.001	y	0.002
29	b:n flux	p	p	y	<0.001		
36	b:n flux	p	p	y	<0.001		
8	% TBSA	p	p	y	<0.001		
15	% TBSA	p	p	y	<0.001		
22	% TBSA	p	p	y	<0.001		
29	% TBSA	p	p	y	<0.001		
36	% TBSA	p	p	y	0.005		
-2	TEWL	p	p	n	0.327		
8	TEWL	F	p	y	0.005	y	0.002
15	TEWL	p	p	n	0.015		
22	TEWL	p	p	y	<0.001		
29	TEWL	p	p	y	0.002		
36	TEWL	p	p	y	<0.001		
-2	hardness	p	p	n	0.817		
8	hardness	p	p	y	<0.001		
15	hardness	p	p	y	0.003		
22	hardness	p	p	y	0.003		
29	hardness	p	p	y	0.003		
36	hardness	p	p	y	<0.001		
-2	elasticity	p	p	n	0.929		
8	elasticity	p	p	n	0.235		
15	elasticity	p	p	n	0.451		
22	elasticity	p	p	n	0.919		
29	elasticity	p	p	n	0.204		
36	elasticity	p	p	n	0.016		
36	% collagen	p	p	y	0.008		
36	new:old collagen	F	p	y	0.006	y	0.009

Table 4. Bonferroni Adjusted t-Test Results, sham vs. other treatment groups

		No Treatment					
Day	Parameter	Normality Test	Equal Variance	Statistical Difference?	P value	M-W RS Difference?	P value
-2	lightness	p	p	n	0.741		
8	lightness	p	p	y	<0.001		
15	lightness	p	F	y	<0.001	y	<0.001
22	lightness	p	F	y	<0.001	y	<0.001
29	lightness	F	p	y	<0.001	y	<0.001
36	lightness	F	p	y	<0.001	y	<0.001
-2	red/green	p	p	n	0.034		
8	red/green	p	F	n	0.573	n	0.594
15	red/green	p	p	y	<0.001		
22	red/green	F	p	n	0.270	n	0.214
29	red/green	F	p	n	0.015	n	0.012
36	red/green	p	p	y	0.002		
-2	yellow/blue	p	p	n	0.269		
8	yellow/blue	p	F	y	<0.001	y	<0.001
15	yellow/blue	p	F	y	<0.001	y	<0.001
22	yellow/blue	p	p	y	<0.001		
29	yellow/blue	p	p	y	<0.001		
36	yellow/blue	p	p	y	<0.001		
-2	color difference	p	p	n	0.111		
8	color difference	F	p	y	<0.001	y	<0.001
15	color difference	p	F	y	<0.001	y	<0.001
22	color difference	p	F	y	<0.001	y	<0.001
29	color difference	F	p	y	<0.001	y	<0.001
36	color difference	p	F	y	<0.001	y	<0.001
-2	b:n flux	p	p	n	0.470		
8	b:n flux	p	p	y	<0.001		
15	b:n flux	p	p	y	<0.001		
22	b:n flux	F	p	y	<0.001	y	<0.001
29	b:n flux	p	p	n	0.017		
36	b:n flux	p	p	y	<0.001		
8	% TBSA	p	p	y	0.006		
15	% TBSA	p	p	y	<0.001		
22	% TBSA	p	p	y	<0.001		
29	% TBSA	p	p	y	<0.001		
36	% TBSA	p	p	y	<0.001		
-2	TEWL	p	p	n	0.896		
8	TEWL	F	p	y	<0.001	y	<0.001
15	TEWL	p	F	y	<0.001	y	<0.001
22	TEWL	F	F	y	<0.001	y	<0.001
29	TEWL	F	p	y	<0.001	y	<0.001
36	TEWL	F	p	y	<0.001	y	<0.001
-2	hardness	p	p	n	0.794		
8	hardness	p	p	y	<0.001		
15	hardness	NA	NA	NA	NA		
22	hardness	p	p	y	<0.001		
29	hardness	p	p	y	<0.001		
36	hardness	p	p	y	<0.001		
-2	elasticity	F	p	n	0.429	n	0.915
8	elasticity	p	p	y	<0.001		
15	elasticity	NA	NA	NA	NA		
22	elasticity	p	F	y	<0.001	y	0.007
29	elasticity	p	p	y	<0.001		
36	elasticity	F	p	y	<0.001	y	<0.001
36	% collagen	p	p	y	<0.001		
36	new:old collagen	F	p	y	<0.001	y	<0.001

Table 4. Bonferroni Adjusted t-Test Results, sham vs. other treatment groups

		Sharp/no graft					
Day	Parameter	Normality Test	Equal Variance	Statistical Difference?	P value	M-W RS Difference?	P value
-2	lightness	p	p	n	0.481		
8	lightness	p	F	y	<0.001	y	0.002
15	lightness	p	p	y	<0.001		
22	lightness	p	p	y	<0.001		
29	lightness	F	p	y	<0.001	y	0.002
36	lightness	p	p	y	<0.001		
-2	red/green	p	p	n	0.012		
8	red/green	p	p	y	<0.001		
15	red/green	p	p	n	0.499		
22	red/green	F	p	y	0.003	n	0.039
29	red/green	F	p	y	0.002	y	0.002
36	red/green	p	p	y	0.005		
-2	yellow/blue	p	p	n	0.469		
8	yellow/blue	F	p	y	<0.001	y	0.002
15	yellow/blue	p	p	y	<0.001		
22	yellow/blue	p	p	y	<0.001		
29	yellow/blue	F	F	y	<0.001	y	0.002
36	yellow/blue	p	p	n	0.220		
-2	color difference	p	p	n	0.184		
8	color difference	p	p	y	<0.001		
15	color difference	F	p	y	<0.001	y	0.002
22	color difference	p	F	y	<0.001	y	0.002
29	color difference	F	F	y	<0.001	y	0.002
36	color difference	p	p	y	<0.001		
-2	b:n flux	p	p	n	0.099		
8	b:n flux	p	p	y	<0.001		
15	b:n flux	p	p	y	<0.001		
22	b:n flux	p	p	n	0.056		
29	b:n flux	p	p	n	0.511		
36	b:n flux	p	p	y	<0.001		
8	% TBSA	p	p	n	0.085		
15	% TBSA	p	p	y	0.003		
22	% TBSA	p	p	y	<0.001		
29	% TBSA	p	p	y	<0.001		
36	% TBSA	p	p	y	<0.001		
-2	TEWL	p	p	n	0.973		
8	TEWL	p	p	y	<0.001		
15	TEWL	F	p	y	<0.001	y	0.002
22	TEWL	F	F	y	<0.001	y	0.002
29	TEWL	F	p	y	<0.001	y	0.002
36	TEWL	F	F	y	<0.001	y	0.002

Table 4. Bonferroni Adjusted t-Test Results, sham vs. other treatment groups

		TX1A/no graft					
Day	Parameter	Normality Test	Equal Variance	Statistical Difference?	P value	M-W RS Difference?	P value
-2	lightness	p	p	n	0.475		
8	lightness	F	p	y	<0.001	y	0.002
15	lightness	p	p	y	<0.001		
22	lightness	p	F	y	<0.001	y	0.002
29	lightness	p	p	y	<0.001		
36	lightness	p	p	y	<0.001		
-2	red/green	p	p	n	0.047		
8	red/green	F	p	y	<0.001	n	0.029
15	red/green	p	F	n	0.045	n	0.112
22	red/green	F	F	y	0.010	n	0.039
29	red/green	F	p	y	<0.001	y	0.002
36	red/green	p	p	y	<0.001		
-2	yellow/blue	p	p	n	0.518		
8	yellow/blue	F	p	y	<0.001	y	0.002
15	yellow/blue	p	p	y	<0.001		
22	yellow/blue	p	F	y	<0.001	y	0.002
29	yellow/blue	p	F	n	0.044	n	0.175
36	yellow/blue	p	p	n	0.984		
-2	color difference	p	p	n	0.532		
8	color difference	F	p	y	<0.001	y	0.002
15	color difference	F	p	y	<0.001	y	0.002
22	color difference	F	F	y	<0.001	y	0.002
29	color difference	p	F	y	<0.001	y	0.002
36	color difference	p	p	y	<0.001		
-2	b:n flux	p	p	n	0.409		
8	b:n flux	p	p	y	<0.001		
15	b:n flux	p	p	y	<0.001		
22	b:n flux	F	p	y	0.005	n	0.022
29	b:n flux	p	p	y	0.001		
36	b:n flux	p	p	y	<0.001		
8	% TBSA	p	p	n	0.045		
15	% TBSA	p	p	n	0.200		
22	% TBSA	p	p	n	0.201		
29	% TBSA	p	p	n	0.135		
36	% TBSA	p	p	n	0.137		
-2	TEWL	p	p	n	0.496		
8	TEWL	p	p	y	<0.001		
15	TEWL	p	F	y	<0.001	y	0.002
22	TEWL	F	p	y	<0.001	y	0.002
29	TEWL	F	p	y	<0.001	y	0.002
36	TEWL	F	F	y	<0.001	y	0.002
-2	hardness	p	p	n	0.661		
8	hardness	p	p	y	<0.001		
15	hardness	p	p	y	<0.001		
22	hardness	p	p	y	<0.001		
29	hardness	p	p	y	<0.001		
36	hardness	p	p	y	<0.001		
-2	elasticity	p	p	n	0.480		
8	elasticity	p	p	y	<0.001		
15	elasticity	p	p	y	<0.001		
22	elasticity	p	p	y	<0.001		
29	elasticity	p	p	y	<0.001		
36	elasticity	p	p	y	0.006		
36	% collagen	p	p	y	<0.001		
36	new:old collagen	F	p	y	<0.001	y	0.002

Table 5. One-Way Repeated Measures ANOVA Results, wound contraction over time

Day	Parameter	Normality Test	Equal Variance	Statistical Difference?	P value	Post-surgical Day									
						8 v 36	8 v 29	8 v 22	8 v 15	15 v 36	15 v 29	15 v 22	22 v 36	22 v 29	29 v 36
sharp/graft	% TBSA	p	p	n	0.466										
sharp/no graft	% TBSA	p	p	y	<0.001	y	y	y	y	y	y	y	n	n	n
TX1A/graft	% TBSA	p	p	n	0.652										
TX1A/no graft	% TBSA	p	p	y	<0.001	y	y	y	n	y	y	y	n	n	n
not treated	% TBSA	p	p	y	<0.001	y	y	y	y	y	y	y	y	y	n
sham	% TBSA	p	p	n	0.258										

Table 6. Pathology scores of biopsies taken at 48 hours post-exposure

		FT Epidermal Necrosis (p/a)	Micro-blisters (p/a)	BV Congestion (p/a)	Dermal Hemorrhage (p/a)	Dermal Coagulation (p/a)	Coagulation Depth (s/m/d)	Edema in Dermis (p/a)	Edema in Adipose (p/a)	Edema in Muscle (p/a)	Follicular Necrosis (p/a)	Sweat Gland Necrosis (p/a)	Sweat Gland Epithelial Cell Swelling (p/a)	Muscle Necrosis (0-3)	Adipose Necrosis (0-3)	Inflamm. Cell Infiltration (0-3)
	Totals															
	Count	12	12	12	12	12	12	12	12	12	12	12	12	12	12	12
SM: no	# absent	12	12	12	12	12		12	12	8	12	10	5			
	# present	0	0	0	0	0		0	0	0	0	0	5			
(controls on SM-exposed pigs)	# na						12			4		2	2	4		
	# super						0									
	# mid						0									
	# deep						0									
	# 0													8	12	12
	# 1													0	0	0
	# 2													0	0	0
	# 3													0	0	0
	Totals															
	Count	3	3	3	3	3	3	3	3	3	3	3	3	3	3	3
SM: no	# absent	3	3	3	3	3		3	3	2	3	3	2			
	# present	0	0	0	0	0		0	0	0	0	0	1			
(controls on sham pigs)	# na						3			1				1		
	# super						0									
	# mid						0									
	# deep						0									
	# 0													2	3	3
	# 1													0	0	0
	# 2													0	0	0
	# 3													0	0	0
	Totals															
	Count	72	72	72	72	72	72	72	72	72	72	72	72	72	72	72
SM: yes	# absent	0	72	0	1	61		0	0	24	1	19	33			
	# present	72	0	72	71	11		72	72	20	64	38	24			
	# na						61			28	7	15	15	28		
	# super						1									
	# mid						5									
	# deep						5									
	# 0													43	72	0
	# 1													1	0	72
	# 2													0	0	0
	# 3													0	0	0

Table 7. Pathology scores of samples taken at 36 days post-surgery

			Dermal Collagen Invading Muscle (0-3)	Full Re-epith. (p/a)	Marked Epidermal Hyperplasia (p/a)	Marked Hyper-keratosis (p/a)	Marked Para-keratosis (p/a)	Micro-granulomas (p/a)	MG Distribution (F/MF)	Rete Ridge Pattern (p/a)	Hair Follicles (p/a)
		Totals									
		Count	24	24	24	24	24	24	24	24	24
SM:	no; ventral control sites	# absent		0	24	24	24	24		0	0
	on SM-exposed pigs	# present		24	0	0	0	0		24	24
Tx:	none	# focal							0		
Grafted:	no	# m. focal							0		
		# na							24		
		# 0	24								
		# 1	0								
		# 2	0								
		# 3	0								
		Totals									
		Count	6	6	6	6	6	6	6	6	6
SM:	sham sites 1,4	# absent		0	6	6	6	6		0	0
Tx:	none	# present		6	0	0	0	0		6	6
Grafted:	no	# focal							0		
		# m. focal							0		
		# na							6		
		# 0	6								
		# 1	0								
		# 2	0								
		# 3	0								
		Totals									
		Count	6	6	6	6	6	6	6	6	6
SM:	sham sites 2,5	# absent		0	6	6	6	6		0	0
Tx:	none	# present		6	0	0	0	0		6	6
Grafted:	no	# focal							0		
		# m. focal							0		
		# na							6		
		# 0	6								
		# 1	0								
		# 2	0								
		# 3	0								
		Totals									
		Count	6	6	6	6	6	6	6	6	6
SM:	sham sites 3,6	# absent		0	6	6	6	6		0	0
Tx:	none	# present		6	0	0	0	0		6	6
Grafted:	no	# focal							0		
		# m. focal							0		
		# na							6		
		# 0	6								
		# 1	0								
		# 2	0								
		# 3	0								
		Totals									
		Count	6	6	6	6	6	6	6	6	6
SM:	sham sites 7,8	# absent		0	6	6	6	6		0	0
Tx:	none	# present		6	0	0	0	0		6	6
Grafted:	no	# focal							0		
		# m. focal							0		
		# na							6		
		# 0	6								
		# 1	0								
		# 2	0								
		# 3	0								

Table 7. Pathology scores of samples taken at 36 days post-surgery

			Dermal Collagen Invading Muscle (0-3)	Full Re-epith. (p/a)	Marked Epidermal Hyperplasia (p/a)	Marked Hyper-keratosis (p/a)	Marked Para-keratosis (p/a)	Micro-granulomas (p/a)	MG Distribution (F/MF)	Rete Ridge Pattern (p/a)	Hair Follicles (p/a)
		Totals									
		Count	12	12	12	12	12	12	12	12	12
SM:	yes	# absent		6	0	0	0	4		0	11
Tx:	sharp surgical	# present		6	12	12	12	8		12	1
Grafted:	no	# focal							2		
		# m. focal							6		
		# na							4		
		# 0	3								
		# 1	2								
		# 2	5								
		# 3	2								
		Totals									
		Count	24	24	24	24	24	24	24	24	24
SM:	yes	# absent		11	0	0	0	11		0	17
Tx:	none	# present		13	24	24	24	13		24	7
Grafted:	no	# focal							6		
		# m. focal							7		
		# na							11		
		# 0	11								
		# 1	4								
		# 2	4								
		# 3	5								
		Totals									
		Count	12	12	12	12	12	12	12	12	12
SM:	yes	# absent		4	0	0	4	1		0	3
Tx:	laser	# present		8	12	12	8	11		12	9
Grafted:	no	# focal							3		
		# m. focal							8		
		# na							1		
		# 0	4								
		# 1	1								
		# 2	3								
		# 3	4								
		Totals									
		Count	12	12	12	12	12	12	12	12	12
SM:	yes	# absent		0	12	12	12	1		0	0
Tx:	Sharp surgical	# present		12	0	0	0	11		12	12
Grafted:	yes	# focal							4		
		# m. focal							7		
		# na							1		
		# 0	10								
		# 1	1								
		# 2	1								
		# 3	0								
		Totals									
		Count	12	12	12	12	12	12	12	12	12
SM:	yes	# absent		0	12	12	12	0		0	0
Tx:	laser	# present		12	0	0	0	12		12	12
Grafted:	yes	# focal							5		
		# m. focal							7		
		# na							0		
		# 0	8								
		# 1	0								
		# 2	1								
		# 3	3								

Table 8. Pathology scores of samples taken at 36 days post-surgery

			Light Microscopy on Pentachrome-Stained Tissue						
			Elastic Fibers in Reticular Dermis (p/a)	Reticular Orientation (H/V/D)	Reticular Fiber Thickness (w/t)	Elastic Fibers in Papillary Dermis (p/a)	Papillary Orientation (H/V/D)	Papillary Fiber Thickness (w/t)	Fibers in Hypodermis (w/t)
		Totals							
		Count	24	24	24	24	24	24	24
SM:	no; ventral control sites	# absent	0			2			
	on SM-exposed pigs	# present	24			22			
Tx:	none	# H		24			0		
Grafted:	no	# V		0			22		
		# D		0			0		
		# na		0			2	2	0
		# w			1			22	3
		# t			23			0	21
		Totals							
		Count	6	6	6	6	6	6	6
SM:	sham sites 1,4	# absent	0			0			
Tx:	none	# present	6			6			
Grafted:	no	# H		6			0		
		# V		0			6		
		# D		0			0		
		# na		0	0		0	0	0
		# w			0			6	2
		# t			6			0	4
		Totals							
		Count	6	6	6	6	6	6	6
SM:	sham sites 2,5	# absent	0			0			
Tx:	none	# present	6			6			
Grafted:	no	# H		6			0		
		# V		0			6		
		# D		0			0		
		# na		0	0		0	0	0
		# w			0			6	1
		# t			6			0	5
		Totals							
		Count	6	6	6	6	6	6	6
SM:	sham sites 3,6	# absent	0			0			
Tx:	none	# present	6			6			
Grafted:	no	# H		6			0		
		# V		0			6		
		# D		0			0		
		# na		0	0		0	0	0
		# w			0			6	0
		# t			6			0	6
		Totals							
		Count	6	6	6	6	6	6	6
SM:	sham sites 7,8	# absent	0			0			
Tx:	none	# present	6			6			
Grafted:	no	# H		6			0		
		# V		0			6		
		# D		0			0		
		# na		0	0		0	0	0
		# w			0			6	0
		# t			6			0	6

Table 8. Pathology scores of samples taken at 36 days post-surgery

		Light Microscopy on Pentachrome-Stained Tissue						
		Elastic Fibers in Reticular Dermis (p/a)	Reticular Orientation (H/V/D)	Reticular Fiber Thickness (w/t)	Elastic Fibers in Papillary Dermis (p/a)	Papillary Orientation (H/V/D)	Papillary Fiber Thickness (w/t)	Fibers in Hypodermis (w/t)
	Totals							
	Count	12	12	12	12	12	12	12
SM: yes	# absent	0			12			
Tx: sharp surgical	# present	12			0			
Grafted: no	# H		2			0		
	# V		0			0		
	# D		10			0		
	# na		0	0		12	12	0
	# w			10			0	6
	# t			2			0	6
	Totals							
	Count	24	24	24	24	24	24	24
SM: yes	# absent	0			24			
Tx: none	# present	24			0			
Grafted: no	# H		8		0	0		
	# V		0			0		
	# D		16			0		
	# na		0	0		24	24	0
	# w			16			0	13
	# t			8			0	11
	Totals							
	Count	12	12	12	12	12	12	12
SM: yes	# absent	0			12			
Tx: laser	# present	12			0			
Grafted: no	# H		2			0		
	# V		0			0		
	# D		10			0		
	# na		0	0		12	12	0
	# w			10			0	8
	# t			2			0	4
	Totals							
	Count	12	12	12	12	12	12	12
SM: yes	# absent	0			0			
Tx: sharp surgical	# present	12			12			
Grafted: yes	# H		3			0		
	# V		0			12		
	# D		9			0		
	# na		0	0		0	0	0
	# w			11			12	7
	# t			1			0	5
	Totals							
	Count	12	12	12	12	12	12	12
SM: yes	# absent	0			2			
Tx: laser	# present	12			10			
Grafted: yes	# H		5			0		
	# V		0			10		
	# D		7			0		
	# na		0	0		2	2	0
	# w			11			10	7
	# t			1			0	5

Table 9. Pathology incidence summary table.

TISSUE	LESION	SM-Exposed TOTAL AFFECTED	SM-Exposed OUT OF	Sham-Exposed TOTAL AFFECTED	Sham-Exposed OUT OF
Liver	no significant lesions (nsl)	10	12	3	3
	hepatitis, portal (mild)	2	12	0	0
Gall Bladder	no significant lesions (nsl)	6	7	1	1
	edema, submucosal + lymphatic dilation	1	7	0	1
Kidney	no significant lesions (nsl)	8	9	1	1
	nephritis, interstitial w/ tubular and glomerular protein	1	9	0	1
Heart (LV)	no significant lesions (nsl)	12	12	3	3
Spleen	no significant lesions (nsl)	11	12	3	3
	congestion, acute, marked	1	12	0	3
Pancreas	no significant lesions (nsl)	12	12	3	3
Adrenals	no significant lesions (nsl)	12	12	3	3
U. Bladder	no significant lesions (nsl)	10	11	2	2
	cyctitis	1	11	0	2
Lung	no significant lesions (nsl)	1	12	0	3
	pneumonia, interstitial	11	12	3	3
	type II pneumocyte hyperplasia	3	12	0	3
	peribronchiolar lymphoid hyperplasia	4	12	1	3
	syncytial cells	1	12	0	3
	multinucleated giant cells	1	12	0	3
	pleural and interlobular dilated lymphatics	1	12	0	3
Thymus	no significant lesions (nsl)	0	11	0	3
	medulla: syncytia	9	11	1	3
	medulla: multinucleate cells	2	11	2	3
	thymitis, granulomatous	1	11	0	3
	thymitis, eosinophilic	3	11	0	3
	hemorrhage	1	11	0	3
Inguinal L.N.	no significant lesions (nsl)	0	12	0	3
	lymphoid hyperplasia	12	12	2	3
	lymphadenitis, granulomatous	8	12	0	3
	eosinophilia	12	12	3	3
	sinus histiocytosis	7	12	1	3
	medullary histiocytosis	4	12	2	3
Stomach	no significant lesions (nsl)	10	12	3	3
	gastritis (mild)	2	12	0	3
S. Intestine	no significant lesions (nsl)	9	12	3	3
	enteritis (mild to moderate)	3	12	0	3
L. Intestine	no significant lesions (nsl)	9	12	3	3
	enteritis (mild to moderate)	3	12	0	3
Brain	no significant lesions (nsl)	9	12	2	3
	gliosis (mild)	1	12	0	3
	encephalitis (mild)	2	12	1	3
Bone Marrow	no significant lesions (nsl)	10	10	3	3
Sternum	no significant lesions (nsl)	8	8	1	1

Table 9. Pathology incidence summary table.

TISSUE	LESION	SM-Exposed TOTAL AFFECTED	SM-Exposed OUT OF	Sham-Exposed TOTAL AFFECTED	Sham-Exposed OUT OF
Rib	no significant lesions (nsl)	3	3	2	2
Skin	no significant lesions (nsl)				na
	dermatitis	4	4		na
Trachea	no significant lesions (nsl)	3	3		na
Esophagus	no significant lesions (nsl)	3	3		na
Tongue	no significant lesions (nsl)	2	2		na
Diaphragm	no significant lesions (nsl)	2	2		na
Thyroid	no significant lesions (nsl)	3	3		na
Skeletal muscle	no significant lesions (nsl)	2	2	1	1

Table 10. Hematology results

Time	SM	Tx	Grafted		WBC	RBC	HGB	HCT	MCV	MCH	MCHC	PLT	MPV	PCT	NEU %	LYM %	MONO %	EOS %	BASO %
BSM	sham	none	n	Min	10.20	5.80	10.20	28.3	48.5	17.4	35.1	505	7.02	0.355	29.0	45.1	6.47	0.079	1.980
				Max	14.10	6.38	11.20	31.4	53.5	18.7	35.9	631	8.26	0.521	41.3	58.5	11.10	0.284	3.840
				Mean	11.97	6.00	10.77	30.2	50.4	17.9	35.5	566	7.73	0.441	34.4	53.9	8.89	0.215	2.687
				SD	1.98	0.33	0.51	1.7	2.7	0.7	0.4	63	0.64	0.083	6.3	7.6	2.32	0.118	1.007
				SEM	1.14	0.19	0.30	1.0	1.6	0.4	0.2	36	0.37	0.048	3.6	4.4	1.34	0.068	0.582
BSURG	sham	none	n	Min	8.04	5.71	9.87	27.7	48.1	17.3	35.4	448	7.70	0.349	22.1	32.1	6.42	0.029	1.870
				Max	14.90	5.93	11.10	31.3	52.9	18.8	36.8	648	8.62	0.551	49.2	69.2	15.50	0.480	3.180
				Mean	11.25	5.80	10.39	29.0	49.9	17.9	35.9	517	8.28	0.429	39.1	47.2	10.94	0.190	2.590
				SD	3.45	0.12	0.64	2.0	2.6	0.8	0.8	114	0.50	0.108	14.8	19.5	4.54	0.252	0.665
				SEM	1.99	0.07	0.37	1.2	1.5	0.4	0.5	66	0.29	0.062	8.5	11.2	2.62	0.145	0.384
PS08	sham	none	n	Min	11.30	4.80	8.48	23.5	46.9	17.1	35.3	524	7.25	0.391	27.5	27.1	6.41	0.092	1.240
				Max	18.10	5.34	9.24	26.2	50.0	17.7	36.4	615	8.46	0.520	60.4	61.3	11.10	0.270	2.850
				Mean	13.83	5.05	8.76	24.6	48.6	17.4	35.7	567	7.73	0.439	39.9	49.0	8.66	0.185	2.197
				SD	3.72	0.27	0.42	1.4	1.6	0.3	0.6	46	0.64	0.070	17.9	19.0	2.35	0.089	0.847
				SEM	2.15	0.16	0.24	0.8	0.9	0.2	0.4	26	0.37	0.041	10.3	11.0	1.36	0.052	0.489
PS15	sham	none	n	Min	11.00	4.95	8.55	23.7	46.4	16.5	35.6	557	6.20	0.346	25.4	34.0	0.64	0.030	0.280
				Max	14.70	5.68	9.66	26.7	47.9	17.3	36.2	754	8.60	0.649	51.9	73.5	11.50	0.254	2.650
				Mean	12.63	5.44	9.20	25.6	47.1	16.9	36.0	646	7.67	0.503	36.3	55.3	6.46	0.146	1.770
				SD	1.89	0.42	0.58	1.7	0.8	0.4	0.3	100	1.29	0.152	13.8	19.9	5.47	0.112	1.297
				SEM	1.09	0.24	0.34	1.0	0.4	0.2	0.2	58	0.74	0.088	8.0	11.5	3.16	0.065	0.749
PS22	sham	none	n	Min	9.52	4.49	7.64	21.3	45.6	16.8	35.8	463	7.86	0.363	17.4	29.9	0.53	0.193	0.423
				Max	15.40	6.10	10.20	27.8	47.5	17.3	37.0	627	10.60	0.558	56.4	81.5	11.00	0.518	2.860
				Mean	11.50	5.22	8.86	24.2	46.6	17.0	36.5	530	9.12	0.484	32.2	58.4	7.21	0.348	1.831
				SD	3.38	0.82	1.28	3.3	1.0	0.3	0.6	86	1.38	0.106	21.1	26.2	5.80	0.163	1.262
				SEM	1.95	0.47	0.74	1.9	0.5	0.1	0.4	50	0.80	0.061	12.2	15.1	3.35	0.094	0.729
PS29	sham	none	n	Min	11.00	5.17	8.96	24.7	46.1	16.5	35.8	512	7.22	0.369	17.6	54.4	0.47	0.167	0.193
				Max	12.50	5.95	9.82	27.4	47.7	17.3	36.3	587	9.30	0.546	36.5	75.3	6.63	0.206	2.290
				Mean	11.87	5.57	9.40	26.1	46.9	16.9	36.0	557	8.02	0.449	26.3	68.0	3.98	0.187	1.524
				SD	0.78	0.39	0.43	1.4	0.8	0.4	0.3	40	1.12	0.090	9.5	11.8	3.17	0.020	1.157
				SEM	0.45	0.23	0.25	0.8	0.5	0.2	0.1	23	0.65	0.052	5.5	6.8	1.83	0.011	0.668
PS36	sham	none	n	Min	6.95	5.17	8.60	24.2	46.2	16.6	35.5	478	7.04	0.359	11.9	65.8	3.19	0.138	0.985
				Max	10.90	5.81	9.67	27.0	46.8	17.1	37.1	510	9.20	0.447	29.6	78.3	10.30	0.557	1.650
				Mean	9.35	5.43	9.13	25.2	46.5	16.8	36.2	496	8.40	0.415	19.9	71.2	7.19	0.372	1.362
				SD	2.11	0.33	0.54	1.5	0.3	0.3	0.8	16	1.18	0.049	9.0	6.4	3.64	0.214	0.341
				SEM	1.22	0.19	0.31	0.9	0.2	0.2	0.5	9	0.68	0.028	5.2	3.7	2.10	0.123	0.197

Table 10. Hematology results

Time	SM	Tx	Grafted		WBC	RBC	HGB	HCT	MCV	MCH	MCHC	PLT	MPV	PCT	NEU %	LYM %	MONO %	EOS %	BASO %
BSM	y	debrided	n	Min	10.50	5.47	8.74	24.1	39.7	14.2	34.2	430	8.37	0.369	33.2	23.2	1.22	0.092	0.013
				Max	23.80	7.08	10.30	29.3	50.6	17.8	36.9	949	10.90	0.976	63.7	54.3	13.30	0.418	2.470
				Mean	15.18	6.05	9.64	27.1	45.1	16.0	35.6	654	9.53	0.620	47.1	42.0	9.18	0.251	1.534
				SD	4.87	0.56	0.60	2.2	4.5	1.4	1.0	229	1.06	0.219	12.9	13.0	4.42	0.130	0.965
				SEM	1.99	0.23	0.24	0.9	1.8	0.6	0.4	93	0.43	0.089	5.3	5.3	1.81	0.053	0.394
BSURG	y	debrided	n	Min	8.89	5.28	8.77	23.4	39.6	14.2	35.5	407	8.63	0.380	38.9	33.6	0.56	0.031	0.000
				Max	26.20	6.72	9.98	27.7	49.0	17.7	37.5	810	9.87	0.750	63.4	53.7	13.10	0.341	3.200
				Mean	15.75	5.78	9.31	25.7	44.6	16.2	36.2	599	9.35	0.556	47.0	43.6	7.69	0.163	1.552
				SD	6.00	0.50	0.46	1.7	4.1	1.4	0.8	172	0.46	0.148	8.8	8.0	5.05	0.112	1.502
				SEM	2.45	0.20	0.19	0.7	1.7	0.6	0.3	70	0.19	0.060	3.6	3.3	2.06	0.046	0.613
PS08	y	debrided	n	Min	10.30	5.21	7.99	21.6	38.8	14.3	34.8	364	7.90	0.348	41.0	19.1	6.47	0.046	0.335
				Max	27.10	5.72	9.63	26.8	47.8	17.2	36.9	727	11.90	0.609	68.6	45.0	12.00	0.622	3.150
				Mean	17.97	5.56	8.85	24.5	44.0	15.9	36.2	539	9.32	0.492	54.3	34.2	9.59	0.223	1.751
				SD	5.58	0.18	0.73	2.4	4.1	1.3	0.8	158	1.40	0.118	10.5	10.1	2.21	0.212	1.053
				SEM	2.28	0.08	0.30	1.0	1.7	0.5	0.3	65	0.57	0.048	4.3	4.1	0.90	0.087	0.430
PS15	y	debrided	n	Min	10.60	5.55	8.32	23.1	39.2	14.2	35.5	398	7.50	0.341	36.4	25.6	2.54	0.100	0.031
				Max	20.60	6.05	10.20	28.6	47.3	16.9	36.2	963	11.80	0.734	64.9	57.0	13.30	0.658	2.020
				Mean	14.30	5.87	9.25	25.7	43.8	15.8	35.9	674	9.55	0.634	49.8	41.4	7.32	0.314	1.153
				SD	3.82	0.21	0.80	2.3	3.6	1.2	0.3	187	1.54	0.147	9.9	10.0	3.50	0.206	0.740
				SEM	1.56	0.09	0.33	0.9	1.5	0.5	0.1	77	0.63	0.060	4.0	4.1	1.43	0.084	0.302
PS22	y	debrided	n	Min	11.70	5.18	8.24	23.4	39.1	13.8	34.8	352	8.66	0.394	33.2	42.6	0.46	0.036	0.000
				Max	18.00	6.49	9.89	27.4	47.0	17.0	36.5	886	12.30	0.800	53.9	66.3	11.20	0.610	3.590
				Mean	14.30	5.83	9.07	25.3	43.6	15.6	35.8	603	10.16	0.595	42.4	52.1	4.39	0.228	0.928
				SD	2.40	0.43	0.65	1.7	3.6	1.3	0.7	215	1.67	0.163	8.9	10.6	4.71	0.197	1.508
				SEM	0.98	0.17	0.27	0.7	1.5	0.5	0.3	88	0.68	0.067	3.6	4.3	1.92	0.081	0.616
PS29	y	debrided	n	Min	7.66	5.42	7.99	22.3	38.7	14.0	34.7	414	7.71	0.337	26.2	43.4	0.39	0.112	0.000
				Max	19.60	6.39	10.40	29.0	46.7	16.9	37.0	819	10.80	0.792	44.4	70.6	10.90	0.345	2.530
				Mean	12.58	5.91	9.26	25.8	43.6	15.7	36.0	574	9.52	0.542	36.0	56.5	5.97	0.188	1.405
				SD	4.15	0.40	0.78	2.3	3.8	1.3	0.8	170	1.29	0.165	6.9	9.0	4.11	0.083	1.129
				SEM	1.69	0.16	0.32	0.9	1.5	0.5	0.3	69	0.53	0.067	2.8	3.7	1.68	0.034	0.461
PS36	y	debrided	n	Min	10.60	5.74	8.17	22.5	38.6	14.2	36.0	357	7.92	0.305	30.0	40.6	0.26	0.093	0.000
				Max	15.30	6.39	10.40	28.1	46.7	17.2	37.7	770	9.72	0.700	48.2	69.4	10.70	0.378	3.560
				Mean	12.30	5.96	9.48	25.8	43.4	15.9	36.7	583	9.02	0.522	38.4	54.6	5.57	0.253	1.178
				SD	1.67	0.25	0.78	2.1	3.6	1.3	0.6	187	0.67	0.159	6.8	11.1	4.74	0.103	1.434
				SEM	0.68	0.10	0.32	0.9	1.5	0.5	0.2	76	0.27	0.065	2.8	4.5	1.94	0.042	0.585

Table 10. Hematology results

Time	SM	Tx	Grafted		WBC	RBC	HGB	HCT	MCV	MCH	MCHC	PLT	MPV	PCT	NEU %	LYM %	MONO %	EOS %	BASO %
BSM	y	debrided	y	Min	7.66	4.85	8.87	24.9	45.3	16.0	35.3	461	7.15	0.357	25.1	42.7	6.15	0.030	0.437
				Max	13.70	6.67	34.80	30.6	51.2	52.2	114.0	748	10.50	0.641	45.4	66.6	17.10	0.146	2.450
				Mean	11.05	5.88	14.03	27.9	47.6	23.1	49.1	558	8.99	0.497	36.7	52.4	9.14	0.088	1.661
				SD	2.09	0.64	10.19	1.9	2.5	14.3	31.8	113	1.34	0.100	9.3	11.0	4.00	0.048	0.764
				SEM	0.86	0.26	4.16	0.8	1.0	5.8	13.0	46	0.55	0.041	3.8	4.5	1.63	0.019	0.312
BSURG	y	debrided	y	Min	9.53	4.91	9.19	24.5	44.1	15.7	34.9	492	7.28	0.389	43.1	32.8	2.18	0.030	0.516
				Max	18.40	6.47	10.30	29.1	50.0	18.7	37.5	719	9.64	0.682	51.2	49.8	14.30	0.494	3.190
				Mean	12.56	5.74	9.74	26.7	46.7	17.1	36.6	572	8.99	0.517	47.2	42.3	8.51	0.144	1.830
				SD	3.30	0.58	0.49	1.7	2.3	1.1	0.9	82	0.88	0.103	2.9	6.6	4.03	0.173	1.116
				SEM	1.35	0.24	0.20	0.7	0.9	0.4	0.4	33	0.36	0.042	1.2	2.7	1.65	0.071	0.456
PS08	y	debrided	y	Min	12.30	5.16	8.97	24.2	43.0	15.6	35.9	514	7.75	0.456	38.2	24.4	4.71	0.030	0.137
				Max	21.80	6.07	9.73	26.9	49.6	18.4	37.8	789	8.88	0.681	62.5	50.5	11.60	0.669	3.240
				Mean	15.13	5.61	9.41	25.5	45.6	16.8	36.9	615	8.52	0.523	47.4	41.9	8.43	0.252	2.023
				SD	3.54	0.30	0.29	1.0	2.6	1.1	0.8	98	0.41	0.088	8.5	9.5	2.61	0.242	1.131
				SEM	1.45	0.12	0.12	0.4	1.1	0.4	0.3	40	0.17	0.036	3.4	3.9	1.06	0.099	0.462
PS15	y	debrided	y	Min	8.28	4.76	8.58	23.1	42.3	15.7	36.1	471	6.82	0.405	31.9	34.0	0.73	0.031	0.000
				Max	24.80	6.71	10.60	28.4	48.6	18.0	37.6	748	9.71	0.594	57.8	66.8	12.10	0.658	3.370
				Mean	14.68	5.85	9.66	26.2	45.0	16.6	36.8	607	8.38	0.503	45.6	45.7	6.76	0.258	1.693
				SD	6.28	0.65	0.67	1.8	2.4	0.8	0.6	112	0.97	0.074	9.2	11.5	4.69	0.212	1.318
				SEM	2.56	0.27	0.27	0.7	1.0	0.3	0.2	46	0.39	0.030	3.8	4.7	1.91	0.087	0.538
PS22	y	debrided	y	Min	9.81	5.25	8.46	22.9	41.3	15.2	35.7	466	7.13	0.364	26.2	45.2	0.23	0.114	0.016
				Max	16.00	6.36	10.00	27.5	48.3	18.1	37.4	582	9.85	0.573	45.8	65.7	11.10	0.399	4.770
				Mean	12.00	5.74	9.39	25.6	44.6	16.4	36.7	522	8.60	0.449	34.8	56.0	7.13	0.187	1.882
				SD	2.20	0.38	0.54	1.6	2.3	1.0	0.6	51	1.04	0.073	7.9	7.5	4.03	0.109	1.929
				SEM	0.90	0.15	0.22	0.7	0.9	0.4	0.3	21	0.43	0.030	3.2	3.1	1.64	0.044	0.788
PS29	y	debrided	y	Min	9.21	5.15	9.08	24.5	42.2	15.0	35.6	483	7.29	0.428	19.3	57.1	2.22	0.062	0.000
				Max	16.70	6.62	10.20	28.6	47.5	17.7	37.3	639	9.82	0.542	39.0	71.6	12.20	0.331	2.800
				Mean	12.32	5.83	9.42	25.8	44.2	16.2	36.7	559	8.67	0.483	29.7	63.7	5.38	0.176	1.091
				SD	3.04	0.49	0.41	1.4	1.8	0.9	0.8	58	0.84	0.050	9.1	6.2	3.77	0.104	1.206
				SEM	1.24	0.20	0.17	0.6	0.7	0.4	0.3	24	0.34	0.020	3.7	2.5	1.54	0.043	0.492
PS36	y	debrided	y	Min	9.90	4.78	7.92	21.5	41.9	15.0	35.7	463	7.67	0.386	0.0	18.1	0.00	0.000	0.000
				Max	18.40	6.47	10.00	27.2	47.4	17.9	37.8	1153	12.20	1.410	32.3	81.3	10.70	0.260	2.430
				Mean	13.62	5.66	9.17	24.9	44.2	16.3	36.8	597	9.20	0.582	21.2	61.0	3.37	0.160	0.635
				SD	3.02	0.71	0.82	2.4	1.9	1.0	0.7	273	1.63	0.406	12.6	23.1	3.76	0.088	0.934
				SEM	1.23	0.29	0.33	1.0	0.8	0.4	0.3	111	0.66	0.166	5.1	9.4	1.54	0.036	0.381

Table 11. Clinical chemistry results

Time	HD	Tx	Grafted		CPK	MM %	MB %	BB %	LDH	LD1 %	LD2 %	LD3 %	LD4 %	LD5 %	LD1/LD2	AST	ALT	ALP	AMY	BUN	CRE	B/C	TP	ALB	GLOB	A/G	TBIL	CAL	PHOS	GLU	NA	K	CHLOR	MAG
BSM	sham	none	n	Min	750	70.6	4.5	9.7	407	27.6	25.2	21.3	9.4	4.9	1.08	53	34	131	1737	8.5	1.0	8.5	4.9	3.5	1.3	2.5	0.1	10.4	6.5	115	144	3.5	93	1.81
				Max	1569	85.8	13.5	15.9	626	36.4	26.2	24.9	12.1	15.0	1.43	77	105	238	2517	15.7	1.1	14.3	5.1	3.8	1.4	2.9	0.2	11.0	8.8	135	146	3.9	100	2.05
				Mean	1077	78.9	8.8	12.3	501	30.8	25.6	23.4	10.8	9.5	1.20	61	63	169	2209	11.9	1.0	11.5	5.0	3.7	1.3	2.8	0.1	10.7	7.3	126	145	3.7	97	1.94
				SD	434	7.7	4.5	3.2	113	4.9	0.5	1.9	1.4	5.1	0.20	14	37	60	415	3.6	0.1	2.9	0.1	0.2	0.1	0.2	0.1	0.3	1.3	10	1	0.2	4	0.12
				SEM	251	4.4	2.6	1.9	65	2.8	0.3	1.1	0.8	3.0	0.11	8	22	35	240	2.1	0.0	1.7	0.1	0.1	0.0	0.1	0.0	0.2	0.8	6	1	0.1	2	0.07
BSURG	sham	none	n	Min	380	72.8	4.7	6.4	280	37.6	13.3	19.3	9.3	5.7	1.50	41	50	125	1554	9.9	1.1	9.0	5.0	3.6	1.3	2.4	0.1	10.6	7.0	118	145	3.7	95	1.89
				Max	542	88.9	13.4	17.2	598	52.4	25.0	21.6	13.6	5.8	3.94	58	120	210	2351	12.7	1.1	11.5	5.1	3.7	1.5	2.8	0.2	11.3	9.2	140	148	4.2	101	2.54
				Mean	483	79.4	8.1	12.5	435	44.4	18.5	20.4	11.0	5.8	2.64	50	74	156	2030	11.5	1.1	10.5	5.1	3.7	1.4	2.6	0.1	11.0	8.2	129	146	3.9	97	2.17
				SD	90	8.4	4.7	5.5	155	7.5	5.9	1.2	2.3	0.1	1.23	9	40	47	421	1.4	0.0	1.3	0.1	0.1	0.1	0.2	0.1	0.4	1.1	11	2	0.3	3	0.34
				SEM	52	4.9	2.7	3.2	89	4.3	3.4	0.7	1.3	0.0	0.71	5	23	27	243	0.8	0.0	0.8	0.0	0.0	0.1	0.1	0.0	0.2	0.6	6	1	0.2	2	0.19
PS08	sham	none	n	Min	330	73.3	7.2	6.9	327	29.2	16.9	17.3	5.1	4.3	0.99	47	54	154	1931	3.4	0.8	3.8	4.4	3.0	1.3	2.1	0.2	10.4	8.7	92	140	3.5	93	1.74
				Max	908	84.0	9.1	18.3	475	56.3	29.4	26.5	9.4	6.7	3.33	55	95	184	2548	12.5	0.9	13.9	5.1	3.8	1.8	2.9	0.3	11.0	9.0	116	146	3.9	97	2.47
				Mean	596	77.3	8.2	14.5	421	38.7	24.6	23.1	7.9	5.7	1.81	50	71	165	2185	6.5	0.9	7.3	4.8	3.4	1.4	2.4	0.2	10.7	8.8	100	144	3.7	95	2.22
				SD	292	5.8	1.0	6.6	82	15.3	6.8	5.0	2.4	1.2	1.32	4	22	16	323	5.2	0.1	5.7	0.4	0.4	0.2	0.5	0.1	0.3	0.2	14	3	0.2	2	0.42
				SEM	168	3.4	0.6	3.8	47	8.8	3.9	2.9	1.4	0.7	0.76	3	12	9	186	3.0	0.0	3.3	0.2	0.2	0.1	0.3	0.0	0.2	0.1	8	2	0.1	1	0.24
PS15	sham	none	n	Min	453	73.6	6.5	9.1	309	28.8	22.5	21.9	10.1	6.3	0.95	43	56	122	1891	2.3	0.8	2.6	4.6	2.9	1.4	1.7	0.1	9.6	7.9	103	139	3.6	86	1.71
				Max	829	80.7	10.2	16.6	521	30.2	30.2	26.7	11.1	11.8	1.34	61	110	169	2655	9.5	1.0	11.9	5.3	3.9	1.7	2.8	0.3	11.3	9.2	111	147	5.0	98	2.37
				Mean	665	76.0	8.8	13.1	429	29.6	26.0	24.4	10.5	9.5	1.16	54	83	150	2278	4.8	0.9	5.7	5.0	3.4	1.5	2.3	0.2	10.7	8.7	106	143	4.1	93	1.96
				SD	192	3.9	2.0	3.8	109	0.9	3.9	2.4	0.5	2.9	0.20	10	27	25	382	4.0	0.1	5.3	0.4	0.5	0.2	0.5	0.1	1.0	0.7	4	4	0.8	6	0.36
				SEM	111	2.2	1.2	2.2	63	0.5	2.3	1.4	0.3	1.7	0.11	6	16	14	221	2.3	0.1	3.1	0.2	0.3	0.1	0.3	0.1	0.6	0.4	2	2	0.5	4	0.21
PS22	sham	none	n	Min	667	73.5	8.4	4.6	402	17.8	13.1	14.9	9.0	7.8	1.07	44	78	102	1766	4.6	0.9	5.1	4.5	2.7	1.3	1.5	0.1	10.0	8.5	112	139	3.6	91	1.68
				Max	6047	83.1	12.3	15.3	544	39.9	23.1	24.9	11.4	41.6	3.05	64	108	156	2645	9.6	1.0	10.7	5.2	3.9	1.8	3.0	0.2	11.4	9.5	117	150	3.9	101	1.89
				Mean	2738	79.5	10.6	9.9	481	30.2	17.6	19.4	10.4	22.4	1.85	56	89	136	2250	7.0	0.9	7.5	4.9	3.5	1.5	2.5	0.2	10.8	9.1	115	144	3.7	95	1.82
				SD	2896	5.2	2.0	5.4	72	11.3	5.1	5.1	1.2	17.4	1.05	11	17	30	446	2.5	0.1	2.8	0.4	0.7	0.3	0.8	0.1	0.7	0.5	3	6	0.2	5	0.12
				SEM	1672	3.0	1.2	3.1	42	6.5	2.9	2.9	0.7	10.1	0.61	6	10	17	258	1.4	0.0	1.6	0.2	0.4	0.2	0.5	0.0	0.4	0.3	2	3	0.1	3	0.07
PS29	sham	none	n	Min	1469	85.3	4.7	3.4	401	21.6	15.7	13.4	8.3	28.5	1.15	46	82	138	2127	4.4	0.8	5.5	5.1	3.2	1.3	1.6	0.1	10.7	8.8	96	143	3.5	91	1.45
				Max	6037	91.9	5.1	9.6	1036	25.9	20.4	16.9	11.5	37.2	1.38	116	94	159	2873	11.0	1.0	12.4	5.3	3.8	2.0	2.9	0.2	11.0	9.7	112	146	4.1	101	1.89
				Mean	3449	89.4	4.9	5.7	667	23.1	18.4	14.8	9.7	34.0	1.27	72	87	147	2340	8.4	0.9	9.6	5.2	3.6	1.8	2.4	0.2	10.9	9.4	105	144	3.7	98	1.65
				SD	2344	3.6	0.2	3.4	330	2.4	2.4	1.9	1.6	4.8	0.11	39	6	11	292	3.5	0.1	3.6	0.1	0.3	0.4	0.7	0.1	0.2	0.5	8	2	0.3	6	0.22
				SEM	1353	2.1	0.1	2.0	190	1.4	1.4	1.1	0.9	2.8	0.07	22	4	6	169	2.0	0.1	2.1	0.1	0.2	0.2	0.4	0.0	0.1	0.3	5	1	0.2	3	0.13
PS36	sham	none	n	Min	896	84.8	5.1	6.4	362	25.3	9.5	15.0	5.8	15.0	1.42	23	50	87	1360	5.6	0.6	5.6	2.9	2.2	0.7	2.4	0.1	6.8	5.9	63	93	2.8	59	1.09
				Max	3343	88.4	6.4	10.1	396	32.8	22.2	21.2	11.7	36.2	3.45	52	70	134	2680	7.9	1.0	13.2	5.5	4.0	1.5	3.1	0.1	11.0	9.2	121	149	4.0	109	1.82
				Mean	2112	86.3	5.6	8.1	379	30.3	16.5	18.0	8.8	26.5	2.12	38	61	115	2058	7.0	0.9	8.8	4.5	3.3	1.2	2.7	0.1	9.4	7.9	97	130	3.5	88	1.53
				SD	1224	1.9	0.7	1.9	17	4.3	6.4	3.1	3.0	10.7	1.16	15	10	25	663	1.2	0.2	3.9	1.4	0.9	0.5	0.4	0.0	2.3	1.7	30	32	0.6	26	0.39
				SEM	706	1.1	0.4	1.1	10	2.5	3.7	1.8	1.7	6.2	0.67	8	6	14	383	0.7	0.1	2.3	0.8	0.5	0.3	0.2	0.0	1.3	1.0	18	19	0.4	15	0.22

Table 11. Clinical chemistry results

Time	HD	Tx	Grafted		CPK	MM %	MB %	BB %	LDH	LD1 %	LD2 %	LD3 %	LD4 %	LD5 %	LD1/LD2	AST	ALT	ALP	AMY	BUN	CRE	B/C	TP	ALB	GLOB	A/G	TBIL	CAL	PHOS	GLU	NA	K	CHLOR	MAG
BSM	y	debrided	n	Min	360	66.2	6.6	4.1	345	34.1	17.2	19.0	5.4	4.1	1.39	34	41	146	1892	6.6	0.8	6.6	4.9	3.6	1.1	2.5	0.1	10.2	8.2	100	142	3.6	94	1.96
				Max	517	83.7	12.5	21.3	590	44.3	25.9	24.5	12.2	10.1	2.49	66	95	219	2408	15.4	1.2	19.3	5.6	4.0	1.6	3.6	0.2	11.5	9.5	137	150	5.0	105	2.56
				Mean	427	76.5	9.5	14.0	459	39.3	22.6	21.8	9.8	6.5	1.79	48	63	179	2086	10.9	1.0	11.0	5.3	3.9	1.4	2.9	0.1	10.7	8.6	119	146	4.1	99	2.2
				SD	61	6.3	2.4	5.9	97	4.1	3.3	2.2	2.4	2.4	0.45	11	20	26	189	2.9	0.2	4.5	0.3	0.2	0.2	0.4	0.0	0.5	0.5	12	3	0.5	4	0.2
				SEM	25	2.6	1.0	2.4	40	1.7	1.3	0.9	1.0	1.0	0.18	5	8	11	77	1.2	0.1	1.8	0.1	0.1	0.1	0.2	0.0	0.2	0.2	5	1	0.2	2	0.1
BSURG	y	debrided	n	Min	264	69.4	3.2	4.1	244	36.5	14.8	20.2	6.8	3.3	1.35	22	41	101	1568	8.8	0.6	8.9	4.1	2.9	1.2	2.2	0.1	8.4	7.6	102	117	3.3	80	1.51
				Max	948	92.6	16.4	24.3	571	45.3	27.7	24.2	14.7	8.8	2.90	84	117	193	2082	14.7	1.2	17.3	5.5	4.0	1.7	3.1	0.2	11.3	8.8	136	157	4.5	107	2.68
				Mean	534	78.9	7.7	13.4	448	40.2	22.0	22.4	10.0	5.4	1.97	46	75	150	1738	11.7	1.0	12.7	5.1	3.7	1.4	2.6	0.1	10.3	8.0	123	143	4.0	98	2.0
				SD	295	8.0	4.8	8.4	118	3.1	5.5	1.4	2.9	2.0	0.70	15	24	32	179	2.4	0.2	3.5	0.5	0.4	0.2	0.3	0.1	1.0	0.5	15	13	0.4	10	0.5
				SEM	120	3.3	2.0	3.4	48	1.3	2.2	0.8	1.2	0.8	0.29	6	10	13	73	1.0	0.1	1.4	0.2	0.2	0.1	0.1	0.0	0.4	0.2	6	5	0.2	4	0.2
PS08	y	debrided	n	Min	487	81.7	4.7	3.2	220	37.2	12.2	15.2	7.7	9.8	1.71	39	63	121	1563	6.0	0.7	7.0	4.7	3.0	1.4	1.7	0.1	9.2	7.8	84	128	3.1	87	1.50
				Max	1922	91.3	11.8	9.3	411	43.5	23.7	21.9	14.9	14.6	3.54	67	121	176	2321	12.0	1.2	14.6	5.2	3.8	1.8	2.7	0.9	10.9	9.6	136	148	5.0	102	2.51
				Mean	1251	86.4	7.2	6.3	316	40.5	18.5	18.7	11.4	11.0	2.34	55	82	153	1976	8.6	0.9	10.1	4.9	3.4	1.5	2.3	0.3	10.1	8.7	109	141	3.9	96	2.0
				SD	543	3.7	2.6	2.2	63	2.7	4.5	2.4	2.7	1.9	0.78	12	21	22	276	2.2	0.2	3.1	0.2	0.3	0.2	0.4	0.3	0.7	0.8	18	8	0.6	5	0.3
				SEM	222	1.5	1.0	0.9	26	1.1	1.8	1.0	1.1	0.8	0.32	5	9	9	113	0.9	0.1	1.3	0.1	0.1	0.1	0.2	0.1	0.3	0.3	7	3	0.3	2	0.1
PS15	y	debrided	n	Min	304	74.8	3.0	7.0	251	28.0	13.8	18.1	9.8	5.3	1.03	31	63	113	1786	7.3	0.8	4.9	4.7	2.9	1.3	1.4	0.1	10.1	8.9	70	137	3.8	91	1.90
				Max	1760	85.9	12.8	17.6	493	42.8	27.3	26.3	12.8	14.9	3.01	75	102	169	2465	14.5	1.5	14.5	6.0	4.1	2.1	2.6	1.1	11.5	10.4	164	146	5.0	100	2.71
				Mean	822	81.1	7.1	11.8	344	39.2	19.0	21.4	11.1	9.4	2.22	51	85	149	2157	9.8	1.1	9.8	5.5	3.7	1.8	2.1	0.4	10.7	9.7	107	141	4.4	96	2.1
				SD	535	3.9	3.6	3.7	87	5.5	5.1	3.2	1.0	3.4	0.70	14	15	20	255	2.9	0.2	3.5	0.5	0.4	0.3	0.5	0.4	0.5	0.6	31	4	0.5	4	0.3
				SEM	218	1.6	1.5	1.5	36	2.3	2.1	1.3	0.4	1.4	0.29	6	6	8	104	1.2	0.1	1.4	0.2	0.2	0.1	0.2	0.2	0.2	0.3	13	2	0.2	2	0.1
PS22	y	debrided	n	Min	399	77.8	3.6	5.2	196	28.0	14.3	19.5	7.8	7.5	1.25	33	68	126	1850	6.0	1.0	4.8	5.0	3.2	1.5	1.5	0.1	10.2	8.7	62	138	3.8	75	1.84
				Max	2737	89.5	8.9	13.3	487	39.3	26.0	25.3	13.5	19.9	2.75	51	97	147	2553	13.2	1.6	12.0	5.5	3.9	2.2	2.4	0.9	10.9	10.3	121	164	5.9	104	2.30
				Mean	1177	84.3	5.9	9.8	350	34.4	20.2	21.1	10.8	13.5	1.81	44	83	138	2124	8.8	1.2	7.8	5.4	3.6	1.8	2.1	0.4	10.6	9.4	101	147	4.5	95	2.0
				SD	902	4.6	2.1	3.1	104	4.2	4.4	2.2	2.4	4.6	0.60	6	13	9	289	2.6	0.2	3.2	0.2	0.2	0.3	0.4	0.4	0.3	0.7	21	9	0.8	10	0.2
				SEM	368	1.9	0.9	1.3	42	1.7	1.8	0.9	1.0	1.9	0.24	3	5	4	118	1.1	0.1	1.3	0.1	0.1	0.1	0.2	0.2	0.1	0.3	8	4	0.3	4	0.1
PS29	y	debrided	n	Min	481	76.4	3.6	3.1	166	19.8	9.1	12.1	4.8	9.0	1.16	34	67	96	1587	5.5	0.8	5.3	3.5	2.5	1.0	1.7	0.0	7.5	7.0	81	104	2.7	66	1.38
				Max	5295	93.3	10.5	13.9	540	50.4	24.4	23.2	10.4	50.8	5.40	59	101	168	2881	11.2	1.2	12.4	5.8	4.3	2.1	2.9	0.9	11.0	9.4	127	145	5.0	106	2.32
				Mean	1896	86.1	6.6	7.3	302	35.8	17.5	17.2	8.1	21.4	2.43	44	84	137	2149	8.5	1.0	9.1	5.3	3.6	1.6	2.3	0.2	10.2	8.5	105	135	4.3	94	2.0
				SD	1756	6.0	3.1	4.1	130	12.7	6.4	4.0	2.1	15.9	1.67	10	13	24	368	2.7	0.1	3.1	0.9	0.6	0.4	0.4	0.3	1.3	1.0	17	15	0.9	14	0.4
				SEM	717	2.5	1.3	1.7	53	5.2	2.6	1.6	0.9	6.5	0.68	4	5	10	150	1.1	0.1	1.3	0.4	0.2	0.2	0.2	0.1	0.6	0.4	7	6	0.4	6	0.1
PS36	y	debrided	n	Min	731	84.5	0.5	2.6	271	20.3	15.7	14.8	4.8	8.0	1.26	37	75	131	1922	5.7	0.9	5.7	5.4	3.7	1.4	1.7	0.0	10.0	7.5	71	138	3.4	96	1.77
				Max	5138	96.9	9.6	9.8	626	49.5	25.7	25.5	8.9	40.9	2.69	74	102	161	2696	9.8	1.1	10.9	6.0	4.1	2.2	2.9	0.9	10.9	10.0	112	147	5.3	101	2.50
				Mean	2389	89.0	4.9	6.2	432	32.8	20.3	18.6	7.5	20.9	1.64	50	90	142	2273	8.4	1.0	8.8	5.7	4.0	1.8	2.3	0.3	10.5	9.0	93	143	4.4	98	2.1
				SD	1847	5.2	3.1	3.0	151	10.1	3.7	3.9	1.5	13.5	0.54	13	10	11	293	1.4	0.1	1.9	0.2	0.2	0.3	0.5	0.3	0.3	0.9	16	5	0.8	2	0.3
				SEM	754	2.1	1.3	1.2	62	4.1	1.5	1.6	0.6	5.5	0.22	5	4	4	120	0.6	0.0	0.8	0.1	0.1	0.1	0.2	0.1	0.1	0.3	6	2	0.3	1	0.1

Table 11. Clinical chemistry results

Time	HD	Tx	Grafted		CPK	MM %	MB %	BB %	LDH	LD1 %	LD2 %	LD3 %	LD4 %	LD5 %	LD1/LD2	AST	ALT	ALP	AMY	BUN	CRE	B/C	TP	ALB	GLOB	A/G	TBIL	CAL	PHOS	GLU	NA	K	CHLOR	MAG
BSM	y	debrided	y	Min	378	66.1	3.2	4.4	330	29.9	7.3	11.5	7.1	4.2	1.12	27	51	166	1127	3.0	0.8	2.7	4.1	3.5	0.6	2.4	0.0	9.5	3.4	76	139	3.9	93	1.67
				Max	1650	91.8	16.1	17.7	599	56.7	27.5	28.6	12.2	15.5	7.77	122	82	247	3684	10.8	1.4	9.8	5.8	4.1	1.7	5.8	0.5	11.2	9.6	155	165	4.8	110	2.44
				Mean	896	81.8	7.5	10.6	445	39.2	21.1	22.3	9.8	7.6	2.70	59	66	211	2553	8.2	1.1	7.3	5.0	3.7	1.2	3.4	0.2	10.5	7.9	105	148	4.3	100	2.0
				SD	470	9.7	4.6	5.7	96	10.1	8.6	6.0	1.8	4.2	2.63	33	13	28	888	3.0	0.2	2.5	0.6	0.2	0.4	1.3	0.2	0.6	2.3	28	10	0.4	7	0.3
				SEM	192	4.0	1.9	2.3	39	4.1	3.5	2.5	0.7	1.7	1.07	13	5	11	362	1.2	0.1	1.0	0.2	0.1	0.2	0.5	0.1	0.3	0.9	11	4	0.2	3	0.1
BSURG	y	debrided	y	Min	449	66.7	3.7	6.6	315	29.8	14.3	17.0	5.0	3.6	1.03	44	57	143	1119	4.7	0.9	4.7	4.6	3.3	1.0	2.4	0.0	10.1	7.8	101	139	3.8	93	1.56
				Max	987	86.3	13.5	19.7	538	47.6	29.0	29.4	15.0	9.4	2.96	68	105	185	2651	10.1	1.5	11.1	5.3	3.8	1.5	3.7	0.2	11.2	8.7	124	153	4.8	106	2.32
				Mean	678	80.6	7.9	11.5	417	39.9	21.9	22.6	8.7	6.9	1.99	54	84	175	2147	8.8	1.1	8.4	4.9	3.6	1.3	2.8	0.1	10.6	8.1	115	145	4.1	100	2.0
				SD	201	7.3	3.2	4.6	100	6.9	5.8	4.1	3.8	2.2	0.79	10	17	16	570	2.0	0.2	2.3	0.3	0.2	0.2	0.5	0.1	0.5	0.3	9	5	0.4	5	0.3
				SEM	82	3.0	1.3	1.9	41	2.8	2.4	1.7	1.6	0.9	0.32	4	7	7	233	0.8	0.1	0.9	0.1	0.1	0.1	0.2	0.0	0.2	0.1	4	2	0.2	2	0.1
PS08	y	debrided	y	Min	373	62.0	5.4	5.7	301	30.0	16.8	20.5	5.7	5.6	1.07	47	69	142	934	3.6	0.7	4.0	4.6	3.0	1.5	1.8	0.0	9.2	7.4	89	143	3.5	94	1.60
				Max	2145	87.4	11.1	30.4	494	47.0	31.3	26.8	11.9	15.4	2.80	66	143	208	2672	10.0	1.0	10.0	5.6	3.7	2.0	2.2	0.4	10.9	9.6	129	162	4.4	111	2.47
				Mean	1124	81.8	7.4	10.8	394	37.0	23.0	23.0	8.8	8.1	1.77	59	108	164	2072	6.2	0.9	6.9	5.1	3.4	1.7	2.0	0.2	10.0	8.8	104	149	3.9	101	1.9
				SD	690	9.9	2.1	9.6	78	5.7	6.7	2.6	2.5	3.6	0.71	7	28	25	664	2.4	0.1	2.4	0.4	0.3	0.2	0.2	0.1	0.6	0.6	14	7	0.3	6	0.3
				SEM	282	4.0	0.9	3.9	32	2.3	2.7	1.1	1.0	1.5	0.29	3	11	10	271	1.0	0.0	1.0	0.2	0.1	0.1	0.1	0.1	0.2	0.3	6	3	0.1	2	0.1
PS15	y	debrided	y	Min	401	66.5	4.1	4.8	319	31.9	11.9	17.2	5.2	5.4	1.12	51	71	133	1338	4.6	0.8	5.1	4.8	3.3	1.4	1.8	0.1	10.1	8.0	87	143	3.7	59	1.51
				Max	3575	90.9	9.6	25.7	455	52.6	28.5	22.2	13.7	24.4	3.97	84	150	184	2733	14.8	1.2	18.5	5.8	4.1	1.8	2.4	0.6	11.3	10.6	125	153	4.6	102	2.14
				Mean	1498	83.6	6.1	10.2	406	39.6	20.5	19.8	8.6	11.5	2.29	70	116	158	2269	9.6	1.0	10.2	5.3	3.6	1.7	2.2	0.3	10.7	9.1	102	147	4.0	92	1.9
				SD	1149	9.1	2.2	7.9	50	7.9	7.9	2.0	3.3	6.9	1.20	13	26	19	526	3.9	0.1	4.7	0.3	0.3	0.2	0.2	0.2	0.5	1.0	13	4	0.4	16	0.3
				SEM	469	3.7	0.9	3.2	20	3.2	3.2	0.8	1.3	2.8	0.49	5	11	8	215	1.6	0.1	1.9	0.1	0.1	0.1	0.1	0.1	0.2	0.4	5	2	0.1	7	0.1
PS22	y	debrided	y	Min	805	74.8	4.2	5.3	300	26.1	10.5	12.4	7.5	6.6	0.98	44	79	133	1224	5.3	0.6	5.3	5.0	3.5	1.5	2.0	0.1	10.3	8.1	75	143	3.7	93	1.33
				Max	2589	89.5	13.0	12.2	476	37.4	30.3	24.9	12.2	28.8	3.44	76	157	169	2787	8.1	1.1	12.2	5.8	4.1	1.8	2.6	0.2	11.0	10.2	110	147	3.8	96	2.28
				Mean	1560	84.1	7.9	8.0	375	31.7	21.4	19.8	9.8	17.4	1.71	58	109	148	2328	6.9	0.9	7.9	5.4	3.7	1.8	2.3	0.2	10.6	9.1	96	146	3.8	95	1.8
				SD	617	5.3	3.6	2.3	62	4.3	6.9	4.2	2.0	8.0	0.93	14	32	13	586	1.0	0.2	2.4	0.3	0.2	0.1	0.2	0.1	0.3	0.7	15	2	0.1	1	0.3
				SEM	252	2.2	1.5	0.9	25	1.7	2.8	1.7	0.8	3.3	0.38	6	13	5	240	0.4	0.1	1.0	0.1	0.1	0.1	0.1	0.0	0.1	0.3	6	1	0.0	0	0.1
PS29	y	debrided	y	Min	653	83.6	2.1	2.8	412	30.3	13.4	13.9	4.5	8.9	1.53	37	80	141	1319	3.4	0.9	3.1	5.3	3.7	1.5	2.2	0.1	9.9	8.4	100	144	3.7	91	0.38
				Max	3428	95.1	9.1	9.5	561	49.0	24.8	20.5	12.1	29.7	3.16	70	147	172	3153	12.5	1.1	13.9	5.8	4.3	1.7	2.9	0.3	11.3	10.3	122	150	4.1	99	2.13
				Mean	2070	88.6	5.6	5.9	461	39.1	18.1	17.8	8.9	16.2	2.29	54	111	156	2418	8.0	1.0	8.2	5.5	3.9	1.6	2.4	0.2	10.7	9.2	107	148	3.9	96	1.7
				SD	1233	4.5	2.6	2.2	54	6.6	5.0	2.9	3.1	7.7	0.68	12	30	14	626	3.2	0.1	4.0	0.2	0.2	0.1	0.3	0.1	0.6	0.8	9	2	0.2	3	0.7
				SEM	503	1.8	1.1	0.9	22	2.7	2.1	1.2	1.3	3.1	0.28	5	12	6	255	1.3	0.0	1.6	0.1	0.1	0.0	0.1	0.0	0.2	0.3	4	1	0.1	1	0.3
PS36	y	debrided	y	Min	775	84.0	4.9	1.9	382	19.8	11.0	15.0	5.7	7.4	1.22	44	69	140	1371	5.0	1.0	5.0	5.0	3.7	1.2	2.2	0.0	10.2	8.2	97	145	3.5	92	1.33
				Max	5506	93.2	6.4	10.6	891	35.5	26.2	22.1	13.5	38.1	2.83	110	144	175	3235	13.4	1.4	9.6	5.7	4.2	1.8	3.3	0.3	11.3	9.7	153	161	4.5	106	2.14
				Mean	2552	89.1	5.6	5.4	565	30.9	18.9	18.0	9.8	22.3	1.78	60	107	157	2477	8.2	1.1	7.3	5.4	3.9	1.5	2.7	0.2	10.6	9.2	114	149	3.9	97	1.8
				SD	1794	3.4	0.6	3.3	199	5.7	6.2	3.3	2.9	11.6	0.68	25	27	13	622	2.9	0.2	1.8	0.3	0.2	0.2	0.4	0.1	0.4	0.5	20	6	0.3	5	0.3
				SEM	733	1.4	0.3	1.3	81	2.3	2.5	1.3	1.2	4.7	0.28	10	11	5	254	1.2	0.1	0.7	0.1	0.1	0.1	0.2	0.0	0.2	0.2	8	3	0.1	2	0.1

Table 12. Vancouver scar assessments

Time	Tx	Grafted		Vascularity (0-3)	Pigmentation (0-2)	Pliability (0-5)	Height (0-3)
PS22	sharp	n	Mean	1.7	0.0	1.3	0.4
			SD	0.7	0.0	0.6	0.5
			SEM	0.2	0.0	0.2	0.2
PS29	sharp	n	Mean	1.8	0.0	1.1	0.1
			SD	0.9	0.0	0.8	0.3
			SEM	0.3	0.0	0.2	0.1
PS36	sharp	n	Mean	2.7	0.0	0.6	0.0
			SD	0.5	0.0	0.5	0.0
			SEM	0.1	0.0	0.1	0.0
PS22	none	n	Mean	1.5	0.0	1.0	0.5
			SD	0.6	0.0	0.0	0.6
			SEM	0.3	0.0	0.0	0.3
PS29	none	n	Mean	2.1	0.0	1.3	0.5
			SD	0.6	0.0	0.7	0.7
			SEM	0.1	0.0	0.2	0.2
PS36	none	n	Mean	2.6	0.0	1.3	0.5
			SD	0.6	0.0	0.6	0.7
			SEM	0.1	0.0	0.1	0.1
PS22	TX1A	n	Mean	2.5	0.0	0.8	0.8
			SD	0.9	0.0	0.7	0.5
			SEM	0.3	0.0	0.2	0.1
PS29	TX1A	n	Mean	2.3	0.0	1.0	0.2
			SD	1.0	0.0	0.6	0.4
			SEM	0.3	0.0	0.2	0.1
PS36	TX1A	n	Mean	2.7	0.0	0.7	0.3
			SD	0.5	0.0	0.5	0.5
			SEM	0.1	0.0	0.1	0.1
PS22	sharp	y	Mean	0.4	0.0	0.9	1.1
			SD	0.5	0.0	0.3	0.7
			SEM	0.1	0.0	0.1	0.2
PS29	sharp	y	Mean	0.6	0.0	0.8	0.9
			SD	0.7	0.0	0.4	0.8
			SEM	0.2	0.0	0.1	0.2
PS36	sharp	y	Mean	0.3	0.0	0.5	0.7
			SD	0.5	0.0	0.5	0.5
			SEM	0.1	0.0	0.2	0.1
PS22	TX1A	y	Mean	0.8	0.0	1.0	1.3
			SD	0.5	0.0	0.4	0.5
			SEM	0.1	0.0	0.1	0.1
PS29	TX1A	y	Mean	0.9	0.0	0.8	1.0
			SD	0.8	0.0	0.4	0.6
			SEM	0.2	0.0	0.1	0.2
PS36	TX1A	y	Mean	0.8	0.0	0.8	1.0
			SD	0.5	0.0	0.4	0.6
			SEM	0.1	0.0	0.1	0.2

Table 13. Biological Mediators of Interest

1. *Inflammatory Mediators*

   IL-1∀, IL-1∃, IL-6, IL-8, interleukin-1 converting enzyme (ICE), IL-1 receptor antagonist (IL-1ra), IL-10, MIP-1∀, MIP-2, TNF∀, MCP-1

2. *Angiogenic Mediators*

   TGF-∃, TNF∀, vascular endothelial growth factor, fibroblast growth factor-2 (FGF-2), wound angiogenesis factor (WAF)

3. *Extracellular Matrix Components*

   elastin, collagens I and III, fibronectin, tenascin

4. *Receptors for Extracellular Matrix Components*

   various ∀ and ∃ subunits of integrins, especially ∃1, ∃4, ∀2, ∀3, ∀5, ∀6, and ∀v

5. *Suprabasal Markers of Terminal Differentiation*

   involucrin, keratin 10 and keratin 16

6. *Transcription Factors*

   AP-2 (important in epithelial-specific gene expression), and NF-6B

7. *Enzymes of the Matrix Metalloproteinase (MMP) Family*

   collagenase, gelatinase B

8. *Basement Membrane Components*

   laminin, collagens IV and VII

9. *Adhesion Molecules*

   ICAM-1, ICAM-2, E-selectin (ELAM-1), P-selectin, VCAM-1, GMP-140, PECAM-1

10. *Tissue Type Plasminogen Activator (t-Pa)*

11. *Growth Factors*

epidermal growth factor (EGF)
platelet-derived growth factor (PDGF, especially the BB dimer)
basic fibroblast growth factor (bFGF)
acidic fibroblast growth factor (aFGF)
heparin binding epidermal growth (HB-EGF)
connective tissue growth factor (CTGF)
fibroblastic/keratinocyte growth factor-7 (FGF-7 or KGF)
insulin-like growth factor-I (IGF-I)
keratinocyte-derived autocrine factor (KAF)
platelet-derived endothelial growth factor (PD-EGF)
transforming growth factor-alpha (TGF-∀)
transforming growth factor-beta (TGF-∃)
vascular endothelail growth factor (VEGF)
tumor necrosis factor alpha (TNF-∀)
tumor necrosis factor beta (TNF-∃)
IL-1
tissue inhibitors of metalloproteinase (TIMPs)

12. *Growth-Inhibitory Cytokines*

beta fibroblast interferon (IFN-∃)
gamma interferon (IFN-∗)

Table 14. Candidate Treatment Regimens

1. Pharmacologic Agents

    a. anti-inflammatory
    b. antibacterial
    c. HD scavengers
    d. poly(ADP-ribose) polymerase (PARP) inhibitors
    e. protease inhibitors
    f. DNA repair enzymes
    g. Antioxidants (topical)
    h. xanthine oxidase inhibitors
    i. angiogenic inducers
    j. mast cell inhibitors
    k. preservation of blood flow into damaged tissue

2. wound debridement

    a. chemical
    b. CO_2 laser
    c. sharp surgical tangential excision

3. wound dressings

4. scar management

5. skin substitutes

6. growth factor cocktails

7. early skin fixation followed by debridement

8. wound cleansers

9. treatment adjuncts to reduce stress and (possibly) improve healing rate

10. nutritional supplements

11. topical or hyperbaric O_2 therapy

12. sub-atmospheric pressure

13. low energy photon therapy (infrared and/or red light)

14. vacuum-assisted closure

15. electrical stimulation

16. heat transfer gels

17. combination therapies